TOPICAL REVIEW • OPEN ACCESS

Flexible diodes for radio frequency (RF) electronics: a materials perspective

To cite this article: James Semple *et al* 2017 *Semicond. Sci. Technol.* **32** 123002

OPEN ACCESS
IOP Publishing
Semiconductor Science and Technology
Semicond. Sci. Technol. **32** (2017) 123002 (45pp)
https://doi.org/10.1088/1361-6641/aa89ce

Topical Review

Flexible diodes for radio frequency (RF) electronics: a materials perspective

James Semple[1,5], Dimitra G Georgiadou[1,5], Gwenhivir Wyatt-Moon[1], Gerwin Gelinck[2,3] and Thomas D Anthopoulos[1,4,5]

[1] Department of Physics and Centre for Plastic Electronics, Blackett Laboratory, Imperial College London, Exhibition Road, London SW7 2BW, United Kingdom
[2] Holst Centre/TNO, Hightech Campus 31, PO Box 8550, 5605 KN, Eindhoven, The Netherlands
[3] Department of Applied Physics, Eindhoven University of Technology, PO Box 513, 5600 MB, Eindhoven, The Netherlands
[4] Division of Physical Sciences and Engineering, King Abdullah University of Science and Technology, Thuwal 23955-6900, Saudi Arabia

E-mail: thomas.anthopoulos@kaust.edu.sa, j.semple12@imperial.ac.uk and d.georgiadou@imperial.ac.uk

Received 12 December 2016, revised 5 August 2017
Accepted for publication 1 September 2017
Published 30 October 2017

Abstract

Over the last decade, there has been increasing interest in transferring the research advances in radiofrequency (RF) rectifiers, the quintessential element of the chip in the RF identification (RFID) tags, obtained on rigid substrates onto plastic (flexible) substrates. The growing demand for flexible RFID tags, wireless communications applications and wireless energy harvesting systems that can be produced at a low-cost is a key driver for this technology push. In this topical review, we summarise recent progress and status of flexible RF diodes and rectifying circuits, with specific focus on materials and device processing aspects. To this end, different families of materials (e.g. flexible silicon, metal oxides, organic and carbon nanomaterials), manufacturing processes (e.g. vacuum and solution processing) and device architectures (diodes and transistors) are compared. Although emphasis is placed on performance, functionality, mechanical flexibility and operating stability, the various bottlenecks associated with each technology are also addressed. Finally, we present our outlook on the commercialisation potential and on the positioning of each material class in the RF electronics landscape based on the findings summarised herein. It is beyond doubt that the field of flexible high and ultra-high frequency rectifiers and electronics as a whole will continue to be an active area of research over the coming years.

Keywords: radio frequency diodes, RFID, printed electronics, flexible electronics

(Some figures may appear in colour only in the online journal)

1. Introduction

Future societies will benefit from a constantly increasing degree of automation in all aspects of everyday life. The ultimate connectivity from machine to machine and from human to machine via wireless networks is already becoming a reality under the wider notion of the *Internet of Things* (IoT) or the *Internet of Everything* [1]. The full traceability and

[5] Authors to whom any correspondence should be addressed.

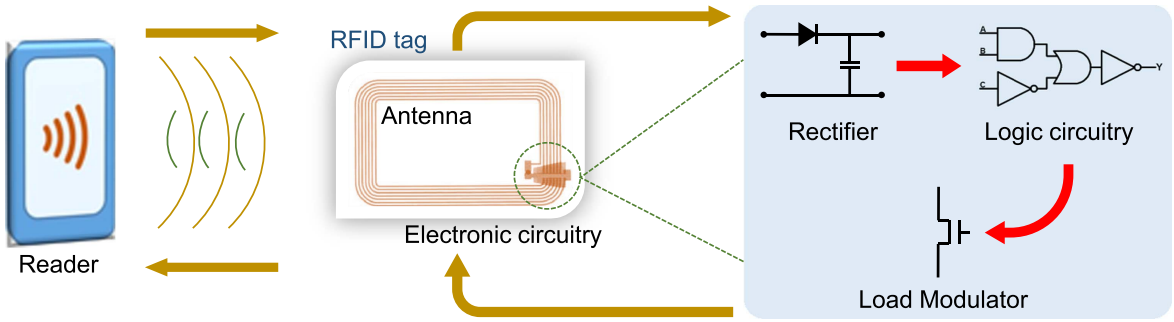

Figure 1. Schematic of the operation of passive RFID tags operating at 13.56 MHz, comprising an antenna, a DC rectifier, logic circuitry and a load modulator. The tag is powered directly by the incoming RF signal without the need for an on-board power supply.

monitoring of 'things', including vehicles, sensitive biological substances, medicines and luxury products, will affect the domains of transportation, health and commerce, and make day-to-day living easier and more secure. Furthermore, the full automation of sorting processes is expected to save valuable time and reduce labour costs in both the public and private sectors, for example, in libraries, laundry facilities, airlines, and fashion apparel retailers to name but a few.

The key elements that lie at the heart of such applications are a radio frequency (RF) reader/emitter in association with a RF identification (RFID) tag, a unique microelectronic component that is attached to an object and carries and/or transmits data related to it. It is comprised of three main components: an antenna, a rectifier, including a diode, and logic circuitry consisting of several transistors. The working principle is illustrated in figure 1: the antenna picks up the alternating current (AC) signal from the reader, which is then rectified. The rectified direct current (DC) signal powers the code generator (logic circuitry) that has an identification code stored in its memory. Therefore, the rectifier generates the DC supply voltage for the code generator, which drives the modulation transistor between the on- and off-state with the code sequence. Load modulation can be obtained in two different modes, depending on the position of the load modulation transistor in the RFID circuit. RFID tags powered by the energy of the RF carrier wave produced by the reader are called passive tags, while those powered by a battery are called active tags. For low-cost applications, passive tags are essential. While alternative technologies, such as surface acoustic wave devices or tuned resonators, can also be implemented for RFID applications, the aforementioned approach, traditionally based on complementary metal-oxide semiconductor (CMOS) circuitry, is by far the most common [2]. Currently based on silicon dies, CMOS circuitry (including rectifiers) is expected to be replaced in the near future by flexible circuitry, which may offer advantages in both more seamless integration and lower cost.

The seminal paper on RFID was published almost 70 years ago by an electronic engineer who foresaw the progression of radar 'on-off' technology to a more complicated radio wave communication through signal modulation [3]. However, a prerequisite for the emergence of the first applications was the maturity of microelectronics and integrated circuits (ICs) to occur. The 'RFID spring' actually occurred in the 1970s when a vast amount of research publications and patents were filed, and the first attempts at commercialisation were made through electronic article surveillance systems to prevent shoplifting [4]. The subsequent developments in RFID occurred in the application field of animal tagging and transportation, for instance in automatic fare collection.

A limitation to even more widespread application has been the maximum read distance. As such, there has been a drive to use higher frequencies, which enable larger read distances. For example, while high frequency (HF) tags operating at 13.56 MHz are usually restricted to a read distance below 10 cm, ultra high frequency (UHF) devices are capable of operating over some metres, enabling their operation in warehouse inventory and logistics of perishable goods for example. As a consequence, there was an increasing demand for more efficient rectifier circuitry or low power devices, which was effectively satisfied through faster switching speeds and lower drive voltages that were obtained with silicon-based rectifiers. New technological developments during the 1990s expanded the functionality of RFID through fabrication of microwave (operating at the GHz regime) Schottky diodes on a regular CMOS IC [5]. Alongside the progress made towards higher frequencies, the 21st century introduced the smallest microwave tags built so far by using just two components: a single custom CMOS IC (which included the rectifier) and an antenna. This miniaturisation paved the way to a plethora of niche applications, since the tags resembled sticky labels (like commonly employed barcodes) that could be easily attached to almost any type of objects. Nowadays the size of tags is limited solely by the constraints of the antenna, the latter—as well as the search for better non-volatile memory—being design challenges still to be resolved [6].

From the application viewpoint, another particularly attractive field that stems from 13.56 MHz RFID is the near-field communication (NFC) sector. NFC is a protocol for the contactless bidirectional communication between devices in proximity, at least one being a mobile device. NFC essentially extends the capability of contactless card technology, enabling mobile devices to perform secure payment transactions, access digital content and allow connectivity and data exchange between electronic devices at a distance smaller than 5–10 cm [7]. Bluetooth Low Energy or Bluetooth Smart and Zigbee are communication protocols operating at

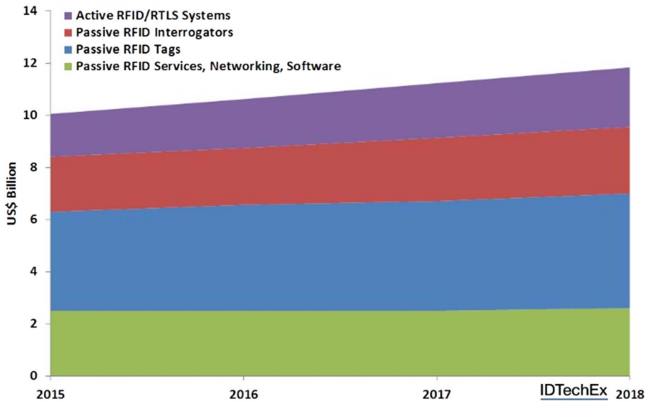

Figure 2. Total RFID Market Projections in US$ billions. Provided and reprinted with permission from IDTechEx Ltd.

2.4 GHz corresponding to 10–100 m range and characterised by low energy consumption, which target applications like wearable monitoring devices (heart rate monitors, smart watches and fitness trackers), other sensing applications such as thermometers, proximity sensors, weight scales, tyre pressure monitoring systems and numerous devices that use wireless technologies to provide their smart functionality [8]. Other lower power RF communications technologies, such as *Z*-Wave, operating in the sub-1 GHz (900 MHz) regime, are primarily designed for home automation in products such as lamp controllers and sensors [9].

Finally, the trend to go to higher frequencies, enabling higher readout distances, addresses the need for low-power communication, which paves the way for applications in the RF energy harvesting domain. By taking advantage of RF-to-DC conversion technology, the possibility of low power (μW to some mW) [10, 11] electronic devices without the need for batteries can be realised. This is a critical enabler for the envisioned IoT. The energy harvested by these devices may be provided, for instance, by mobile phones that operate within the UHF band (300 MHz–3 GHz) and more specifically, within the global system for mobile communication frequency bands currently used by all mobile networks (i.e. roughly at 850 MHz/1.9 GHz in America and 900 MHz/1.8 GHz in Europe and other parts of the globe) [11]. Interestingly, a recent case study showed how much energy could be potentially harvested from ambient (freely available) RF sources located in urban or semi-urban environments, such as London underground stations [12].

From the above it becomes obvious that the total RFID market is very large and will keep growing, as indicated by the already more than 800 companies globally active in this field. According to recent market analysis reports, the value of the passive RFID tag market is currently estimated at >$8 billion (figure 2) with projections indicating that the total RFID market will be worth $18.68 billion by 2026 [13].

It is interesting to note that the top RFID reader suppliers are focused on application areas that require either higher volumes or higher-priced devices, such as smartcard applications (e.g. security/access control, ID) or active solutions, such as real time locating systems or tolling [14].

To enable an entire host of new applications, such as barcode replacement, a fabrication cost reduction that will render the single tag price below $0.01 USD must be generated by means of substantially increasing the production volume as well as shrinking the tag size—especially the antenna [15]. UHF tags with higher operating frequencies (which require smaller antennas) thus have a competitive cost advantage as compared to HF tags, while at the same time being ideal for longer-range communication, as discussed above. This, of course, provided that the manufacturing cost of the low power rectification components and required integrated circuitry remains low. The latter has been successfully obtained by following a miniaturisation strategy, which yields the largest number of devices per wafer, e.g. by dicing the starting device wafer down to the smallest possible die size, combined with cost effective ways of integrating such small Si RFID die onto the antenna, bringing thus the cost of certain RFID tags at around $0.05 [16]. However, to achieve further price reduction, the cost of the attachment process has to be reconsidered and alternative routes towards ease of manufacturing should be sought.

To this end, the technology platform known as printed or flexible electronics [17–19], which commonly refers to electronic devices, such as organic light-emitting diodes (OLEDs) [20, 21], organic photovoltaics [22–24], and thin-film transistors (TFTs) based on solution-processed organic or inorganic materials (inks) that can be printed directly on flexible, lightweight, thin substrates with potentially low cost, has seen tremendous advancements within the last two decades and is considered to be a key enabler also for RF applications [25, 26]. In fact, Philips Research in the Netherlands [27] and PolyIC in Germany [28–30] both reported—already 10 years ago—on 'full plastic RFID tags' operating at 13.56 MHz, which were based on organic/polymer diodes and transistors printed on plastic (e.g. polyester foil) substrates. The great advantage, especially for UHF applications, presented by using printing manufacturing technologies, such as roll-to-roll, is that the rectifier and antenna can be printed directly onto the substrate reducing the production process steps from three (i.e. antenna moulding, chip production, assembly of components in the silicon-based tags) to one. Nevertheless, it should be noted that this is currently an emerging field and there are several fundamental challenges, such as low yield and low device performance, still to be overcome to compete with very large scale integration Si processes and enter niche or new markets (e.g. low cost items tagging).

In this review, we summarise the latest progress made and the status of flexible RF diodes and rectifiers, a critical component for the realisation of flexible RFID tags, with specific emphasis given to materials, material processing and device aspects. To this end, different device architectures, classes of materials, and manufacturing processes are compared in terms of device and system performance, functionality, stability and lifetime. The main aim of this article is to highlight recent advances in *flexible* RF diodes and circuits as well as discuss the main challenges. A review of the progress of flexible-substrate-compatible materials will also be provided.

More specifically, we first refer to basic device physics related to Schottky diode and TFT-based rectifiers and then present the physical quantities commonly used as figures of merit to evaluate the device performance. An overview of the desired materials properties is also given in the theoretical section. The following sections are categorised according to the respective material class that is described therein and include silicon (Si)-based RF devices, as Si is the key material of todays dominant semiconductor technology, with emphasis given to flexible-Si (and related traditional semiconductor) RF devices. Next, we summarise published results on rectifiers based on metal oxide semiconductors (MOSs), which have shown remarkable progress in terms of performance over the last decade. First, we draw the theoretical background picture by introducing basic elements of the fundamental charge transport mechanisms, followed by a discussion of the various thin-film deposition methods and their relation to specific materials aspects. This highlights how progress within the field of process and materials engineering has paved the way to high performing flexible RF electronics. Next, we introduce the emerging class of organic semiconducting materials, which have demonstrated great promise for application in low-cost RF rectifiers. Their attractiveness lies in the fact that they may comprise both n- and p-type semiconductors and the majority of these materials are compatible with printing technologies. Finally, the last section of the review is devoted to nanomaterials, such as carbon nanotubes (CNTs), graphene and other related two-dimensional (2D) materials, which have shown great intrinsic high-frequency performance. The various challenges associated with the manufacturing of devices based on such nanomaterials will also be discussed alongside potential solutions.

2. Theoretical background

The defining performance factors for RFID systems include the transmission frequency of the signal (from 125 kHz up to 5.8 GHz in the microwave (MW) range), the physical coupling method (electric, magnetic or electromagnetic) and the read range of the system (from a few millimetres to above 100 m) [31]. These key criteria are closely interrelated and in many cases define the specific field of application as well as the cost of the tag [32]. In general, (far field) electromagnetically coupled tags have the greatest read range. However, the required size of electromagnetic antennae in the low frequency (LF) and high frequency (HF) bands would be prohibitively large, which leads to the use of magnetic or electric coupling in these frequency ranges. Read range can also be stretched in all cases by optimising the antenna efficiency, maximising the efficiency of the rectifier as well as boosting the power of the output signal.

Figure 3 summarises the read range, frequency and end-use applications of each of the commercially employed RFID bands. While the LF band spans 30–300 kHz, the specific frequencies employed for LF devices are 125 and 135 kHz. Similarly, for the HF band (3–30 MHz) and the UHF band (>300 MHz) the frequencies of interest are 13.56 MHz for the HF band and 433, 868 and 915 MHz for the UHF band. It should be noted that, while HF has traditionally been the most popular band by market value (figure 4) [33], recent data indicate that UHF tags are set to become the dominant fraction in the coming years with innovations stemming from advances in plastic electronics being a major drive.

One of the principal roadblocks to flexible RFID technology has been the manufacture of a mechanically flexible/deformable rectifier. Typically, low-cost rectifiers produced on flexible substrates have struggled to operate at the required frequencies. Key to the frequency performance of the rectifier circuit is the diode, which is the focal point of this review. Significant effort shall be made to address device structural optimisation as well as material performance concerning the production of a HF and mechanically flexible diode. First, however, DC rectifying circuitry will be briefly explained, followed by an introduction to the relevant figures of merit.

2.1. DC rectifier circuits and their operational principle

DC rectifiers are circuits fabricated with the purpose of converting AC signals to DC. The critical component in any rectifier circuit is the diode(s). The diode is the component that limits the maximum frequency that can be rectified and (typically) determines the level of the rectified DC output and is thus the focus of this review. Schottky diodes have been widely studied owing to their intrinsic HF response. However, transistors can also be operated as diodes (transdiode mode) and thus have also been employed.

2.1.1. Rectifier circuitry. Diodes are by definition two-terminal electronic devices allowing the flow of current in one direction only. To achieve a DC output, the diode is typically integrated with a capacitor.

In the simplest case, a diode is incorporated into a low-pass filter, as shown in figure 5(a). When a sinusoidal input signal is applied, the diode outputs a half wave signal, namely only the polarity that can be conducted through the diode, which charges one side of the capacitor. So long as the half wave signal charges the capacitor faster than it can discharge significantly, a DC output with a small AC ripple is produced as shown in the dashed waveform in figure 5(b). The RC time constant of the capacitor affects the magnitude of the ripple (lower ripple for higher capacitance), whereas the operational frequency of the rectifier is dictated by the diode performance alone. This ripple can be further reduced by employing more complex circuitry, for example, by taking advantage of the full input sine wave by means of a full wave bridge rectifier, as shown in figure 5(c). In figure 5(d) the output signal of the full wave bridge rectifier diodes is shown in the solid line waveform, while again the capacitor has the effect of outputting the dashed signal from the circuit. In this case, the shorter time between the charging cycles of the capacitors leads to a reduction in the magnitude of the AC ripple.

In the cases where it is advantageous to output a high value of DC voltage (for example, energy harvesting of weak signals to charge batteries, driving high voltage logic components), voltage multipliers are implemented. Figure 5(e) shows how

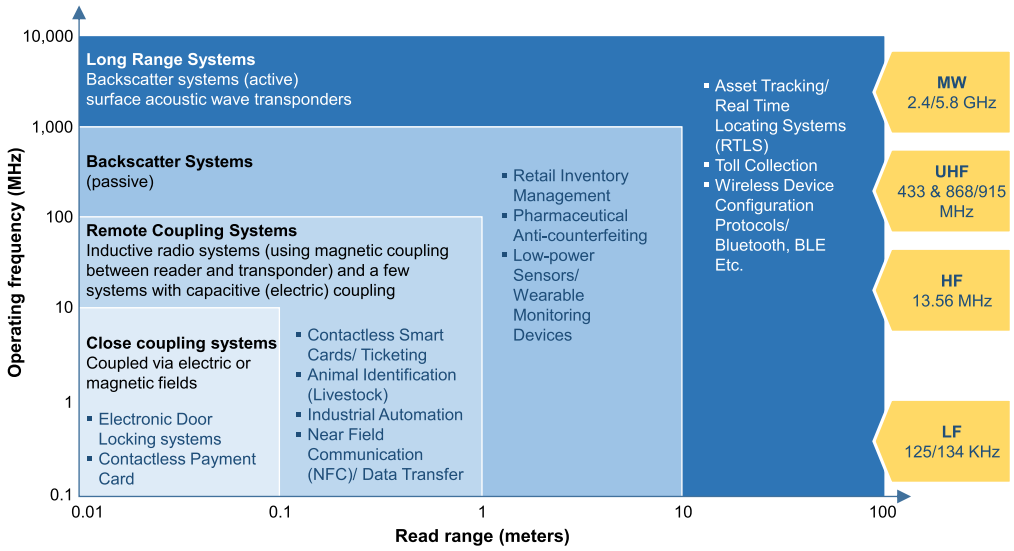

Figure 3. Classification of examples of RF applications according to their operating frequency and read range requirements. The benchmark frequencies and the physical coupling system are also mentioned for each frequency range.

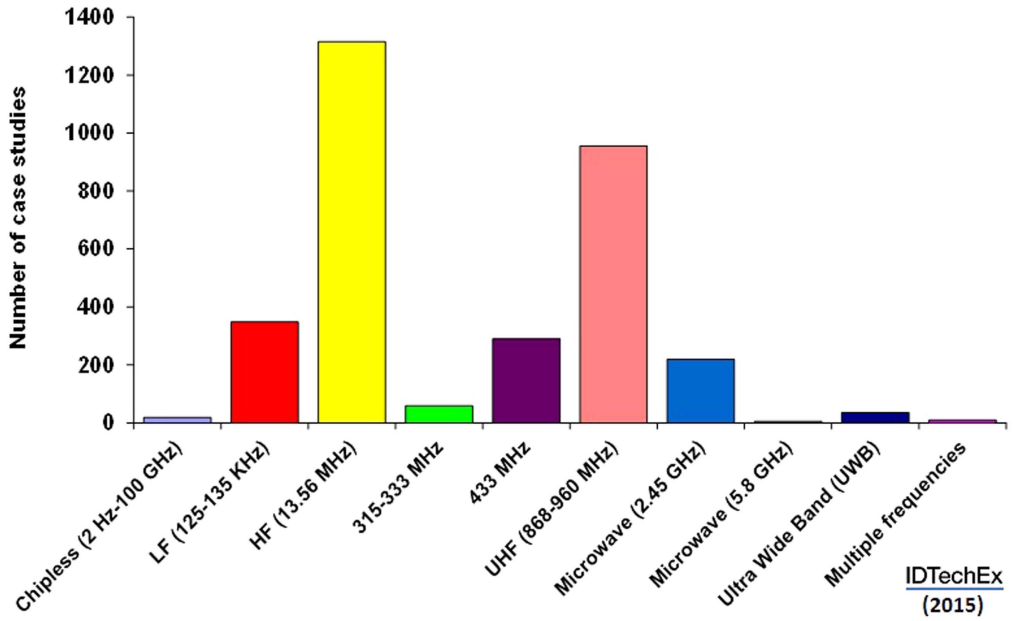

Figure 4. Number of cases reported by frequency band reflecting a breakdown of the current RFID market. Adapted and reprinted with permission from IDTechEx Ltd.

cascaded diode and capacitor cells can be combined to make a charge pump circuit, in this case a voltage quadrupler. By subtracting or adding these cells, voltage doublers, triplers and higher order multipliers can be realised, although the output is limited in terms of current capacity. A double half wave rectifier, or Delon circuit, shown in figure 5(f), works on a similar principle, taking advantage of the full sine wave input to produce a DC signal with double the peak of the input sine wave.

Ideally, the selected diode configuration should favour one or more of the following, according to the end-application: high cut-off frequency, f_C; high conversion efficiency, $\eta_{rectifier}$; large output voltage, V_{DC}, and driving current, I. For example, to give an estimate of the lowest limits for the above values (for instance when targeting energy harvesting, i.e. low power applications), a commercial Schottky diode implemented into a rectifier circuit operating at 2.45 GHz outputs a DC voltage of 36.2 mV with a conversion efficiency of 1.3% over a 10 kΩ load resistor and for input power −20 dBM (corresponding to 0.01 mW), while $\eta_{rectifier}$ increases to 23% for input power 0 dBM (1 mW) [34]. In another instance, a $V_{DC} = 1$ V was outputted by an all-printed Si-based diode operating at 1.6 GHz, with a current of 3 μA at 1 V in DC I–V measurement, upon harvesting the emitted energy from a mobile phone while performing a call, and was able to power an electrochromic display element [35]. From the above examples it becomes obvious that for certain applications (e.g. low incident power), large V_{DC} may

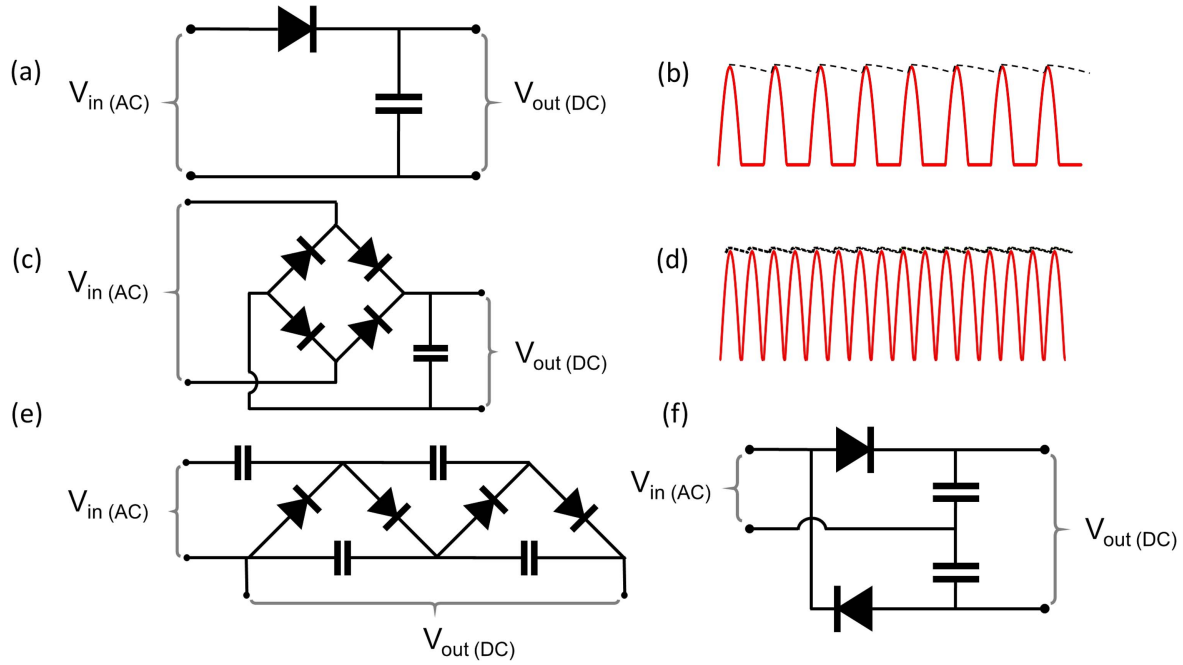

Figure 5. Rectifier circuits and corresponding output signals based on (a), (b) a simple diode and (c), (d) a full wave bridge rectifier. Output waveforms without and with the capacitor are shown as solid and dashed lines, respectively. (e) Voltage quadrupler as an example of charge pump circuit. (f) Double half wave rectifier circuit also known as Delon circuit.

be compromised with high conversion efficiency and vice versa.

Having all the above requirements in mind, we will explain why the ideal diode candidate is most often a Schottky diode. Its merits will then be compared and contrasted with the well-established TFT technology.

2.1.2. Schottky diodes. A Schottky diode is a type of metal–semiconductor (MS) junction, where the mismatch in the Fermi levels of the metal and semiconductor cause a bending in the energy level of the majority carrier band edge of the semiconductor (conduction band edge for n-type and valence band edge for p-type) at the interface. The degree of band bending defines the barrier height for charge carriers to overcome at the MS junction [36]. In many well-studied semiconductor systems, the MS barrier height in a Schottky diode tends to be lower than the junction barrier in a PN diode. This in turn leads to lower turn-on voltages and higher values of the current (both forward and reverse biased) in Schottky diodes, which is why they are the diode of choice for low voltage applications.

An additionally important feature for high-speed operation is that Schottky diodes are unipolar devices. The limiting factor in terms of switching speed in bipolar PN junction diodes and PIN diodes is the fact that charge is stored at the interface (or in the intrinsic region in the case of the PIN diode), and must be discharged when switching the sign of the applied bias. This gives rise to a reverse recovery time (t_{rr}), a value that is on the order of nanoseconds in the best case [37]. When the time between positive and negative half cycles of the signal is not sufficient for this discharge to occur (i.e. it is less than t_{rr}), the diode conducts in both half cycles and rectification ceases. The unipolar nature of Schottky diodes, however, means that no charge is stored and switching speed is thus not limited by such a reverse recovery time. In this case, only a capacitive loading must be considered, which has far less impact on switching speed.

2.1.3. Transdiode transistors versus Schottky diodes. Apart from diodes, TFTs have also been employed in RF rectifying circuits. TFTs are three terminal switching devices, analogous to MOS field effect transistors (MOSFETs), the workhorse of traditional Si-based ICs. Though typically requiring a secondary variable voltage to the gate electrode to rectify signals, transistors may also be configured as simple diodes by directly connecting the gate and the drain electrodes. In this state, the transistor is always in the saturation region, acting as a MOS diode with *I–V* characteristics similar to the PN junction diode, and it is referred to as operating in transdiode mode.

To understand how such a diode-connected transistor operates, we may consider first that the general condition for a transistor being in the saturation regime is:

$$V_{DS} > V_{GS} - V_{th}, \tag{1}$$

where V_{DS}, V_{GS} and V_{th} represent the drain, gate and threshold voltages, respectively. In the case of the transdiode transistor $V_{DS} = V_{GS}$. Thus, from the above inequality, in the diode-connected mode the transistor will always be in the saturation regime. Current in saturation mode for a transistor is given by the well-known square law dependence:

$$I_D = \frac{\mu C_G W}{2L}(V_{GS} - V_{th})^2, \tag{2}$$

where μ is the semiconductor mobility, C_G is the specific capacitance of the gate dielectric per unit area due to overlap

of the gate with the source/drain (S/D) electrodes, and W and L are the width and length of the channel, respectively. Thus, one would expect to see higher currents from a Schottky diode, as the current is given by an exponential dependence on voltage according to the Shockley diode equation:

$$I = I_0(e^{\frac{qV}{nkT}} - 1), \tag{3}$$

where k is the Boltzmann constant, T the temperature, q the electron charge, n is the diode ideality factor, and I_0 the reverse bias saturation current. Furthermore, the V_{th} in a transistor tends to be significantly higher than the on-voltage for a Schottky diode (typically < 0.5 V), thus leading to lower values of $\eta_{rectifier}$ when using transdiode transistors. Several efforts have been made to boost the latter by either lowering the V_{th} [38] or by using self-V_{th} cancellation techniques [39, 40].

With these less ideal device characteristics, as compared to Schottky diodes, the question arises as to why one would employ transistors in DC rectifiers at all. Indeed, Schottky diodes consistently and significantly outperform transistors based on the same materials in terms of frequency response, as will be discussed in section 2.2.4. In short, the answer lies in the fabrication process. In current Si-based RFID technology, MOSFETs are employed as diode components due to their compatibility with existing semiconductor device fabrication facilities.

A further consideration, with regard to the fabrication of diodes for large-area applications, is the difficulty in processing planar asymmetric electrodes in a cost-effective manner. Planar diodes (as opposed to vertical 'sandwich' structures) are not always necessary, but become of relevance when the semiconductor material is incompatible with vertical architectures (see section 6). MOSFETs/transistors, on the other hand, require symmetric contacts, which are more easily processed. Finally, the logic circuitry employed in RFID tags is currently based on MOSFETs, meaning both logic circuitry and rectifier can be manufactured on the same line.

Thus, there is a trade-off between processability and ultimate device performance, which accounts for the high rate of reports of high speed transistors as compared to Schottky diodes. The verdict is still out on which of these device types will be adopted in future technologies. Therefore, both Schottky diodes and transistors are considered in this review.

2.2. Important figures of merit

2.2.1. Operating frequency. There are several quantities that can be used to assess the frequency response depending on the type of the device. As such cut-off frequency (f_C) is a somewhat generic term, which may refer to different frequencies depending on the context. Therefore, in this section we elucidate the different types of cut-off frequencies generally encountered and make an effort to discern each by looking at the specific definition.

One highly practical definition of f_C is the half-power point (f_{-3dB}), the frequency at which a circuit/device outputs half of the maximum possible output power (i.e. the output at lower frequencies). This is the equivalent of observing a power attenuation of approximately -3 dB. An analogous way of stating this is the frequency at which the voltage reaches $1/\sqrt{2} \approx 0.707$ of its peak value. Most often this interpretation is used when measuring a DC output (i.e. when a diode/TFT is incorporated in a rectifier circuit). Thus the f_{-3dB} value is practical, as it is representative of how the diode/TFT performs in a practical setup and not complete isolation. Nevertheless, values of device performance in isolation can be useful in assessing the ultimate frequency capabilities of the device/technology.

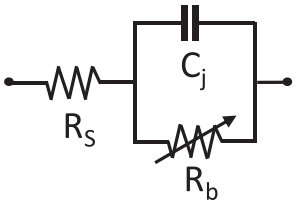

Figure 6. Equivalent circuit model for a Schottky diode, showing series resistance (R_S) and a parallel junction capacitance (C_j) and barrier resistance (R_b).

One such method in defining the upper frequency limit of rectification is to examine equivalent circuit models. In *Schottky diodes*, this upper frequency limit can be derived from the equivalent circuit model shown in figure 6. In this simple RC circuit, comprising resistive and capacitive elements connected in series, the output voltage (V_{out}) is given by the equation:

$$V_{out} = V_{in}\frac{X_C}{\sqrt{R_S^2 + X_C^2}}, \tag{4}$$

where the series resistance, R_s (attributed to spreading resistance, bulk semiconductor resistance and contact resistance), is considered to be in series with a nonlinear barrier resistance, R_b, which gives rise to rectifying characteristics, and X_c is the reactance associated with the capacitive element (C_j) given as:

$$X_C = \frac{1}{\omega C_j} = \frac{1}{2\pi f C_j}, \tag{5}$$

where f is the frequency.

From equations (4) and (5) it becomes clear that at low frequencies of $X_C \gg R_S$, the current transport is dominated by the resistive element and input signal rectification occurs. On the contrary, at significantly high frequencies ($X_C < R_S$) the current flow is shorted through the capacitive element and thus rectification ceases. The threshold frequency ($f_{C\text{-Schottky}}$) for the latter to happen is defined as the frequency at which $X_C = R_S$ [41]:

$$f_{C\text{-Schottky}} = \frac{1}{2\pi R_S C_j}. \tag{6}$$

Therefore, minimisation of the series resistance and junction capacitance are critical for HF operation of the diode.

The most common figure of merit for evaluating the frequency performance of *TFT-based rectifiers* is the transition frequency (f_T). This is the frequency at which the

current gain is unity, and is given by [36]:

$$f_T = \frac{g_m}{2\pi C_G} = \frac{\mu_{eff}(V_{GS} - V_{th})}{2\pi L\left(2L_{OL} + \left(\frac{2}{3}\right)L\right)}, \quad (7)$$

where g_m is transconductance ($g_m = dI_D/dV_{GS}$), C_G is parasitic capacitance caused by gate overlap with the source and drain electrodes (L_{OL}), and μ_{eff} is the effective mobility. The latter may be smaller than the intrinsic charge carrier mobility of the active semiconducting material, as it also takes into account the contact resistance and other parasitic effects.

Another value that can be used to characterise the speed of a transistor is the maximum (oscillation) frequency, f_{max}, which is the frequency at which the power gain is unity. f_{max} correlates with f_T through the following formula [36]:

$$f_{max} = \sqrt{\frac{f_T}{8\pi R_G C_{GD}}}, \quad (8)$$

where R_G is the resistance of the gate and C_{GD} is the gate/drain capacitance. In fundamental derivations, f_T would not take into account the overlap capacitance and f_{max} would be a more accurate representation of the speed of the device. However this has been compensated for by using the gate overlap and effective mobility, and both equations give a fuller model of the frequency.

Finally, for a *TFT in transdiode mode*, a different model for frequency response is required. Uno *et al* [42] considered the transit time as the inverse of the maximum frequency response, $f_{TD\text{-}max}$, of the diode and derived the following equation:

$$f_{TD\text{-}max} = \frac{\mu}{2L^2} V_{in}\left(\frac{\sqrt{1-B^2}}{\cos^{-1}B} - B\right), \quad (9)$$

where V_{in} is the amplitude of the input signal and $B = \frac{V_{out}}{V_{in}}$. This value is roughly π times higher than the transition frequency, and there is no relation to drain and gate capacitance, as these electrodes are now connected electrically.

2.2.1.1. Measurement of frequency response. The first distinction that must be made in terms of frequency measurements is between *extrinsic* and *intrinsic frequency* response. Extrinsic frequencies are those which are directly measured; they thus refer to the response of the device as a whole, incorporating effects such as contact resistance and effects due to the connection of the device to external components. Intrinsic frequency refers to the expected ultimate frequency response of the active material in the diode. These values are extracted with various de-embedding techniques. Intrinsic frequency values are often quoted to give an indication of the upper limit performance of a particular material.

The focus of this review is on both the improvement in materials and device structuring aspects to achieve HF response. As such, values of extrinsic frequency response, which give a more realistic picture of the device as a whole, shall be given unless explicitly stated.

The frequency performance of rectifying elements (diodes and TFTs) can be measured in several ways. Each of these has their own advantages and disadvantages. It is thus important to clarify how the reported frequencies were measured to render their values comparable. Theoretical values of $f_{C\text{-}Schottky}$ may be extracted by measuring the relevant parameters, i.e. resistance and capacitance. However, as these values can be heavily frequency dependent, their extraction from quasi-static DC measurements may be unreliable. The same logic holds for extracting theoretical values of f_T and f_{max} in TFTs. A more accurate route lies in the measurement of the frequency dependent real and imaginary values of impedance. According to what was discussed above, the impedance (Z) of an RC network is given by:

$$Z = R - \frac{j}{2\pi fC} \quad (10)$$

and the cut-off frequency for a diode is defined as the point at which real and imaginary impedance values are equal. In practice, both of these values can be extracted from single port scattering (s_{11}) parameters measurement using a vector network analyser. For TFTs, values of f_T and f_{max} may be extracted using dual port measurements to extract the hybrid (h) parameters.

A direct measurement of f_{-3dB} is often the most accurate and practical measurement approach. In practice, however, diodes/transdiode TFTs are incorporated in rectifier circuits (figure 5(a)), and thus the measured value is a DC rather than AC voltage. Measuring DC voltages is often far simpler than measuring HF AC signals, but this method is also employed for practical reasons as the main applications of many of these HF devices are in AC/DC rectifiers. As diodes/TFTs are expected to be the limiting factor in the circuit in terms of speed, the f_{-3dB} of a rectifier circuit gives a good estimation of the individual diode performance.

2.2.2. Conversion efficiency of rectifying circuit. The RF-to-DC power conversion efficiency of the rectifier, $\eta_{rectifier}$, is the ratio of rectified output power and input power. It can thus be expressed as [43]:

$$\eta_{rectifier} = \frac{P_{DC}}{P_{in}} = \frac{V_{DC}^2}{R_L P_{in}}, \quad (11)$$

where P_{DC} is the rectified output power, P_{in} is the input power, and R_L is the output load resistance. It thus becomes obvious that $\eta_{rectifier}$ is frequency dependent.

2.2.3. Mechanical flexibility of circuits. To give an idea of the mechanical flexibility, an often used parameter is the radius of curvature. In first order approximation this bending radius, ρ, is related to the mechanical strain, ε, and the total substrate and device thickness, t, as:

$$\varepsilon = \frac{t}{2\rho}. \quad (13)$$

For most semiconductors, some deviation from un-flexed device characteristics occurs under moderate bending due to strain-induced mobility variation. At a certain bending radius the electrical characteristics break down due to permanent deformation of one or more device components. Operating

stability under repeated bending cycles is also important for devices to be employed in dynamic environments. It is thus crucial to choose device component materials that are suitable for operating under such demanding environments [44].

2.2.4. Material considerations. Apart from the selection of the circuitry design and device type, the most important optimisation variable relates to the active material used. This is especially important for devices manufactured on flexible substrates; the intrinsic properties of the materials should be considered in line with their film deposition process parameters, which at the same time should be compatible with large volume and large-area manufacturing to substantially reduce the production cost.

Considering the desire for HF operation and high efficiency, one would expect a classical inorganic semiconductor with a high degree of crystallinity, low defect density and high mobility to fit the bill. Indeed, a strong correlation between semiconductor charge carrier mobility and frequency performance has been observed in this review and is depicted for different material classes in figure 7(a).

If we account for deposition on thin flexible substrates, solution processability is often desirable due to its lower cost as opposed to vacuum deposition. In this case the material should be processed from orthogonal and, ideally, environmentally friendly solvents. Optimisation of the fluid parameters of the ink solutions (viscosity, surface tension, drying parameters, to name but a few) according to deposition technique (roll-to-roll, inkjet, screen printing) must be addressed without compromising the intrinsic materials properties. If vacuum-based deposition techniques are to be employed they must be large-area compatible, preferably with the potential for high-throughput manufacturing. In either case, thermal processing (annealing) should be kept at as low temperatures as possible depending on the substrate used (e.g. below 150 °C for polyethylene terephthalate, PET, 180 °C for polyethylene naphthalene, PEN, and 300 °C for polyimide, PI, or polyether ether ketone, PEEK) [45]. A further consideration for device fabrication is that the resulting devices should exhibit low values of series resistance and capacitance in order to be able to achieve HF operation. Thus, in general it is favourable to incorporate semiconductors in devices with appropriately small footprint, while still being compatible with large-area and high-throughput manufacturing.

Finally, considering material performance on flexible substrates, the devices should be capable of operating under some degree of mechanical flexing and retaining this performance over time and after repeated bending cycles. Figure 7(b) shows the cut-off frequency versus bending radius for some materials classes in an effort to highlight the state-of-the-art high performance high flexibility devices.

In this review, we summarise the developments made in the active materials used for RF rectification with emphasis on deposition on flexible substrates. However, to accurately encompass all progress made from the materials point of view, we have also included some works demonstrating high performance functional devices on rigid substrates.

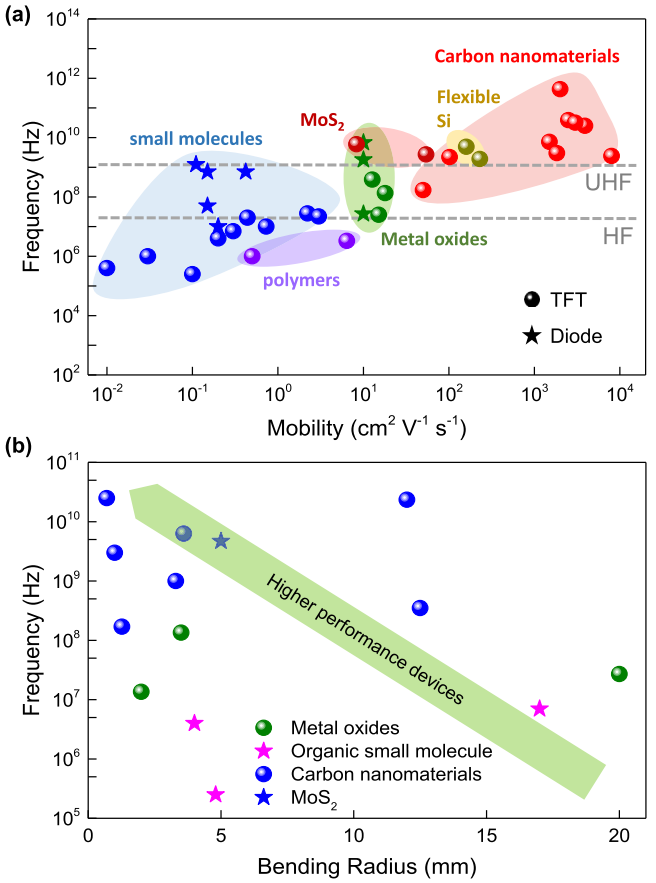

Figure 7. (a) Reported operating frequency versus charge carrier mobility for diodes and TFTs fabricated on flexible substrates and discussed in this review article. As expected, the operating frequency of the device increases with increasing carrier mobility. Threshold frequencies for HF (13.56 MHz) and UHF (860 MHz) RFID operation are shown in dashed grey lines. Organic materials, including polymers and small molecules, exhibit the lowest frequency performance of the semiconductors studied. Nevertheless, their performance is sufficient to operate in the HF and into the UHF regime. Metal oxide semiconductors show promise for UHF operation, while carbon nanomaterials show the highest levels of mobility and frequency response. Notably, diodes consistently outperform TFTs of the same material class. A corresponding table of references is included in the appendix (table A1). (b) Device frequency performance as a function of bending radius. Carbon nanomaterials including graphene and CNTs exhibit the highest frequency response and are capable of sustaining the highest strains.

3. Silicon-based flexible RF electronics

Silicon (Si) in its single crystalline phase represents the state-of-the-art for RF electronics. The thickness of the silicon chip (hundreds of micrometres) limits its mechanical flexibility. The process of thinning the Si wafer has actually been known about since the 1960s, when the thickness of Si was reduced down to 100 μm with the aim of reducing the total weight of the solar cells, and this is regarded by many as the dawning of flexible electronics era [46]. However, incorporation of these thinned Si circuits onto flexible (plastic) substrates remains challenging. Using this method, mechanically strained RF MOSFETs have been demonstrated. Excellent RF performance, such as a low minimum noise figure (NF_{min}) of

Table 1. Summary of recent advances in flexible Si-based RF electronic devices.

A. Thinned Si RF MOSFETs				
Si wafer thickness	f_T (GHz)	f_{max} (GHz)	Year	Reference
30 μm	59	—	2005	[47]
5.7 μm—n-type	150	160	2011	[48]
5.7 μm—p-type	100	130	2011	[48]
B. Si nanomembranes (SiNMs)/microstructured Si (μs-Si)				
Technology progress	f_T (GHz)	f_{max} (GHz)	Year	Reference
μs-Si single-crystal Si TFTs on PI	0.515	—	2006	[64]
rf top-gated single-crystal Si TFTs on PET	1.9	3.1	2006	[53]
Control of parasitic s/d resistance and s-to-g/d-to-g capacitance	2.04	7.8	2007	[55]
Improved nanomembrane transfer method	3.8	12.0	2010	[56]
Double-gate flexible SiNM TFTs on biodegradable CNF substrate	4.9	10.6	2015	[61]
NIL 100 nm trench SiNM TFTs on PET	5.0	38.0	2016	[69]
C. Si microparticles				
Structure of all-printed diodes		f_{-3dB} (GHz)	Year	Reference
PET/Al (50 nm)/Si-in-SU8 (cross-linked, 4 μm)/$NbSi_2$-in-SU8 (4 μm)/carbon (6 μm)/Ag (3 μm)		1.6	2014	[35]
PET/Al/CNF:Si-μPs/Ni:Carbon		1.8	2016	[70]

0.92 dB, high associated gain (14 dB at 10 GHz) and high $f_T = 59$ GHz were obtained after thinning down the Si substrate to 30 μm and mounting it on plastic substrates, after which the devices were subjected to tensile strain [47]. In another instance, high-performance industrial MOSFETs thinned down to 5.7 μm and transferred onto a 125 μm thick polyethylene naphthalate (PEN) foil were demonstrated with f_T and f_{max} as high as 150/160 GHz for n-MOSFETs and 100/130 GHz for p-MOSFETs, respectively [48–50]. In the following subsections, some of the most innovative methods to incorporate Si materials in flexible electronic devices will be described. The important figures of merit related to the performance characteristics of these Si-based devices are summarised in table 1.

3.1. Single crystalline Si nanomembranes

2D geometries of monocrystalline semiconductor sheets with nanoscale (less than a few hundred nanometres) thicknesses and with minimum lateral dimensions—at least two orders of magnitude larger than the thickness—are referred to as nanomembranes [51]. Such materials, in contrast with thin films, may exist as freestanding, isolated forms and be transferred onto arbitrary substrates. Although the approaches that will be discussed below address adequately the challenge of matching well-established mature Si semiconductor technologies with flexible and lightweight plastic substrates, the total cost remains quite high. This is due to the high temperatures and high vacuum that are usually required to form an excellent quality semiconducting material, and such routes usually target applications that are highly demanding in terms of outstanding RF device performance (e.g. military) [52].

A novel dry-printing method for transferring single-crystal Si membranes from a silicon-on insulator onto flexible polymer substrates, the so-called single-crystalline Si nanomembrane (SiNMs) transfer method, has been introduced by the group of Ma (figure 8) [53–58]. By applying this technique, RF top-gated single-crystal Si TFTs have been monolithically integrated on PET polymer substrates and values of f_T and f_{max} of 1.9 GHz and 3.1 GHz were obtained respectively at $V_{DS} = 4$ V and $V_{GS} = 5$ V [54]. The performance was further improved through control of parasitic S/D resistance and source-to-gate/drain-to-gate capacitance upon targeted optimisation of the transistor layout design, which resulted in f_T of 2.04 GHz and f_{max} of 7.8 GHz [55], while subsequent improvements in the process of the nanomembrane transfer method increased further the attained frequencies to 3.8 GHz and 12 GHz, respectively [56]. More interestingly the same group successfully applied this transferrable SiNM method to the fabrication of flexible microwave PIN diodes (figure 8) [57, 58].

The versatility of this technique was further demonstrated by applying it to single-crystal germanium (Ge) nanomembranes to form flexible devices displaying GHz response (insertion loss of <1.3 dB at up to 30 GHz and isolation >10 dB at up to $\sim$13 GHz) [59, 60], and later by demonstrating microwave flexible SiNM-based TFTs [61] and Schottky diodes [62] on biodegradable substrates, such as cellulose nanofibrillated fibre (CNF), towards potential green

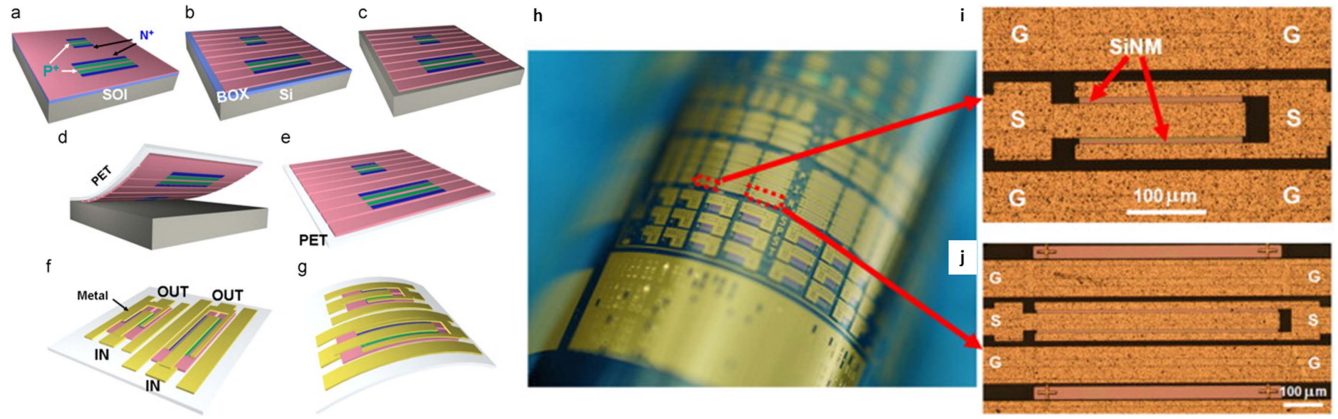

Figure 8. (a)–(f) Process schematic of fabricating flexible microwave single-crystalline Si nanomembrane PIN diode on plastic substrate. (g) Illustration of the flexible single-crystalline SiNM PIN diodes under bending condition. (h) Optical image and (i), (j) microscopic images of the finished PIN diodes arrays on a bent PET substrate. (i) Total diode width is 400 mm (two identical parallel diode channel, each channel has a width of 200 mm). Diode intrinsic region length is 2 mm. Total diode area is 80 mm^2. (j) Microscopic image of the 240 mm^2-PIN diode fabricated on a plastic substrate. Total diode width is 1200 mm (two identical parallel diode channels, each channel has a width of 600 mm). Adapted with permission from [57]. Copyright © 2010 Elsevier Ltd.

portable devices. Double-gate flexible SiNM TFTs built on a CNF substrate have shown an electron mobility of 160 $cm^2\,V^{-1}\,s^{-1}$ and f_T and f_{max} of 4.9 GHz and 10.6 GHz, respectively [61]. Furthermore, four GaAs based Schottky diodes and an MIM capacitor were fabricated with this technique and combined into a simple IC to form a full bridge rectifier that could rectify a 21 dBm input signal to an output power of 2.43 mW at 5.8 GHz, which is one of the most popular frequencies in wireless local area network, commonly used in high speed Wi-Fi systems [62]. This fabrication process therefore allows simultaneous (monolithic) integration of the active TFTs and passive PIN diodes along with other passive components on the same plastic substrate.

A similar dry transfer method, based on soft lithography, for the fabrication of well-organised arrays of printed silicon ribbons, i.e. microstructured silicon (μs-Si), on low-cost plastic substrates has been introduced by the group of Rogers [63]. They employed this technique to fabricate mechanically flexible single-crystal silicon MOSFETs on PI substrate, which showed $f_T = 515$ MHz at channel lengths of 2 μm [64]. Later, they optimised and extended this method to print GaAs nanowires (width $\sim$2 μm) on flexible PET substrates, which were then combined with Ohmic contacts to form high-speed MS field-effect transistors [65]. By varying the gate length, the authors demonstrated an f_T of 1.55 GHz for the shortest gate length of 2 μm, while simulation results showed that upon further decrease of the gate length, cut-off frequencies up to 3 GHz are achievable. One way to circumvent this is by employing S/D contacts self-aligned to the gate electrode to allow minimal parasitic capacitances and resistances. The group of Javey [66] demonstrated III–V MOSFETs with T-shaped gate electrodes, using the previously developed 'XOI platform' [67]. The devices comprised InAs microribbons with a width and spacing of $\sim$5 μm and a nominal thickness of $\sim$15 nm, which have shown a field-effect mobility of around 2300 $cm^2\,V^{-1}\,s^{-1}$. These structures were then employed in a self-aligned InAs XOI RF transistor (dual channel with $L = 75$ nm and $W = 50$ μm), transferred onto a highly resistive silicon substrate, and exhibited an f_T of $\sim$165.5 GHz (figure 9). The same devices fabricated on flexible PI substrate provided an f_T of 105 GHz, while at the same time showed excellent mechanical robustness with minimal performance change under various curvature radii down to 4.8 mm.

Given that patterning sub-1 μm features via conventional photolithography over large-area becomes cost prohibitive, other patterning techniques have been considered. To this end, nanoimprint lithography (NIL) appears to be a viable solution, since nanotrenches as short as 50 nm can be fabricated with this process [68]. Recently, Seo *et al* applied NIL patterned 100 nm channel lengths to form flexible SiNM-based RF transistors with 2 μm gate length, which were capable of attaining a record-breaking f_{max} of 38 GHz [69]. The robustness of these three-dimensional (3D) trench transistor structures was proven by bending them hundreds times under high-strain conditions, namely a convex radius of curvature of 28.5 mm, corresponding to an external strain of 0.55%.

The main drawback of the above mentioned methods—with the exception of NIL, which is compatible with roll-to-roll printing processes—is that they are rather complicated and time-consuming from a manufacturing point of view due to the amount and complexity of steps involved (e.g. lithographic patterning, ion implantation, dry etching, HF etching), which could be an issue for large-area/volume production. Therefore, while in principle high quality semiconductors can be made flexible in this way, their implementation in large volume passive RFID technology will not be low cost.

3.2. Silicon microparticles

An alternative route that takes advantage of the well-established high performance Si technology has been proposed from a

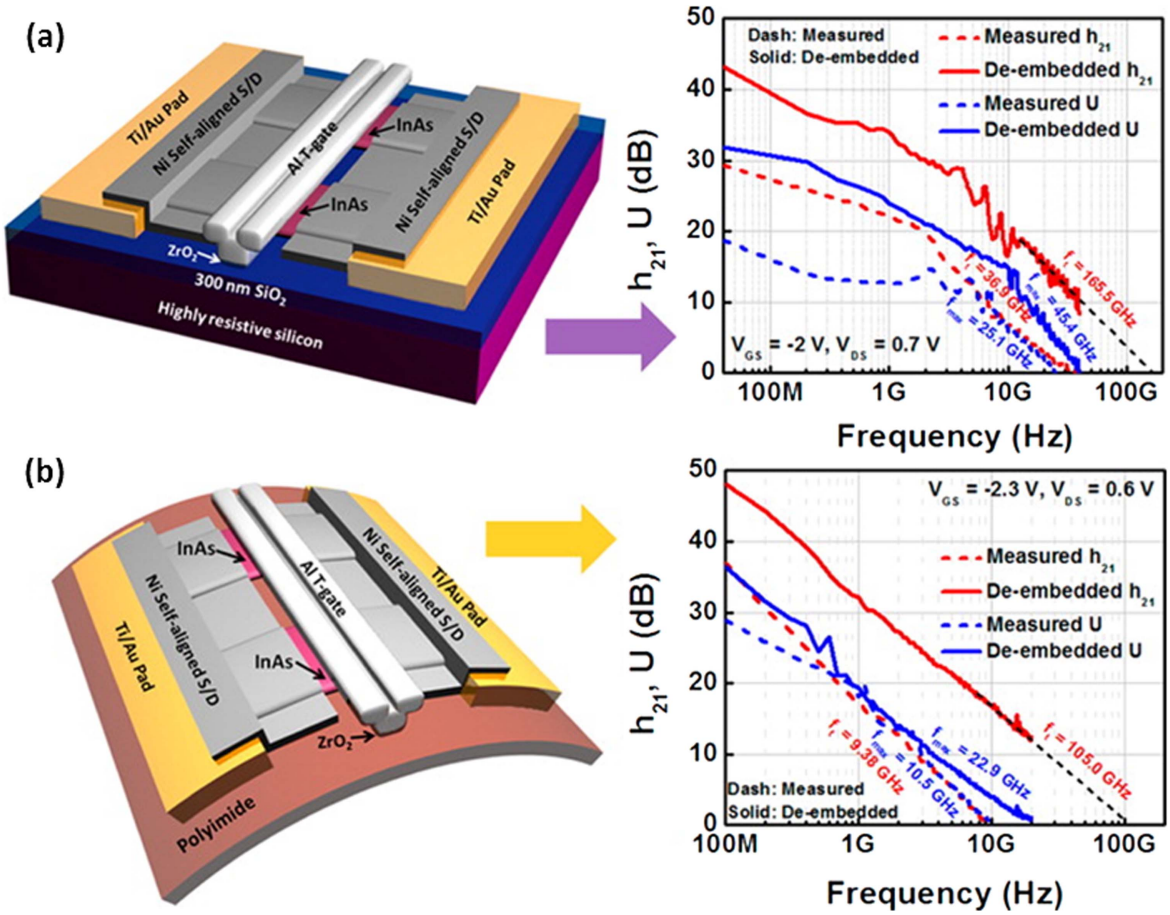

Figure 9. Schematic of self-aligned InAs XOI MOSFETs with an aluminium/ZrO_2 T-shaped gate stack, and self-aligned nickel S/D extensions on (a) rigid (Si) and (b) flexible (PI) substrates and as-measured (dash) and de-embedded (solid) current gain (h21) and Mason's unilateral gain (U) derived from the *S*-parameters from 40 MHz to 40 GHz and from 100 MHz to 20 GHz, respectively. Reprinted with permission from [66]. Copyright © 2012 American Chemical Society.

collaboration between research teams in Linköping University in Sweden and R&D departments in De La Rue, UK, and Acreo, Sweden Their approach involved the use of Si microparticles (Si μPs) embedded in a polymer binder to successfully demonstrate all-printed rectifying diodes operating at 1.6 GHz (figure 10) [35]. This diode was able to rectify the energy harvested from the antenna of a mobile phone, while making a call to power a printed electrochromic display. The best performing devices had the structure PET/Al (50 nm)/Si-in-SU8 (cross-linked, 4 μm)/$NbSi_2$-in-SU8 (4 μm)/carbon (6 μm)/Ag (3 μm), while the fully printed circuit on the PET substrate included an Al-foil antenna, the aforementioned diode and an electrochromic display based on polymer poly(3,4-ethylenedioxythiophene):polystyrene sulfonate (PEDOT:PSS). The Si μPs were formed by using ball milling to crash an n-doped Si wafer into particles in air. These were then implanted into the polymer binder (SU8) layer to ensure that the charge carriers will pass through only a couple of individual Si μPs to avoid losses in mobility due to electron scattering at the interfaces.

The same group recently demonstrated a simplification of this method using cellulose nanofibers (CNF) as the binder material to form PET/Al/CNF:Si-μPs/Ni:Carbon adhesive tape Schottky diodes, which operate up to 1.8 GHz [70]. Interestingly, the freestanding composite semiconducting film can be easily delaminated from the PET/Al substrate and transferred to any other substrate thus enabling reconfigurable GHz-operating flexible diode circuits.

4. Metal oxide semiconductors

4.1. Introduction

Wide bandgap metal oxides have been investigated as semiconductors since the demonstration of the first SnO_2 and In_2O_3 TFTs in 1964 (which were in fact proposed in a self-aligned gate TFT architecture for HF applications) [71], followed by the first ZnO TFT reported by Jacobs in 1968 [72]. The optoelectronic properties of metal oxides (particularly ZnO) and the potential for integration in flexible electronics led to a surge of research in the early 2000s. From a large-area industrial standpoint, however, these materials suffered from lack of uniformity, so they were unsuitable for wide scale adoption, the principle cause being the presence of grain boundaries. This changed rapidly with the first demonstration of amorphous indium gallium zinc oxide (a-IGZO) transparent TFT in 2004 [73]. Nomura *et al* demonstrated that, while

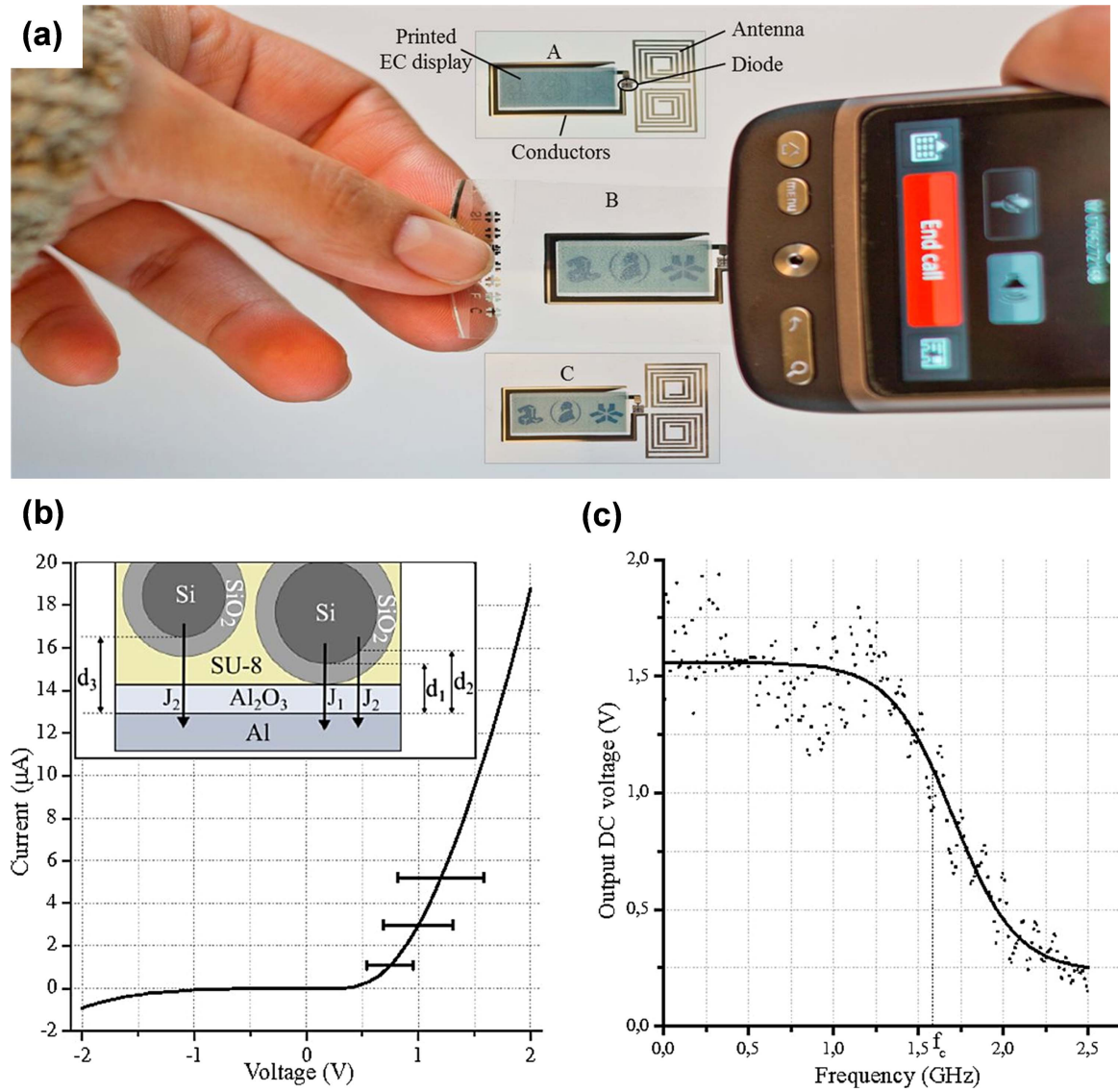

Figure 10. (a) Demonstration of e-label application: A. The antenna–diode–display circuit. B. The mobile phone is held close to the antenna, while making a call. The display starts to switch on. C. The display is switched on after 10 s. (b) The average *I–V* curve based upon 16 representative devices. The error bars show the SD and thus represent the voltage range needed to obtain a certain current level. Using a threshold of 3 μA, an average input voltage of 1 V is needed to switch the diode on. The Inset shows two different current mechanisms for different insulator thicknesses. (c) Frequency response of the device with an input power of 3 W. Adapted and reproduced with permission from [35]. Copyright © 2014 National Academy of Sciences.

materials such as ZnO and In_2O_3 tended to crystallise, IGZO could be made in an amorphous phase, while retaining the high charge carrier mobility, hence promising improved device-to-device uniformity. These TFTs were fabricated on flexible PET substrates and exhibited a Hall mobility exceeding 10 $cm^2\,V^{-1}\,s^{-1}$.

Since this initial work, interest in IGZO has soared, owing primarily to the drive for a replacement to amorphous silicon (a:Si) in flat panel display technology. The reduction in pixel size in liquid crystal displays called for TFTs with higher mobility, while the emergence of active matrix organic light emitting diode displays, which required more than one TFT per pixel, has further increased demand for higher mobility active layers [74]. IGZO exhibits a roughly tenfold increase in mobility over a:Si, the traditional transistor material of choice for display technology. While low temperature polysilicon exhibits even higher mobilities of up to 100 $cm^2\,V^{-1}\,s^{-1}$, IGZO is again the material of choice due to its higher level of uniformity, owing to its lack of grain boundaries and simpler manufacturing process. As a result of this, market forecasts put the amount of metal oxide backplanes in use by the display industry at 8 square kilometres by 2024 [75]. Despite its meteoric rise to industrial adoption, IGZO is still a relatively young material. As such, research is just now beginning to emerge on the HF performance of IGZO. Due to its high mobility, its processing compatibility

with flexible substrates and its current and predicted maturity, IGZO and related metal oxides are expected to be instrumental to HF flexible electronics.

4.2. Common processing routes of metal oxide-based rectifiers

The quality of metal oxide thin films depends on the thin film deposition method. Common vapour deposition techniques include physical vapour deposition [76], pulsed laser deposition [77, 78] and atomic layer deposition [79, 80]. Thermal evaporation has also been employed for some binary oxide thin films [81, 82]. Undoubtedly, the demonstration of large-area sputtered devices from the display industry has been key to the adoption of this method [83]. The potential of solution processed MOSs in the future should not be discounted. In fact, an effective solution-processing route might present the most cost effective option for metal oxides deposition on large-area thin flexible substrates.

4.2.1. Sputtering of metal oxide films. So far, the most investigated large-area deposition method for metal oxides has been sputtering [76]. Various metal oxides, including IGZO, have been deposited via sputtering and implemented in TFT rectifying circuits. For example indium zinc oxide (IZO) TFTs have been demonstrated with $f_T = 155$ MHz and $f_{max} = 180$ MHz [84]. In another instance, Wang *et al* [85] investigated the implementation of high-k dielectrics with ZnO TFTs for low voltage applications and fabricated a ZnO TFT with a Gd_2O_3 gate dielectric with values of $f_T = 180$ MHz and $f_{max} = 240$ MHz.

4.2.2. Solution-processing of metal oxides. The solution processing of MOSs is distinct from the other material classes presented in this paper in the sense that the goal is to chemically convert a precursor solution to a stable metal oxide thin film; such a process requires a significant amount of thermal energy, usually through thermal annealing processing steps [86]. Aside from precursor conversion, the residue of organic contaminants from precursor materials or solvents also calls for high temperature processing [87]. However, annealing at temperatures higher than 200 °C–300 °C is not compatible with most plastic substrates, except for high cost engineering plastics. Recently significant progress has been made towards realising low-temperature flexible-substrate-compatible metal oxide thin films.

Kim *et al* [88] have fabricated layers of In_2O_3, zinc tin oxide (ZTO), IZO and indium tin oxide (ITO) at temperatures as low as 200 °C using a self-energy-generating combustion chemistry technique. The process utilizes acetyl-acetonate as the fuel source and metal nitrates as oxidisers to generate an *in situ* exothermic reaction at localised higher temperatures than the substrate temperature. TFTs with an electron mobility of $\sim 6\ cm^2\ V^{-1}\ s^{-1}$ were demonstrated.

Even higher field-effect mobilities of $10\ cm^2\ V^{-1}\ s^{-1}$, reproducible and stable turn-on voltages $V_{on} \approx 0$ V and high operational stability TFTs based on IZO and IGZO amorphous metal oxide semiconducting thin-films were obtained via solution-processing route [89]. The materials were synthesised using a 'sol–gel on chip' hydrolysis approach from soluble metal alkoxide precursors in anhydrous conditions (low O_2 and H_2O levels) and then subjected to aqueous hydrolysis annealing at temperatures as low as 230 °C.

Kim *et al* [90] have shown that photochemical activation can be used instead of thermal annealing to form In_2O_3, IZO and IGZO thin films. Samples were exposed to deep ultraviolet radiation which had the added effect of heating the samples to ~150 °C. Semiconductor mobility, as measured from TFT analysis, compared favourably to reference samples annealed at this temperature. The authors demonstrated IGZO TFTs on parylene substrates with mean field effect mobilities centred at $3.77\ cm^2\ V^{-1}\ s^{-1}$ for 49 measured devices. Ring oscillators from these TFTs exhibited maximum oscillation frequencies of ~340 kHz, indicating some promise for the optimised HF application of the material.

Lin *et al* [91] reported a carbon-free ZnO hydrate precursor route towards the fabrication of ZnO thin films with mobilities in the range 4–5 $cm^2\ V^{-1}\ s^{-1}$ on PEN substrates operating at voltages lower than 1.5 V. Such a value of mobility from the processing of the polycrystalline ZnO active layer at 160 °C is highly encouraging. A further promise of this approach may be the ability to combine layers of thin metal oxide films to realise oxide heterointerfaces that are able to sustain quasi-2D electron gas, thus further suppressing scattering (primarily due to impurities) and increasing device mobility. The same group combined less than 10 nm thick layers of In_2O_3, Ga_2O_3 and ZnO, and found evidence for quantisation of electrons in a quasi-2D electron gas [92]. As a result, mean values of mobility of $11\ cm^2\ V^{-1}\ s^{-1}$ were measured for metal oxide heterojunction TFTs on PEN substrates, which were fabricated at 175 °C, and mobilities greater than $40\ cm^2\ V^{-1}\ s^{-1}$ were measured when devices were fabricated at 200 °C on glass substrates.

4.3. Solution-processed ZnO diodes and rectifiers

Recently, the Anthopoulos group employed the aforementioned low temperature ZnO solution processing route to fabricate Schottky diodes on PEN substrates [93, 94] (figure 11). The devices were formed in a uniquely lateral nano-gap architecture with electrode spacing on the order of 10 nm utilising the process of adhesion lithography (a-Lith) [95]. The nanoscale spacing of the electrodes leads to low values of device series resistance, while the lateral architecture leads to a sub-picofarad value of junction capacitance. Furthermore, the structure afforded by the technique of a-Lith effectively negates unwanted scattering from ZnO grain boundaries, thus maximising device performance and device-to-device uniformity. As a result of this, no drop in the DC output of the devices up to the measurement limit of 20 MHz was observed when measured in a half wave rectifier setup. Output voltages of up to 1.2 V for a ±4 V AC input were observed.

In another instance, ZnO based semiconducting ink was used to form a hybrid ZnO paste for the active layer of the diode that was part of a 13.56 MHz rectenna circuit,

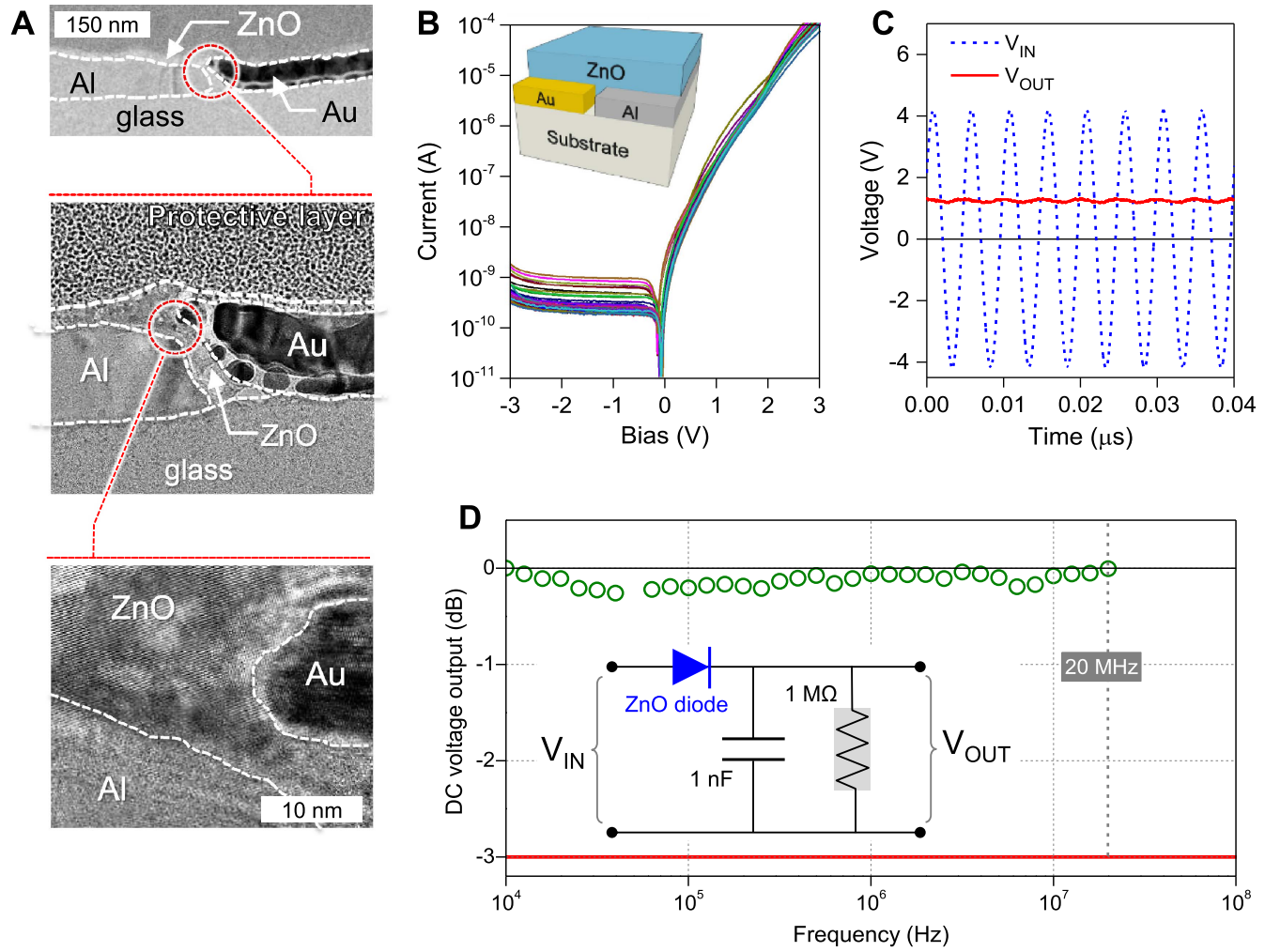

Figure 11. (a) High resolution transmission electron microscope (HR-TEM) images of the cross-section of a ZnO coplanar nano-Schottky diode. Dashed lines indicating the different materials/layers are added for clarity. The high-magnification TEM image of the ZnO region located between the metal electrodes reveals the nanocrystalline nature of the ZnO layer. The image shows nanocrystalline domains up to 5 nm in diameter. (b) Quasi-static *I–V* characteristics of 38 ZnO coplanar nano-Schottky diodes fabricated on the same substrate. (c) AC input and DC output signals of a ZnO diode-based rectifier circuit operating at 13.56 MHz. (d) Bode plot of the DC output signal versus AC input signal frequency up to 20 MHz (measurement limit). Inset in (d) shows the circuitry of the DC rectifier circuit used. Reproduced from [93].

comprising also an antenna and a capacitor, all of which were gravure printed on PET foil [96]. The single diode circuit outputted a $V_{DC} = 4$–4.5 V for a ± 5 V AC input at 13.56 MHz, corresponding to half-wave rectifier efficiency of 90%. When three diodes and three capacitors were printed on the same substrate, the gravure printed rectenna could supply more than 20 V DC to the load circuit and provide at least 0.3 W power from a standard 13.56 MHz RFID reader held at a distance of 2 cm. This diode was later integrated into a fully roll-to-roll gravure printed wireless (13.56 MHz) sensor-signage tag for smart packaging applications, comprising the wireless power transmission device, namely the rectenna (antenna, diode and capacitor), a humidity sensor and an electrochromic signage unit all printed on a PET film [97].

4.4. IGZO-based rectifiers

As mentioned above, the majority of reports on the HF performance of rectifiers based on MOSs concern IGZO. All IGZO films were deposited via sputtering, unless stated otherwise. RF rectifiers operating at the most relevant—from a commercial point of view—frequency bands, i.e. 13.56 MHz (HF), 868 MHz (UHF) and 2.45 GHz (microwave), will be summarised next.

4.4.1. Integration in the 13.56 MHz band. The performance of IGZO in the HF band (13.56 MHz) has been well documented. Partly due to this, and partly due to the maturity of IGZO device processing techniques stemming from its wide utilisation at the display industry, much effort has been focused on device integration, optimisation and flexible performance. At this moment, it seems certain that IGZO will play some part in short-term emerging HF flexible electronics and the only question is to what extent.

There are few reports of IGZO-based diodes operating solely in the HF regime, while much of the work on rectifiers in the HF band has been carried out using TFTs rather than

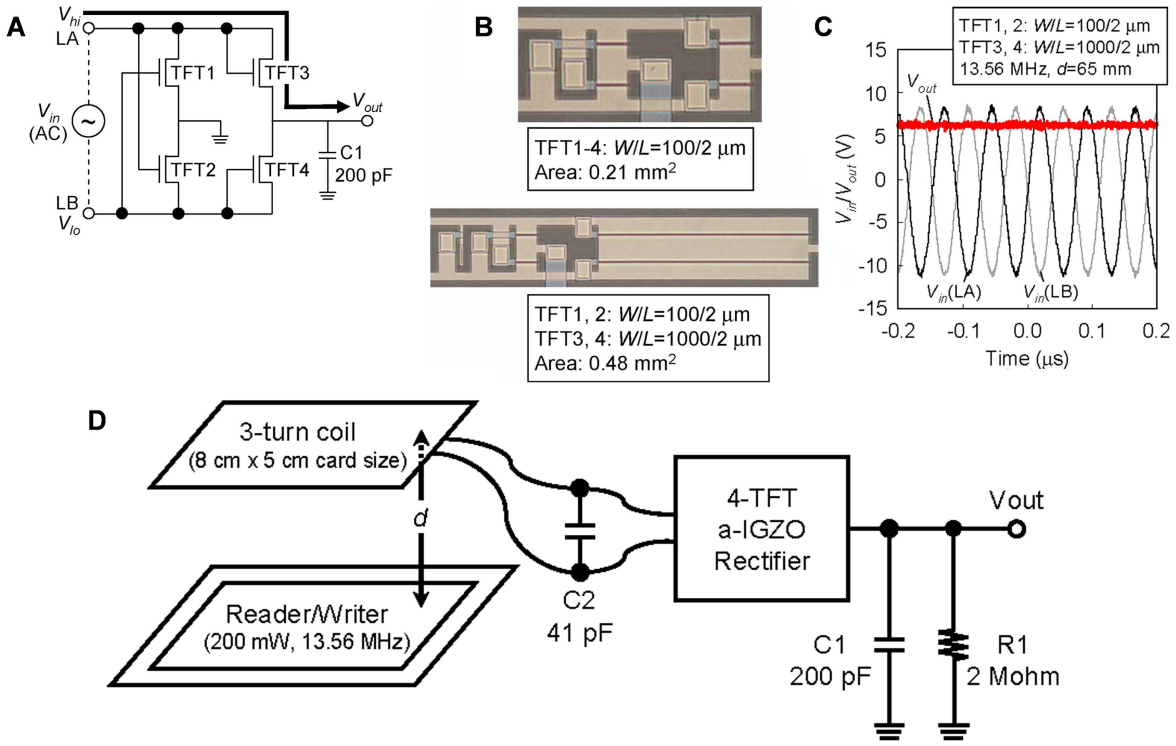

Figure 12. (a) Schematic view of 4-TFT bridge rectifier. TFTs 1 and 2 act as switches, TFTs 3 and 4 act as diodes, and *C*1 acts as voltage smoothing element. The arrow indicates current path when higher voltage (V_{hi}) is inputted into LA and lower voltage (V_{lo}) into LB. (b) Top view of fabricated 4-TFT IGZO rectifiers. (c) Measured full-wave rectifying characteristics of 4-TFT IGZO rectifier. (d) Experimental setup for measuring wireless voltage rectification. 4-TFT IGZO rectifier was connected to resonance capacitor (*C*2), 3-turn coil, smoothing capacitor (*C*1), and load resistance (*R*1; represents subsequent circuits). Reprinted, with permission, from [100]. Copyright © 2010 IEEE.

diodes. One example of HF IGZO diodes was demonstrated by Chen *et al* [98] who fabricated IGZO/p-Cu_2O heterojunction diodes on PEN substrates and attained current densities of 1 A cm^{-2} at +1 V DC with a cut-off frequency of 27 MHz. It is noteworthy that IGZO diodes have also been implemented in the UHF regime, however. More attention shall be given to UHF IGZO diodes in the next section.

A key to the implementation of TFTs as rectifiers is obtaining a low operating voltage. This can be done by fabricating TFTs with a small subthreshold slope, which can be achieved by employing fully depleted channels. In this case, the charge carrier density in the channel must be lower than the maximum amount of gate-controllable charge, and the channel thickness must be smaller than the maximum depletion layer width [99]. Kawamura *et al* [100] achieved this by employing a thin 20 nm IGZO active layer via RF magnetron sputtering in a bottom-gate/top-contact architecture (figure 12). The low subthreshold slope of 160 mV dec^{-1} enabled low-voltage operation. With these devices they built a double half wave rectifier based on two diode-connected TFTs and two TFTs acting as switches. The result was a rectifier outputting a 12 V DC signal at 13.56 MHz for a ±9 V input AC signal.

From a large-scale processing standpoint, it can be advantageous to use the same active material in the rectifier that will be employed in the logic circuit of the device. Complementary logic is most often preferred to unipolar logic due to the lower power consumption of the former. One of the main drawbacks when employing IGZO is the lack of p-type oxide semiconductors available for integration into complementary logic. Addressing this point, Ozaki *et al* [101] showed that logic power consumption could be reduced by a factor of 10 000 by designing active load logic as opposed to saturated load logic, and thus demonstrated the first functioning IGZO IC powered wirelessly at 13.56 MHz. The IC consisted of a reset circuit, a clock circuit consisting of a II-stage ring oscillator, a 4 bit read-only-memory, a memory driver and an encoder. The power consumption was as low as 20 μW and operation was observed for an input AC power of 40 mW from a commercial RF coil antenna at a read distance of 70 mm.

Tripathi *et al* [102] built an 8 bit code generator operating at low power (1.5–2 V) by using thin (100 nm) Al_2O_3 as the gate dielectric in the 300 IGZO TFTs which made up the circuit. The low temperature processing enabled the code generator to be fabricated on flexible PEN, and with it the first IGZO TFT rectifier on a flexible substrate. The transdiode TFT output a DC voltage of 4 V for an AC input of ±5 V_{pp}, substantial enough to drive the associated code generator. Later, Myny *et al* [103] reported a double half wave rectifier employed in a near field communication tag, consisting of a load modulator and code generator on PEN. The power consumption of the IGZO logic here is addressed via the fabrication of dual-gate TFTs, which enable more control

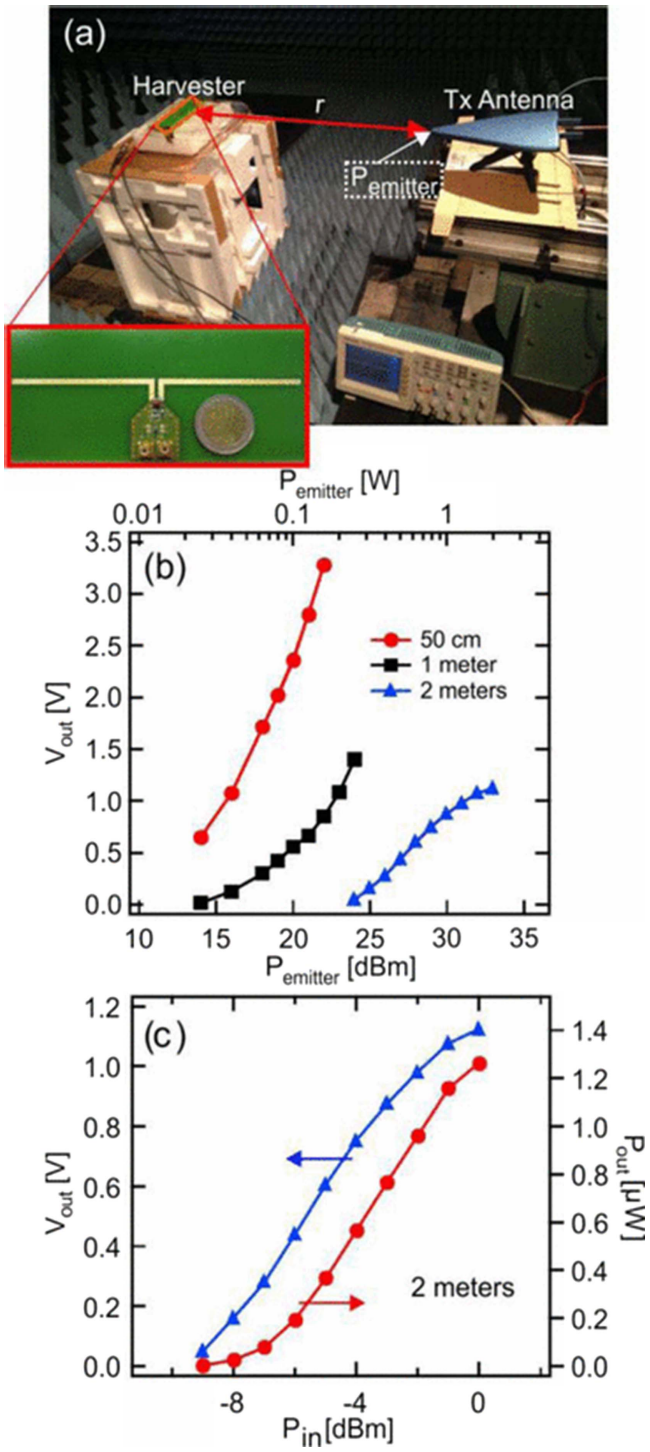

Figure 13. (a) Photograph of the measurement setup. The harvester was measured in an anechoic chamber to avoid standing waves. A directional antenna Tx with a gain of 4 dBi simulated the tag reader and a digital oscilloscope was used to read the resulting DC output voltage. (b) Measured rectified voltage V_{OUT} as a function of the emitted power by the antenna Tx at different distances r from the power emitter. (c) Measured DC output voltage and power as a function of the harvested power P_{in} at $r = 2$ m. All the measurements were performed at $f = 868$ MHz. Reprinted, with permission, from [41]. Copyright © 2014 IEEE.

over the threshold voltage of the TFTs [104]. Further reports by the same group of rectifier and logic circuit based IGZO TFTs on flexible PEN substrates indicate that the devices are stable under flexing, with operation down to a bending radius of 2 mm and a strain of up to 0.8% [105].

From the application point of view, a further advantage of IGZO is that its wide bandgap leads to optical transparency. Given that other transparent metal oxide materials can serve as conductors (e.g. ITO) and insulators (e.g. Al_2O_3), all these compatible materials may be combined to fabricate transparent TFTs. To this end, Cho *et al* [106] fabricated a transparent antenna based on ITO and coupled an AC signal to a transparent ring oscillator via both half wave and full wave IGZO TFT rectifiers. Yang *et al* [107] used a similar TFT fabrication approach and took it a step further by demonstrating a transparent logic circuit coupled to a half wave IGZO TFT rectifier and ITO antenna.

4.4.2. Towards UHF IGZO-based rectifier applications. While IGZO has been demonstrated to be compatible with RFID technology in the 13.56 MHz range, its frequency response is by no means limited to this regime. Munzenrieder *et al* [108] fabricated a self-aligned gate TFT on polyimide (PI), which exhibited an extrinsic value of $f_T = 135$ MHz, as measured via *S*-parameter analysis, and the device performance was maintained up to a tensile bending radius of 3.5 mm. Su *et al* [109] made efforts to maximise current densities from IGZO TFTs on glass by employing thin bi-layer Al_2O_3/SiO_2 gate dielectrics on glass substrates. The result was a device with current density of 22.5 mA mm^{-1} and values of f_T and f_{max} of 384 MHz and 1.06 GHz, respectively.

Further strides towards the realisation of higher frequency IGZO devices have been made through the use of rectifier diodes. As would be expected, Schottky diodes based on IGZO alone have a significantly improved frequency performance as compared to TFTs. Chasin *et al* [110, 111] have demonstrated an IGZO diode on glass with high current densities of 800 A cm^{-2} at +1 V and cut-off frequencies measured via *S*-parameters of 1.8 GHz. Single stage rectifiers based on these diodes showed cut-off frequencies of 1.1 GHz. Optimisation of the contacts was found to be critical in this work, the authors noting the importance of an oxidation step on the Schottky Pd contact, as well as noting that the Ohmic Mo contact was capable of doping the IGZO active layer, so that layer thickness must be monitored [112]. Minimisation of device area also proved important. Building on this work, the same group fabricated a double half wave rectifier on glass capable of delivering 1 V DC at a distance of 2 m from a transmitter antenna at the UHF band 868 MHz [41] (figure 13).

Recently, Zhang *et al* [113] fabricated flexible IGZO Schottky diodes on PET substrates (figure 14). The devices employed Pt as a Schottky contact and Al as the Ohmic contact. Despite current densities of 20 A cm^{-2} at +1 V being

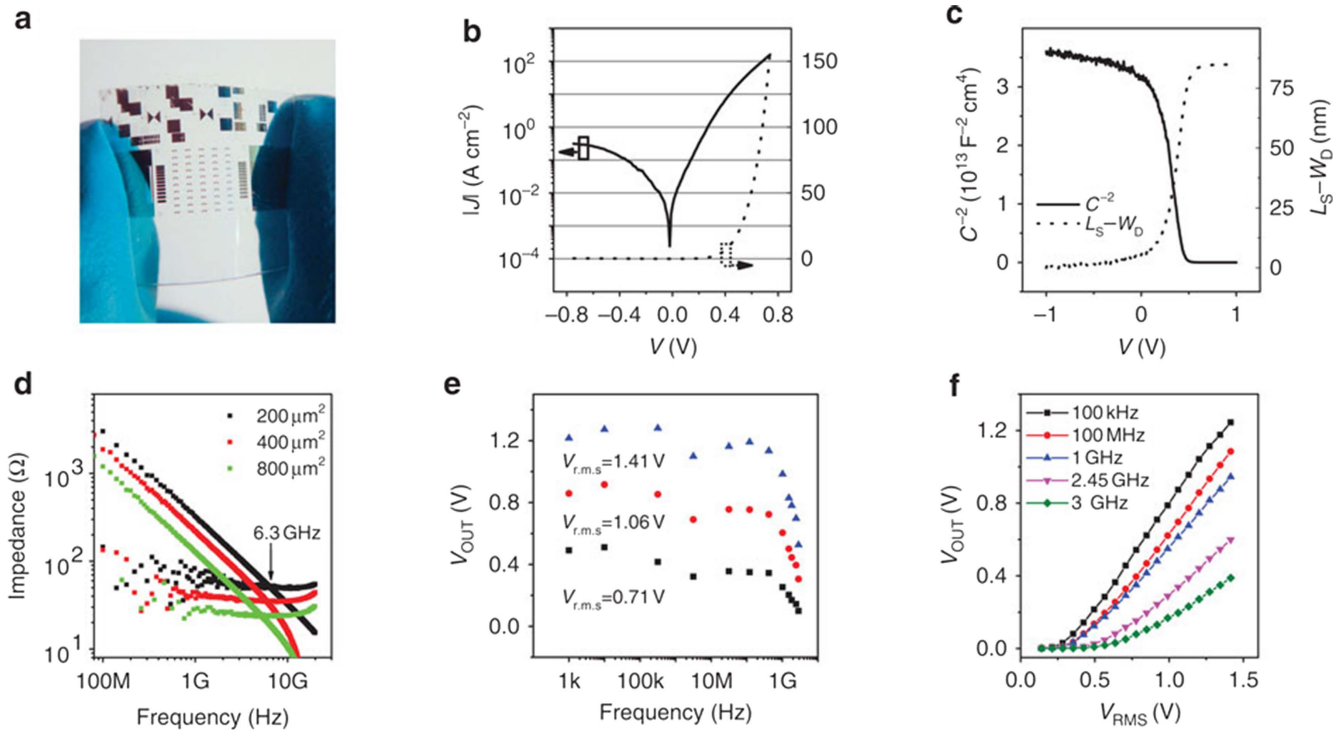

Figure 14. (a) Photograph of flexible IGZO Schottky diodes. (b) *J–V* characteristics of the flexible diode with an 80 nm IGZO layer. (c) Capacitance and depletion width of the diode at different DC voltages. (d) Impedance of the flexible IGZO Schottky diodes as a function of frequency. (e) Output DC voltage as a function of the input signal frequency at different input signal strengths. (f) Output DC voltage as a function of the input RF signal rms voltage at different frequencies. Reprinted by permission from Macmillan Publishers Ltd: Nature Communications [113]. Copyright © 2015.

lower than those demonstrated by Chasin *et al* intrinsic cut-off frequencies of 6.5 GHz were measured, and a rectifier output of 0.6 V for a ±2 V AC input at 2.45 GHz was reported. This exceptional performance was obtained through careful optimisation of IGZO layer thicknesses and oxygen/argon ratios during the sputtering deposition process. The performance characteristics of the above mentioned metal oxide rectifiers are summarised in table 2.

5. Organic materials

Organic semiconducting materials can be generally classified into three main categories [114]: molecular glasses (amorphous small molecules), molecular crystals (single-crystalline or polycrystalline), and polymeric semiconductors. Each of these material classes exhibits advantageous mechanical properties when compared to traditional semiconductor materials, as they can be made bendable, stretchable, lightweight and robust at the same time. Additionally, they can be grown from solutions at low processing temperatures enabling fabrication via high-throughput, low-temperature well-established printing techniques to realise flexible electronics at potentially very low cost.

The semiconducting properties of organic materials stems from the existence of conjugated bonds (alternating single and double bonds) between carbon atoms, which result in the delocalisation of electronic charge across the conjugated part of the molecule [115, 116]. Electronic interactions between the molecular orbitals of neighbouring sites are also weak, so charge transport usually occurs through hopping of electrons rather than band transport, which is responsible for the high mobilities observed in inorganic semiconductor crystals [117].

From the above it can be deduced that to achieve high mobility in organic films (and hence HF operation), a high degree of crystallinity and precise control over the microstructure, molecular packing and chain alignment is desirable [118]. The use of a single crystal of organic material provides near-perfect order over its entirety, which can be cm in size. For example, high-purity acene, i.e. fused polycyclic hydrocarbons, single crystals have been established as exemplary materials for organic TFT devices owing to their intrinsic electronic properties [119]. Finally, recent research efforts have been devoted to relate morphology and microstructure to charge transport in polymeric semiconductors [120], which are extremely attractive due to their ease of processing in large-area substrates, and printed ICs based on uni-or ambipolar polymer semiconductors have been demonstrated [121].

As the properties of organic materials, including chemical structure, molecular weight, electronic bandgap, wetting properties of resulting formulations, and the structural properties of formed solid layers can be easily tuned through chemical synthesis, this material class is highly versatile. Owing to these reasons there has been a great deal of research

Table 2. Summary of the performance characteristics of metal oxide-based rectifiers.

TFT performance						
Material	Device type	Substrate	f_T (MHz)	f_{max} (MHz)	Year	Reference
IZO	TFT	glass	155	180	2008	[84]
ZnO	Gd_2O_3/Au gate TFT	glass	180	240	2009	[85]
	Pr_2O_3/Au gate TFT	glass	95	125		
IGZO	Self-aligned gate TFT	PI	135	—	2013	[108]
	TFT	glass	384	1060	2015	[109]
Rectifier Performance @ 13.56 MHz (HF)						
Material	Device type	Substrate	AC input (V)	DC output (V) (load)	Year	Reference
IGZO	4-TFT bridge rectifier	glass	±18	12 (2 MΩ)	2010	[100]
ZnO ink	Schottky diode Ag/ZnO/Al *gravure printed*	PET	±5	4.5 (1 MΩ)	2012	[96]
ZnO	Schottky diode Au/ZnO/Al *solution processed*	PEN	±4	1.2 (1 MΩ)	2016	[93]
IGZO/Cu_2O	heterojunction diodes ITO/IGZO/Cu_2O /Pt	PEN	±4	3 (1 MΩ)	2014	[98]
Rectifier Performance @ ⩾800 MHz (UHF)						
IGZO	Schottky diode Pd/IGZO/Mo	glass	±3	0.37	2012	[110]
			±5 (800 MHz)	1.26 (1 MΩ)		
	Schottky diode Pd/IGZO/Al	glass	±2	0.6	2013	[111]
			±3 (868 MHz)	1.3 (10 kΩ)		
			±1 (1.5 GHz)	0.56 (1 MΩ)	2014	[41]
	Schottky diode Pt/IGZO/Al	PET	±1.41 (2.45 GHz)	0.6 (1 MΩ)	2015	[113]

conducted in the field of organic semiconductors for use in optoelectronics, logic circuitry and HF electronics.

5.1. TFT geometric considerations

Due to the low carrier mobility, intrinsic to many organic materials, several attempts have been made to optimise TFT performance through altering the device design.

5.1.1. Reducing the overlap of gate with S/D electrodes. Parasitic capacitance can be greatly reduced in TFTs if the gate to S/D overlap, i.e. the contact length ($L_C = L_{gs} + L_{gd}$), is minimised. Zaki *et al* [122] investigated the effect of varying the overlap of the S/D electrodes with the gate electrode via *S*-parameter analysis (figure 15). The authors were able to achieve good alignment using silicon stencil masks and fabricated TFTs with a dinaphtho[2,3-b:2′,3′-f] thieno[3,2-b]thiophene (DNTT) active layer. Here, the authors note that the impact of gate/source capacitance and gate/drain capacitance are not symmetric (see figure 15). Through modelling and experiment they demonstrated a doubling of the device's f_T from 2 to 4 MHz upon varying the source-gate electrode overlap, while keeping the total S/D-gate overlap constant. They also showed that this stencil lithography process is compatible with flexible 125 μm thick PEN substrates by fabricating 1 μm channel length TFTs with small electrode overlap based on a similar small molecule 2,9-didecyl-dinaphtho [2,3-b:2′,3′-f]thieno[3,2-b]thiophene (C_{10}-DNTT) [123]. The TFTs were used to fabricate ring oscillators, which showed >1 MHz operation at low voltage (2–3 V) thanks to the low device dimensions and the high mobility of the semiconductor employed (1.2 $cm^2 V^{-1} s^{-1}$).

5.1.2. Self-aligned gate TFTs. Obviously, the complete elimination of any overlap of electrodes would be ideal for parasitic capacitance minimisation. To this end, a self-aligned gate architecture is highly advantageous. This process usually relies on exposure of a photoresist through the back of a substrate, with the use of one pre-patterned electrode to pattern the other. Promisingly, Uemura *et al* [124] demonstrated vacuum processed TFTs operating at 20 MHz and solution processed devices operating at 10 MHz using DNTT as the active layer. A dual-gate architecture was employed to reduce the S/D contact resistance. This type of architecture rules out the device being operated as a passive

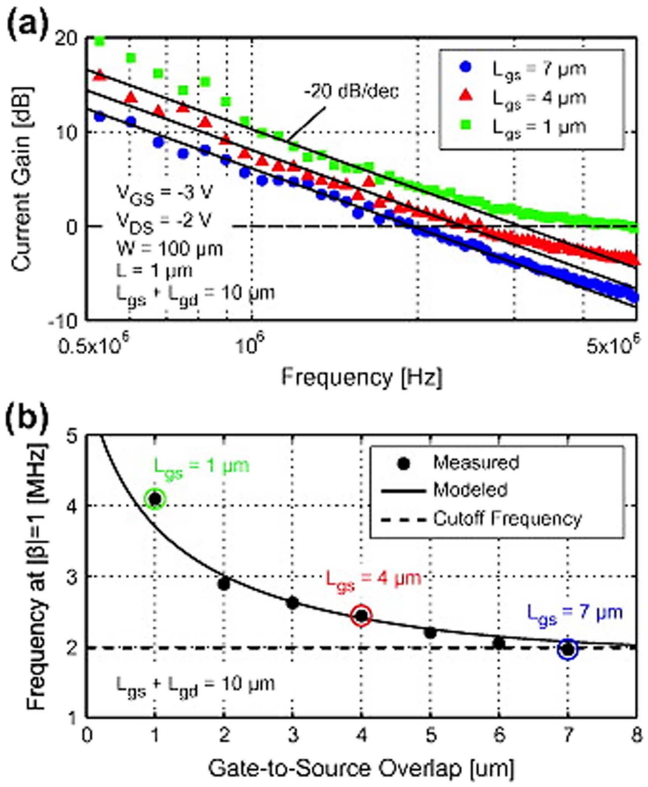

Figure 15. (a) Measured *S*-parameters for asymmetrical organic TFTs with $W = 100\ \mu$m, $L = 1\ \mu$m and $L_{gs} + L_{gd} = 10\ \mu$m. The -20 dB decade^{-1} slopes level off at lower frequencies for OTFTs with smaller L_{gs}. (b) Extracted unity-gain cut-off frequency for all OTFTs with $L_{gs} = 1$–$7\ \mu$m and $L_{gs} + L_{gd} = 10\ \mu$m. The dotted line represents as a reference the simulated prevalent FET-based cut-off frequency $f_T = g_m/(2\pi(C_{gs} + C_{gd}))$, while the solid line represents a modelling approach based on the asymmetric effect of L_{gs} and L_{gd} on TFTs proposed by the authors. Reprinted from [122]. Copyright © (2013), with permission from Elsevier.

component, since gate voltage is needed to achieve optimal device performance. Employing NIL with a self-aligned process allows for the fabrication of short channel lengths with minimised L_C. This route is also promising as it eliminates costly photolithography steps. Vacuum processed small molecule TFTs have been demonstrated employing NIL on flexible substrates. However, the frequency operation of these devices remains below 1 MHz [125, 126].

5.1.3. Ideal contact length determination. While beneficial in the reduction of capacitance, a complete reduction in the contact length to zero can be detrimental to carrier injection. Ante *et al* [127] examined the relationship between contact length, contact resistance, and effective mobility in aggressively scaled staggered organic TFTs. Considering DNTT-based TFTs with varying channel lengths and widths, the authors concluded that by reducing the contact length below the transfer length, i.e. the length where 63% of the charge carrier exchange between the contacts and the semiconductor occurs (which is found to be 10 μm in this specific case), causes the contact resistance to increase considerably, and thus the effective mobility is reduced. As a result of simulations, the authors found a peak in transit frequencies of the devices when the contact length equalled the transfer length, with predicted values of f_T in the low MHz regime for these devices. This conflicts with the simple interpretation of transit frequency presented in section 2.2.1. As a solution, the authors suggest decreasing the transfer length. This could be achieved by means of area selective contact doping. Xu *et al* [128] present an analytical model to determine the ideal contact length for a generic organic semiconductor. By considering the inner Joule heating within the semiconductor they have found that the contact length should be roughly 6 times the organic semiconductor thickness (t) for contact resistance minimisation and hence device optimisation. When channel lengths are significantly reduced (i.e. L approaching t), short channel effects become non-negligible and thus a larger contact length is required.

5.1.4. Vertical 3D transistors. Alternative device structures to conventional self-aligned TFTs have been proposed for frequency optimisation of organic devices. Uno *et al* [129] proposed a vertical 3D transistor based on DNTT and fabricated on PEN. The vertical channel enabled the implementation of a short channel length of 1 μm and was gated from the side using a multicolumnar epoxy supporting structure fabricated via photolithography (the authors showed later that this step could be carried out using NIL) [130]. This architecture allowed top contacting of the active material with one electrode, which had a strong effect on minimising the device contact resistance, and which the authors note is difficult to achieve for short channel lengths when using planar structures with organics. Thanks to these advantages, devices with high current densities of 2.6 A cm^{-2} and small subthreshold swings of 1.6 V decade^{-1} were realised, despite the low mobility of 0.2 cm^2 V^{-1} s^{-1}. The frequency performance of the device was analysed by pulsing the gate voltage for a constant drain voltage and observing a rise in drain current to 70% of its full value in 250 ns, corresponding to a frequency of 4 MHz. The authors later improved the frequency performance of the DNTT vertical TFTs by patterning the gate on the side wall only, so as to minimise the contact length and reduce the channel length to 800 nm [131]. The former had the effect of reducing the capacitance five-fold, to a value of 6 pF. When operated in transdiode mode, the TFTs exhibited a promising cut-off frequency of 20 MHz.

5.2. Organic small-molecule materials for RF diodes

Pentacene is a simple polyacene analogue which has been tested extensively in the field of organic electronics, and was recognised early on as a candidate for high performance devices owing to its high hole mobility (>1 cm^2 V^{-1} s^{-1}), its extended π-system with strong intermolecular overlaps and its low-lying highest occupied molecular orbital (HOMO) level (-5.1 eV), which is suitable for injection of holes from air-stable metal electrodes such as Au [132–134]. As a result of its satisfactory mobility and extensive use, many demonstrations of HF performance of pentacene devices have been made. Additionally, C_{60} buckminsterfullerene has been employed in HF studies, since—similarly to pentacene—it is a relatively high mobility small molecule, which has also been extensively

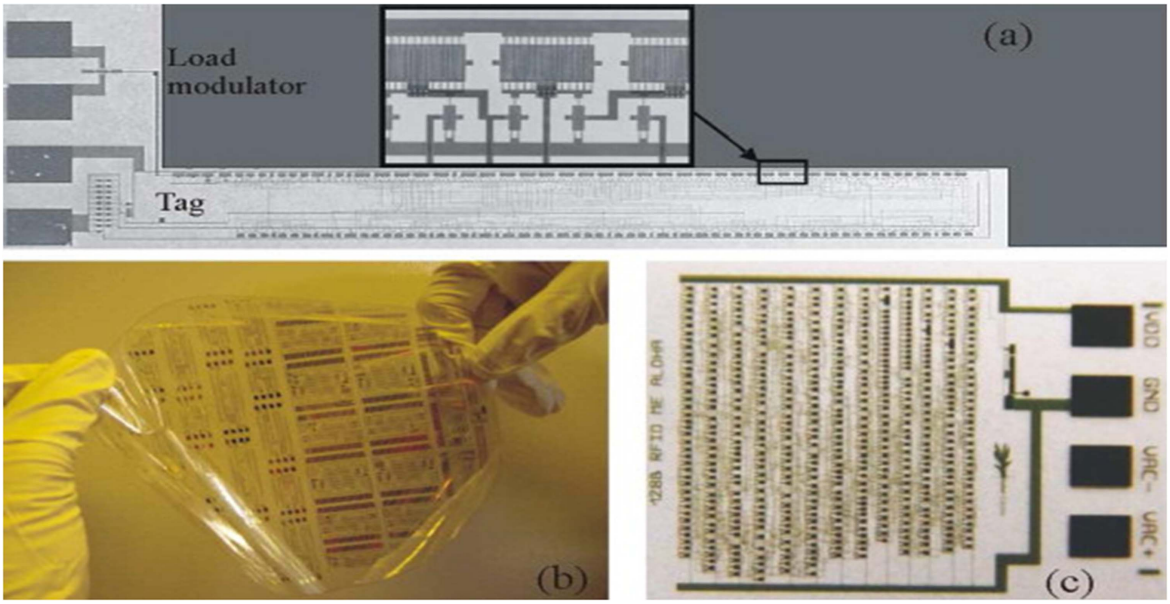

Figure 16. Pictures of (a) the 64 bit transponder foil, (b) the 6″ wafer comprising the transponder chips and (c) the 'generation 2' 128 bit transponder foil whereby the functional area is about 1 cm^2. Reprinted from [147]. Copyright © (2009), with permission from Elsevier.

studied [135, 136]. The use of fullerenes and their derivatives as acceptors in organic photovoltaics, as well as their n-type charge transport, which is not prevalent in many small molecule semiconductors, has led to their wide scale study [137].

5.2.1. Pentacene: the benchmark material for organic Schottky diodes. The first results on pentacene-based ICs powered by near-field coupling at radio frequencies of 125 kHz and over 6 MHz were reported back in 2003 by Baud *et al* [138], where adequate modulation of the RF signal was demonstrated so as to enable external detection of the clock signal generated by the pentacene-based ring oscillators. However, these circuits operated without a diode or AC/DC rectifier stage. Using a similar pentacene TFT technology Marien *et al* [139] designed Dickson voltage triplers based on TFTs in transdiode mode, with an efficiency of 48%, and capable of driving a 9-stage ring oscillator at a clock frequency of 9 kHz.

While these results are promising, it has been the integration of pentacene with Schottky diodes that has led to the greatest advancements in frequency performance. In 2005, Steudel *et al* [140] reported a pentacene diode with a cut-off frequency of 50 MHz while operated in a single half wave rectifier. The pentacene layer used was 160 nm thick and the incorporation of a poly(3,4)ethylenedioxythiophene: polystyrene sulfonate (PEDOT:PSS) layer between the pentacene and the Au Ohmic contact allowed current densities of 2100 A cm^{-2} to be reached. At 14 MHz, the diode output an 11 V DC signal over a 50 kΩ resistor from a ±18 V AC input. While these operating voltages may seem high, the authors noted at the time that at least 10 V would be necessary to drive a circuit made out of organic TFTs. Based on the high voltage operation of the device, the authors note that a small signal analysis of the cut-off frequency, such as taking the inverse of the transit time ($f_{max} = \frac{1}{t_\tau} = \left(\frac{\mu(V_A - V_{DC}}{L^2}\right)$, where V_A is the applied voltage and V_{DC} is the output voltage) is no longer valid. Rather, a dependence based on the speed with which the charges consumed by the load resistance (R_L) at a DC voltage (V_{DC}) during one frequency cycle (ω) can be recharged onto the load capacitance (C_L) by the current going through the organic diode during the fraction of the cycle in which the diode is in forward bias should be considered:

$$f_{max} = \frac{9\mu}{16\pi L^2 V_{dc}}\left[(-3V_{dc} + V_F)\sqrt{V_A^2 - (V_{dc} + V_F)^2} + (V_A^2 + 2V_{dc}^2)\arccos\left(\frac{V_{dc} + V_F}{V_A}\right)\right], \quad (14)$$

where V_F is the transition voltage of the diode, the voltage at which the diode goes from Ohmic conduction to space charge limited conduction. The authors take a similar approach to calculate the maximum frequency operation of a diode-connected TFT [141]:

$$f_{max} = \frac{\mu}{4\pi L(L + L_C)V_{dc}}\left[-V_A\sqrt{1 - \frac{V_{dc}^2}{V_A^2}}(3V_{dc} + 4V_T) + (V_A^2 + 2(V_{dc} + V_T)\arccos\left(\frac{V_{dc}}{V_A}\right)\right]. \quad (15)$$

Based on this analysis they predicted that frequency operation at 13.56 MHz with a transdiode TFT is possible when semiconductors such as pentacene with a measured mobility of 0.15 $cm^2\,V^{-1}\,s^{-1}$ are employed. The model also showed that the maximum frequency attainable in a diode is up to two orders of magnitude greater than for a transdiode TFT. The authors later showed that pentacene Schottky diodes were capable of operating in the UHF regime, by demonstrating integrated half wave rectifiers on PEN foil operating with a 4.5 V DC output for a ±15 V AC input signal at 869 MHz [142]. More recently, a pentacene Schottky diode operating above 1 GHz has been demonstrated and will be discussed in the next section [143].

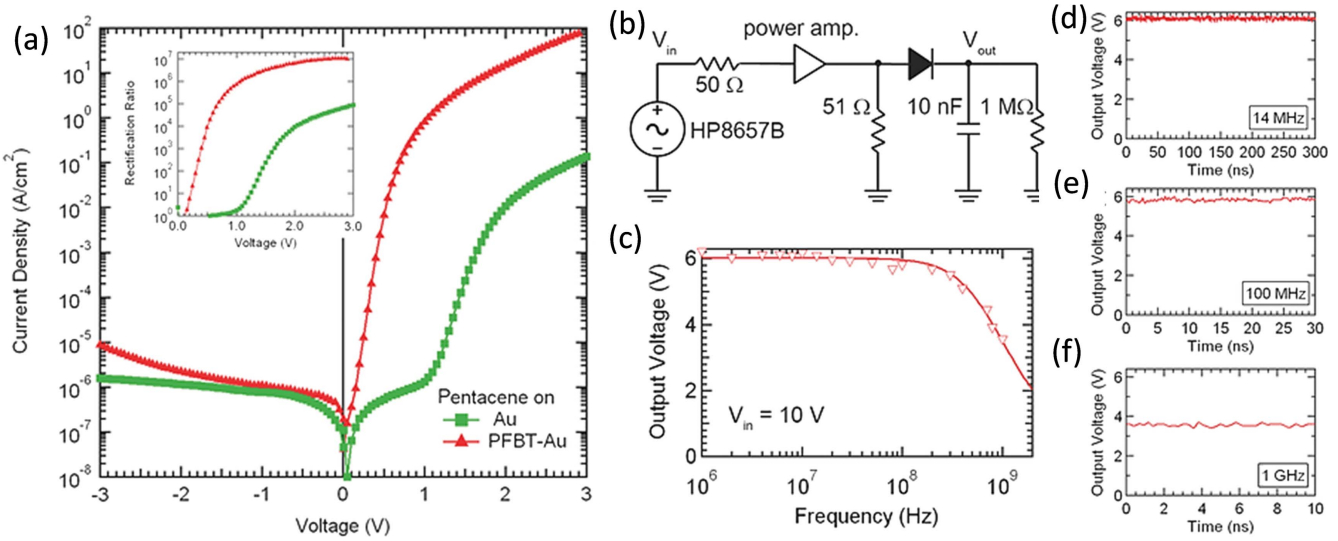

Figure 17. (a) DC current density–voltage characteristics for pentacene diodes both with (filled triangles) and without (filled squares) a PFBT SAM coating on the Au anode. The pentacene films were thermally evaporated with a relatively high deposition rate (3–4 Å s^{-1}) in order to prevent shunts. These diodes had an active area, defined by the overlap of Au and Al electrodes, of 6400 μm^2. The inset shows the corresponding diode rectification ratios. (b) Equivalent circuit for the rectifier frequency dependence measurement system employed in this work. (c) Frequency characteristics for a PFBT-coated Au anode pentacene diode rectifier with a 10 V peak-to-peak sinusoidal input voltage. The time-dependent output voltages of PFBT-coated Au anode pentacene rectifiers operating at (d) 14 MHz, (e) 100 MHz, and (f) 1 GHz are also shown. Reproduced from [143]. Copyright © 2016 John Wiley & Sons, Inc.

Owing to these impressive demonstrations, several groups have made attempts to show that pentacene Schottky diodes can be integrated with other components on flexible substrates. Cvetkovic *et al* [144] demonstrated a pentacene Schottky diode in parallel with a capacitor as a DC rectifier on 12 μm thick polyimide (PI) at frequencies up to 1 MHz. Myny *et al* [145] implemented a double full wave rectifier by incorporating two pentacene Schottky diodes and two capacitors on 200 μm thick PEN foil. With an input signal of $\pm$10.9 V, the output from this setup is 14.9 V at 13.56 MHz input signal frequency, higher than would be achievable with a single diode. Thus the authors demonstrated that the diodes could be realised on plastic foil and integrated without compromising the device performance. Gutierrez-Heredia *et al* [146] built full wave bridge rectifiers based on pentacene diodes and tested them in a frequency up to 5 MHz. However, they note that the individual diodes output a higher DC voltage than the bridge structures when integrated into rectifiers. Finally, Myny *et al* [147] showed that a double full wave rectifier based on pentacene diodes on 150 mm thick PEN foil could be used to power 64 bit and 128 bit transponder chips for RFID at 13.56 MHz (figure 16). The resultant transponders could be read at a read distance of over 10 cm from the RF source. The authors have included details of an encapsulation layer of parylene C and Al but gave no details on the stability or shelf lifetime of the rectifiers in air. The demonstrated RFID tags were based solely on pentacene and hence used unipolar p-channel logic.

5.2.2. Self-assembled monolayers (SAMs) are a diode's best friend. Electrode surface modification has proven to be a key factor in terms of high performance organic electronic devices such as OLEDs, photovoltaics, and organic field-effect transistors (OFETs) [148, 149]. Surface modification can have the effect of aligning energy levels of contacts and semiconductors ideally, as well as attaining optimal semiconductor film morphology. While thin films can be used, as in the case where Steudel *et al* employed PEDOT:PSS in their pentacene Schottky diodes to achieve a higher current density [140], SAMs are often preferred owing to their ease of realising molecularly-thin interlayers, which can nevertheless have a dramatic effect on the properties of the treated electrodes. SAMs can be deposited on a variety of surfaces depending on the anchoring group, and deposition is carried out at low temperatures (typically room temperature) via self-assembly from solution, usually via substrate immersion [150].

In a recent study by Kang *et al* [143], SAM modification of the Ohmic Au electrode in a pentacene Schottky diode was a critical factor in achieving HF operation above 1 GHz (figure 17). In their study the authors employ Raman spectroscopy to probe the molecular orientation of pentacene thin films, finding that Au surfaces treated with 2,3,4,5,6-pentafluorobenzenethiol (PFBT) host more vertically aligned pentacene molecules as opposed to untreated Au surfaces. The change in orientation of the pentacene is attributed to the surface energy modification due to the SAM. Extracted hole mobilities from the space-charge limited current region in the current–voltage characteristics of vertical pentacene Schottky diodes show a correlated increase in mobility from 6.8×10^{-4} to 0.11 $cm^2\,V^{-1}\,s^{-1}$ when the Au surface is SAM treated. The authors attribute the relationship between molecular orientation and extracted device mobility to the diminished presence of grain boundaries in the vertical direction when the pentacene is in the standing up configuration. The secondary effect of the PFBT SAM is in enhancing charge injection. PFBT has long been used to promote injection into p-type semiconductors from Au owing to the dipole moment of

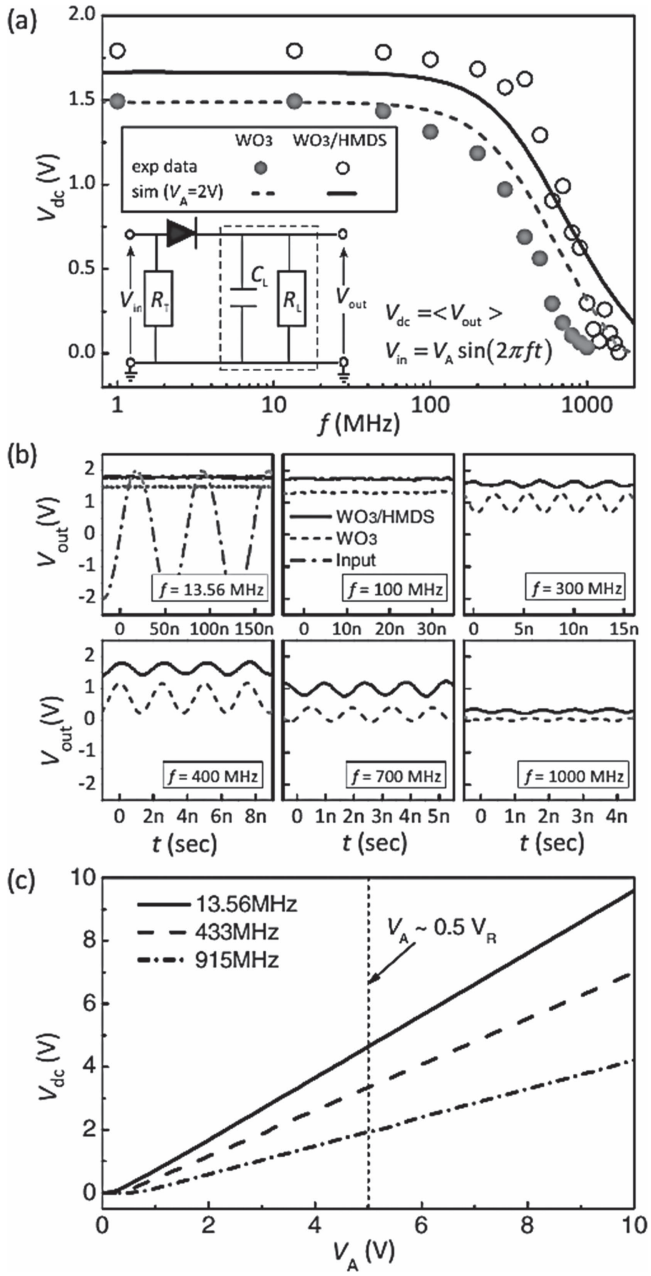

Figure 18. (a) Rectifier setup and measured results for C_{60} Schottky diodes. The shapes are for the experimental data and the lines are for the simulation results. (b) V_{out} obtained at several representative frequencies. V_{in} is also shown for the 13.56 MHz signal. (c) Simulated V_{DC} versus V_A for various carrier frequencies for the devices with HMDS-treated WO_3 layer. Simulation assumed no break-down effect at negative bias. When one considers the actual break-down voltage (V_R) of the proposed devices is ≈10–15 V, the upper limit of V_A that would not cause reverse break-down will be ≈5 V as denoted by the vertical dashed line ($V_A \approx 0.5V_R$). Reproduced from [155]. Copyright © 2011 John Wiley & Sons, Inc.

the small molecule increasing the effective work function of the metal at the surface [133, 151, 152]. Thus, the authors managed to demonstrate pentacene-based Schottky diodes with a high current density of 100 A cm^{-2} and a −3 dB cut-off frequency in a half wave rectifier setup of 1.24 GHz.

Kitamura *et al* [153] used a similar surface modification approach in fabricating pentacene TFTs, using PFBT modified electrodes to enhance charge injection, and measured a maximum transit frequency of 10 MHz for a 2 μm channel length device. In the same study, they employed 4-(dimethylamino)benzenethiol (DABT) treated Au electrodes to fabricate C_{60} fullerene TFTs. The authors previously demonstrated that DABT has the opposite effect of PFBT on the Au surface, effectively reducing the work function due to its dipole moment of 1.57 D (where D is the Debye unit) pointing away from the Au surface [154]. The effect is a change in the Au work function from 4.82 to 4.38 eV, and the realisation of 2 μm channel length TFTs with electron mobilities of 2.22 cm^2 V^{-1} s^{-1} and the highest reported transit frequencies to date for organic TFTs of 27.7 MHz.

Schottky diodes based on C_{60} have also been demonstrated. As with the case of pentacene, the reported frequency operation is much higher when surface modification of electrodes is employed. Im *et al* [155] fabricated vertical diodes where the Schottky and Ohmic contacts were WO_3 and Al respectively (figure 18). At the Ohmic contact, a 2,9-dimethyl-4,7-diphenyl-1,10-phenanthroline (BCP) layer was employed for efficient Ohmic injection and to prevent migration of the Al into the C_{60} layer during thermal evaporation. At the Schottky contact, a hexamethyldisilazane (HMDS) SAM was used to achieve a lower work function of WO_3 (measured 4.3 eV with treatment, 4.6 eV without). The rationale for this change in work function is the same as before, and a dipole moment of 0.41 D pointing away from the metal has been reported. The result of the HMDS treatment was a decrease in the turn on voltage for the diode and a higher DC rectified output at all frequencies. When measured in a half wave rectifier setup, these diodes exhibited an impressive cut-off frequency of 700 MHz. A current density of 46.5 A cm^{-2} at +1 V was reported and the authors note the promise of C_{60} in vertical diodes as, unlike pentacene, charge transport in C_{60} thin films is highly isotropic.

5.2.3. Heterojunction hybrid diodes. Schottky diodes are not the only organic diode type to have been investigated for HF applications. Pal *et al* [156] demonstrated a pentacene/ZnO pn junction diode with a large on-off ratio and current densities up to 160 A cm^{-2} at 5 V. HF performance was analysed by direct observation of the wave rectification and the device was seen to operate up to the measurement limit of 20 MHz. The stability of this device was also investigated and the signal was found to drop by only 10% after 2 months of storage in ambient conditions.

The ability to dope organic semiconductors controllably will be important for both optoelectronic and HF applications [157]. Modulating doping level allows for ideal matching of energy levels with various metal electrodes, as well as controllable alteration to device current voltage characteristics as desired. Kleemann *et al* [158] reported the fabrication of PIN diodes based on doped-pentacene/intrinsic-pentacene/doped-C_{60} heterostructure. The p-type dopant employed for the pentacene is 2,2-(perfluoronaphthalene-2,6-diylidene) dimalononitrile (F6-

TCNNQ), while the n-type dopant for the C_{60} is tetrakis (1,3,4,6,7,8-hexahydro-2H-pyrimido[1,2-a]pyrimidinato) ditungsten(II) ($W(hpp)_4$). The diodes are capable of outputting 1.4 V at 13.56 MHz and ~0.5 V at 300 MHz for an input signal of ±2 V, while the device cut-off frequency is estimated to reach 1 GHz.

5.2.4. Solution processed small molecule devices. A key advantage of organic electronics is their often high solubility in common solvents, as it enables manufacturing solution-phase methods including inkjet printing, and various larger area roll-to-roll compatible methods, such as gravure printing. However, solubility as well as substrate compatibility issues have made it difficult to realise HF organic small molecule thin films such as pentacene or C_{60} from solution phase. Since film morphology plays an important role on charge transport in small molecule semiconductors, this is a critical point which must be addressed. Herwig *et al* [159] developed a precursor chemical route for pentacene based on [n]acenes. Cantatore *et al* [27] used this solution processing route to fabricate pentacene transdiode-operated TFTs on 25 μm thick PI foil which were incorporated into functional 13.56 MHz rectifiers. The rectifiers themselves were integrated with 6 bit organic RFID transponders, providing a powerful demonstration of the potential of solution processed diode technology.

Solution processable precursor materials to traditional high quality vacuum processed small molecule systems certainly have their advantages, but an alternative approach is the use of their functionalized counterparts. Here carefully selected solubilizing side chains are chemically attached onto the semiconducting small-molecule enabling high solubility (e.g. phenyl-C61-butyric acid methyl ester (PCBM), and 6,13-bis(triisopropylsilylethynyl)pentacene (TIPS-pentacene). In fact, ink-jet printed co-planar organic TFTs on flexible foils based on a TIPS-pentacene:polystyrene ink have been demonstrated and implemented in unipolar ICs such as NOT and NAND gates as well as in 19-stage ring-oscillators [160]. Furthermore, nearly 300 inkjet printed TFTs were integrated on a surface area of 34 mm^2 of plastic foil, to realise 8 bit RFID transponder circuits.

With the application of rectification in mind, Higgins *et al* [161] used zone casted TIPS-pentacene in a self-aligned gate TFT and achieved f_T values above 1 MHz despite low mobilities of just 0.03 $cm^2\,V^{-1}\,s^{-1}$. The use of scalable techniques such as zone casting of the active layer, as well as the use of a novel nanoimprint technique, which allows development of TFTs with channel lengths down to 375 nm, is promising.

Another choice is the use of emerging soluble high mobility small molecules. The Takeya group developed a method for the deposition of highly ordered [1]benzothieno [3,2-b]benzothiophene derivative (C_8-BTBT) [162] and decyl substituted dinaphtho[2,3-d:2′,3′-d′]benzo[1,2-b:4,5-b′]dithiophene (C_{10}-DNBDT) [163] from solution to fabricate TFTs with mobilities on the order of 5 and 16 $cm^2\,V^{-1}\,s^{-1}$, respectively. This was achieved via an 'edge-casting' technique whereby a droplet of the solution is sustained at an edge of a structure on an inclined substrate, so that the crystalline domain grows in the direction of inclination. Operating the C_{10}-DNBDT TFTs in transdiode mode led to cut-off frequencies in half wave rectifiers up to 22 MHz when the channel length was reduced to 2 μm [42]. The rectifier was integrated into a 13.56 MHz transponder and used to power a 5-stage ring oscillator based on complementary organic logic. Previously the same group had compared 2,9-di-decyldinaphtho[2,3-b:2′,3′-f]thieno [3,2-b]thiophene (C_{10}-DNTT) based TFTs, where the semiconductor was either vacuum-evaporated or solution-crystallised and measured cut-off frequencies of 20 and 10 MHz, respectively [124]. By applying a vacuum-deposition process of the parent small molecule dinaphtho[2,3-b:2′,3′-f]thieno[3,2-b]thiophenes (DNTT) through a shadow mask from a diagonal direction they had obtained 3D organic transistors comprising vertical extremely short channel lengths (0.8 μm) and reduced parasitic capacitance [131]. Organic rectifiers based on the diode-connected 3D-OFETs showed a cut-off frequency of 20 MHz.

Another alternative to achieving high quality small molecule films from solution is through blending the small molecule with a polymer. Blend systems have been extensively studied for achieving greater control over the deposition and crystallisation of small molecules for high performance TFTs [164–169]. In general, a conjugated polymer acts as a binder for the small molecule. However, insulating polymers such as polystyrene can also be used, and have a similar beneficial effect on film formation [170, 171]. de Zerio Mendaza *et al* [172] found that while C_{60} solutions tended to dewet from SiO_2 substrates during processing, the addition of 9% wt ultrahigh molecular weight polystyrene resulted in even film coverage, and TFTs with field effect mobilities on the order of 1 $cm^2\,V^{-1}\,s^{-1}$ were demonstrated.

Using blends in a Schottky diode may be problematic however, owing to the tendency of blends to vertically phase separate. To this end, Semple *et al* recently reported planar Schottky diodes based on a C_{60}:polystyrene blend [93]. The deposition of high quality films was achieved on pre-patterned planar Al Ohmic and Au Schottky contacts separated on the order of 10–20 nm. The small channel length and low device capacitance resulted in extrapolated cut-off frequencies of 400 MHz when used in a half wave rectifier setup.

5.3. Polymer-based RF devices

Organic semiconductors based on conjugated polymers offer another route towards solution processed HF flexible electronics. These systems offer more flexibility and ease of processing from solution over small molecule systems, but in general suffer from lower mobilities. Recently, Kang *et al* [173], using a commercial polymeric semiconductor, Lisicon® S1200, showed TFTs with transition frequencies above 1 MHz with mobilities of 0.5 $cm^2\,V^{-1}\,s^{-1}$. Using silver ink as the S/D contacts and commercial SAM Lisicon® M001, a driving voltage of 10 V was used to achieve MHz operation. Gate electrodes smaller than 5 μm were gravure printed on PEN at low temperature (140 °C for metal

contacts) in air. Higgins *et al* [174], using a similar self-aligned approach as discussed in the previous section, recently fabricated TFTs with f_T values up to 3 MHz. This performance was achieved by minimising electrode overlap capacitance to 0.03 pF mm^{-1} by employing a gravure printed gate dielectric. The active layer consisted of the donor–acceptor copolymers diketopyrrolopyrole-thieno[3,2-b]thiophene (DPPT-TT) and poly([N,N′-bis(2-octyldodecyl)-naphthalene-1,4,5,8-bis(dicarboximide)-2,6-diyl]-alt-5,5′–(2,2′-bithiophene)) (P(NDI2OD-T2)), which were inkjet printed. Bucella *et al* [175] showed that alignment of P(NDI2OD-T2) polymer by combining pre-aggregating solvents for formulating the semiconductor and adopting a room temperature wired bar-coating technique led to TFTs with incredible mobilities up to 6.4 cm^2 V^{-1} s^{-1}. The high mobility in these devices enabled $f_T = 3.3$ MHz values to be extracted.

In terms of Schottky diodes, Altazin *et al* [176] have provided a model whereby the cut-off frequency in unipolar organic devices is limited by the carrier time-of-flight rather than the diode equivalent capacitance as in a conventional Schottky diode. The result is that the cut-off frequency is given by:

$$f_C = \mu(V_A - V_T)/L^2 , \quad (16)$$

where μ is the semiconductor mobility, V_A is the applied voltage, V_T is the threshold voltage and L is the device length. Based on this very simple model the authors argue that polymer rectifiers may operate in the range of 13.56 MHz despite their inherently lower mobilities if the active layer thickness in minimised. The hypothesis is backed up by the experimental fabrication of devices of varying thickness based on (poly (fluorene-alt-triarylamine) (TFB), where diodes with the lowest thickness (70 nm) exhibited the best RF performance (~1.5 V DC output for ±6 V AC input at 13.56 MHz). Lilja *et al* [177] reported a similar trend for poly(triarylamine) (PTAA)-based Schottky diodes fabricated via gravure printing, for which the highest frequency operation of up to 10 MHz was obtained from diodes based on the thinnest semiconducting layer (~500 nm). Kim *et al* [178] similarly observed a higher frequency performance for thinner diodes fabricated from spin cast films of poly (3-hexylthiophene) (P3HT) for which maximum DC outputs of 3.2 V for AC inputs of ±10 V at 1 MHz, were obtained.

The air stability of these polymer devices is also an issue. Lin *et al* [179] fabricated Schottky diodes based on P3HT and poly(3,3-didodecylquaterthiophene) (PQT12) via spin coating. The PQT-12 device was superior in terms of performance (4 V DC output at ±10 V AC when in rectifier setup). Notably the PQT-12 diode showed some air stability, with minimal changes occurring in the *I–V* characteristics after 120 h in ambient conditions, while the P3HT diode showed a dramatic breakdown in rectification. This is attributed to the higher HOMO level of the PQT-12, making it less susceptible to oxidative doping associated with ambient conditions (e.g. humidity, etc) and more environmentally stable. Bose *et al* [180] report the use of a commercially available amorphous co-polymer of arylamine and a fused aromatic species (FS102, Flexink Ltd) for air stable solution processed diodes. The diodes show current densities of up to 10 A cm^{-2} at 10 V but rectification only occurs at frequencies up to 10 kHz.

The Lupo group employed poly(triarylamine) (PTAA) as an air stable gravure printed active layer [181]. Half wave rectifiers produced 3.5 V DC on application of ±10 V AC signals even after one month in air. The authors note that a decrease in the active layer thickness leads to an even higher output voltage, but also leads to a drop in the yield (from ~97% for thicker active layers to an unspecified lower value). The PTAA diodes have also been integrated via gravure printing into full wave bridge rectifiers. As expected, the full wave rectifiers resulted in a reduced ripple seen in the output. However, the magnitude of the output power also dropped by over a half. This is attributed to the cumulative voltage drop across the diodes. More recently, the same group employed PTAA diodes to build a two-stage charge pump circuit on a PET film, capable of outputting three times the voltage of a single diode half-wave rectifier (8.4 V as compared to 2.8 V over a 1 MΩ load at 13.56 MHz) [182]. Considering further circuit integration of these diodes, they considered the effect of printed PTAA diodes capacitance on rectenna circuit resonance and found that the capacitance in this case is large enough that it must be considered, since it has a significant effect on the DC output voltage [183].

Further integration of printed Schottky diodes has been carried out by many groups. As already mentioned above, Lin *et al* [179] used their printed PQT-12 diode (discussed above) with screen printed capacitors and an antenna to build a demonstrator wireless powerless transmission sheet. The resultant DC voltage transferred from a commercial 13.56 MHz RF radiator was sufficient to power a green LED. Jung *et al* [184] employed a voltage tripler based on hybrid polyaniline (PANI)/cobalt doped zinc oxide nanowire diodes to fabricate an all printed rectifier incorporated into a roll to roll gravure printed 1 bit RFID tag (figure 19). The voltage tripler rectifier was capable of outputting 10 V at a read distance of roughly 1–3 cm from a 13.56 MHz radiator outputting a signal of roughly ±15 V. The output performance characteristics of the rectifiers based on organic materials are summarised in table 3.

6. Carbon-based nanomaterials

Carbon based nanomaterials exhibit a unique combination of thermal, electronic and mechanical properties, making them desirable for a number of applications. While, possibly, the furthest from commercialisation in flexible RF rectifiers, as they face the greatest integration and fabrication challenges, this material class has the potential to outperform competitors in terms of frequency performance and current driving capability, primarily due to their exceptional carrier mobility values.

6.1. Carbon nanotubes

CNTs have been attracting tremendous interest since their discovery by Iijima in 1991 [186], owing to their mechanical stiffness and strength [187], flexibility [188], unprecedented thermal conductivity [189] arising from the carbon–carbon

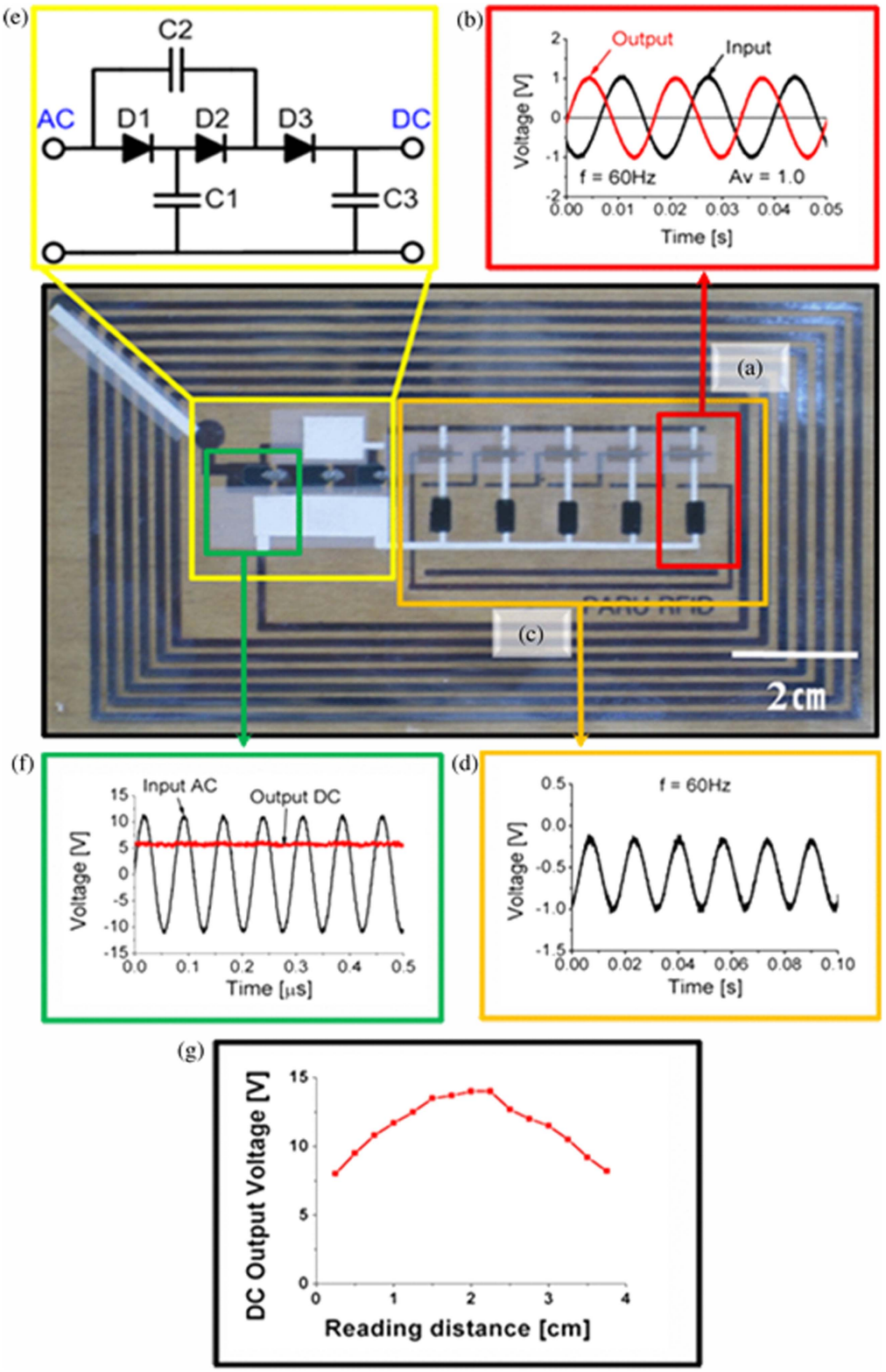

Figure 19. (a) Fully printed and R2R-printable SWCNT inverters with (b) an input and output frequency of 60 Hz and (c) five stages of the SWCNT ring oscillator with (d) an oscillated frequency of 60 Hz. (e) Voltage tripler circuit using three of the printed diodes and three of the printed capacitors to provide more than 10 V DC from the 13.56 MHz RFID reader. (f) Input–output electrical characteristics of a printed diode with a printed capacitor at 13.56 MHz AC. (g) Attained DC outputs of the printed rectenna based on the reading distance from the 13.56 MHz reader (13.56 MHz RFID chip: TRH031M, Protocol: ISO/IEC 14443 A/B, 15693 Standards, Communication distance: up to 10 cm. Antenna size: 75 × 50 mm, 2.7–3.6 operation voltage and 0.3-power down mode current). Reprinted, with permission, from [184]. Copyright © (2010) IEEE.

Table 3. Summary of organic rectifiers' output performance evaluated at 13.56 MHz.

Material	Diode type	Substrate	DC output (V) (R_L)	AC input (V)	Frequency (MHz)	Year	Ref.
Small molecules							
Pentacene	TFT transdiode	Glass	6 V (50 kΩ)	±18	14	2006	[141]
	TFT transdiode	PI	11	±20	0.125	2007	[27]
			25	±60	13.56		
	Schottky diode Au/PEDOT: PSS/pentacene/Al	Si wafer	11	±18	14	2005	[140]
			8 (50 kΩ)		50		
	Schottky diode Au/pentacene/Al	glass	9.8	±15	13.56	2008	[142]
			11		433		
		PEN	4.5 (1 MΩ)		869		
	-II- doubler	PEN	14.9 (1 MΩ)	±10.9	13.56	2008	[145]
	Schottky diode Au/pentacene/Al	PEN (single)	8.1	±10	1	2012	[146]
		PEN (full bridge)	5 (1 MΩ)				
	Schottky diode Au-PFBT/pentacene/Al	Glass	6	±10	1	2016	[143]
			3.8 (1 MΩ)		1000 $f_{cut\text{-}off}$ = 1240		
	p–n diode ITO/ZnO/pentacene/Au	Glass	0.11 (200 Ω)	±2	15	2008	[156]
	PIN diode Al/pentacene:F6-TCNNQ/pentacene/C_{60}:W(hpp)$_4$/Al	Glass	1.4	±2	20	2012	[158]
			0.5 (1 MΩ)		300		
					$f_{cut\text{-}off}$ = 1000 (estimated)		
TIPS-pentacene	Self-aligned gate TFT transdiode	plastic foil	—	—	f_T = 2.23 (V_{GS} = −40 V)	2015	[161]
C_{60}	Schottky diode Al/WO_3-HMDS/C_{60}/BCP/Al	Glass	1.79 (500 kΩ)	±10	13.56	2011	[155]
					$f_{cut\text{-}off}$ = 700		
	Schottky diode Al/C_{60}:PS/Au	glass	1.2 (1 MΩ)	±5	13.56	2016	[93]
					$f_{cut\text{-}off}$ = 400 (extrapol.)		
DNTT	TFT transdiode	Glass	10	±15	1	2015	[131]
			8		15		
					$f_{cut\text{-}off}$ = 20		
C_{10}-DNBDT	TFT transdiode	Glass	10	±15	1	2015	[42]
			8 (200 kΩ)		15		
					$f_{cut\text{-}off}$ = 22		
Polymers							
P3HT	Schottky diode Au/P3HT/Al	Glass	3.2 (1 MΩ)	±10	1	2010	[178]
	Schottky diode IZO/PEDOT:PSS/P3HT/Al	PC	5 (1 MΩ)	±10	5	2011	[179]
PQT12	Schottky diode IZO/PEDOT:PSS/PQT12/Al	PC	4 (1 MΩ)	±10	13.56	2011	[179]
					$f_{cut\text{-}off}$ > 14		
PTAA	Schottky diode Cu/PTAA/Ag	PET	2.7 (1 MΩ)	±10	10	2009	[177]
	Schottky diode Cu/PTAA/Ag	PET	3.5 (1 MΩ)	±10	13.56	2013	[181]
	-II- (2-stage charge pump circuit)	PET	8.4 (1 MΩ)	±10	13.56	2014	[182]
TFB	Schottky diode ITO/PEDOT:PSS/TFB/Al	Glass	1.5 (1 MΩ)	±6	13.56	2014	[185]

sp^2 chemical bond, and unique quasi one-dimensional (1D) electronic structure, which leads to low scattering probability and very high charge carrier mobilities. Their low self-heating characteristics also result in high breakdown voltages, while their low dimensionality gives rise to a very low quantum capacitance. The combination of all these attributes leads to the prospect of CNTs having a major role in the future of high-speed flexible electronics.

The electronic properties of CNTs are highly dependent on their morphology (chirality, diameter etc). As such, around one third of single walled carbon nanotubes (SWCNTs) are metallic and two thirds are semiconducting [190]. Metallic nanotubes may find uses in large-area applications as contacts for diodes and TFTs [191], as well as in the interconnects for integrated circuitry [192], owing to their ability to sustain current densities in excess of 10^9 A cm^{-2} [193]. Meanwhile, semiconducting nanotubes exhibit field-effect mobilities of up to 8×10^4 cm^2 V^{-1} s^{-1} with intrinsic mobilities predicted to exceed 10^5 cm^2 V^{-1} s^{-1} [194]. As a result, CNTs have shown intrinsic current gain cut-off frequencies up to 80 GHz. The potential of the integration of these devices into RF electronics was demonstrated in 2007 when three separate groups reported using nanotube components in the antennae, demodulators and amplifiers to fabricate nanotube radios [195–197]. Rutherglen *et al* [198] provide a detailed review into CNT TFTs for a range of RF applications. One consideration for integration into RFID technology is that semiconducting SWCNTs exhibit dominant p-type conductivity when exposed to air. This is thought to be due to the adsorption of oxygen [199], implying that if CNTs were to be used for logic as well as rectification, a compatible n-type semiconductor would need to be employed to enable complementary logic. Alternatively, a cost-effective encapsulation technology and/or device/circuit processing under inert atmosphere would be required.

6.1.1. Fabrication considerations. A unique consideration of the nanomaterial family in Schottky diode fabrication is that the devices must be lateral rather than vertical as in the case of thin films. Such a constraint is necessary to avoid direct contact and thus shorting of the Schottky and Ohmic contacts. Thankfully nanomaterials, and particularly CNTs, can be fabricated with extremely large aspect ratios (Zhang *et al* reported CNTs grown up to half a metre in length [200]).

A further consideration from this constraint is that asymmetric lateral contacts need to be fabricated. As such, reported channel lengths for CNT Schottky diodes to date have been constrained to >1 μm. To this end, Lu *et al* [201] employed e-beam lithography to form devices with lengths of ~ 3 μm between Al (Schottky) and Au (Ohmic) contacts. Manohara *et al* [202] used a combination of photolithography and angle evaporation to fabricate ~ 2 μm gaps between Ti (Schottky) and Pt (Ohmic) contacts on pre-located CNTs (figure 20). For such a device architecture containing four nanotubes in parallel, the cut-off frequency was predicted from extracted values of series resistance to be 540 MHz, with low voltage operation. Cobas *et al* [203] carried out direct measurements of a CNT Schottky diode at up to 18 GHz employing a microwave signal generator and predicted an ultimate cut-off frequency of 400 GHz based on the device series resistance and junction capacitance. The same authors later conducted direct measurements of the cut-off frequency using four devices with several CNTs in parallel, and found a value of 950 MHz for the 0-bias device cut-off frequency. Applying a positive DC bias, the cut-off frequency increased up to 3.6 GHz at $+1.2$ V [204].

For HF applications, it is important to match the impedance of the device with the source impedance (generally 50 Ω) to minimise signal reflection. The quantum of conductance for a single quantum channel, found by integrating the density of states between source and drain potentials, is e^2/h, where h is the Planck's constant. A CNT has four parallel quantum channels owing to spin and band degeneracy, yielding a total minimum impedance (inverse of conductance) of $4\,h/e^2 \sim 6.45$ kΩ [204]. In practice, device impedance may have to be reduced by placing several CNTs in parallel. The issue of increasing contact resistance with increasing number of CNTs may then have to be addressed. This can be achieved by reducing the channel length. Kim *et al* [205] reported a dramatic scaling of CNT length with contact resistance. A further drive for the reduction of channel length comes from the observation of Cobas *et al* [204] in the observation of the scaling of junction capacitance with channel length. Capacitance was extracted from values of cut-off frequency and it was concluded that stray capacitance between a long CNT channel and a metal electrode dominated junction capacitance in long-channel devices. Importantly, the authors also note that the relationship between device capacitance and the number of CNTs scales sub-linearly, while the resistance scales inversely. Thus, the outlook is that many short nanotubes in parallel will yield devices with the highest cut-off frequencies.

AC dielectrophoresis (DEP) is a process for the aligning of several CNTs over two electrodes. In this process, a drop of CNT containing liquid dispersion is placed over electrodes and an alternating electric field applied so as to induce a dipole moment and align the CNTs between the electrodes. As well as being a viable route toward the large scale aligning of multiple CNTs between electrodes, AC DEP has the further advantage of selectively sorting metallic and semiconducting CNTs [206]. Steiner *et al* [207] fabricated 100 nm channel length TFTs using e-beam lithography and AC DEP of semiconducting single walled CNT dispersions to achieve extrinsic values of f_T and f_{max} of 7 and 15 GHz, respectively. Li *et al* [208] fabricated SWCNT Schottky diodes using AC DEP on photoloithograpically patterned Hf and Au contacts. While they did not measure the AC characteristics of the devices in this instance, it seems DEP is a promising route towards future high-speed CNT Schottky diodes.

6.1.2. Flexible CNT devices. Park *et al* [209] provide a recent general overview of flexible electronics based on CNTs including high-speed flexible CNT-based devices. Importantly, Chen *et al* [210] showed by fabricating IR photodetectors based on symmetric Au contacts that CNT devices based on polymeric

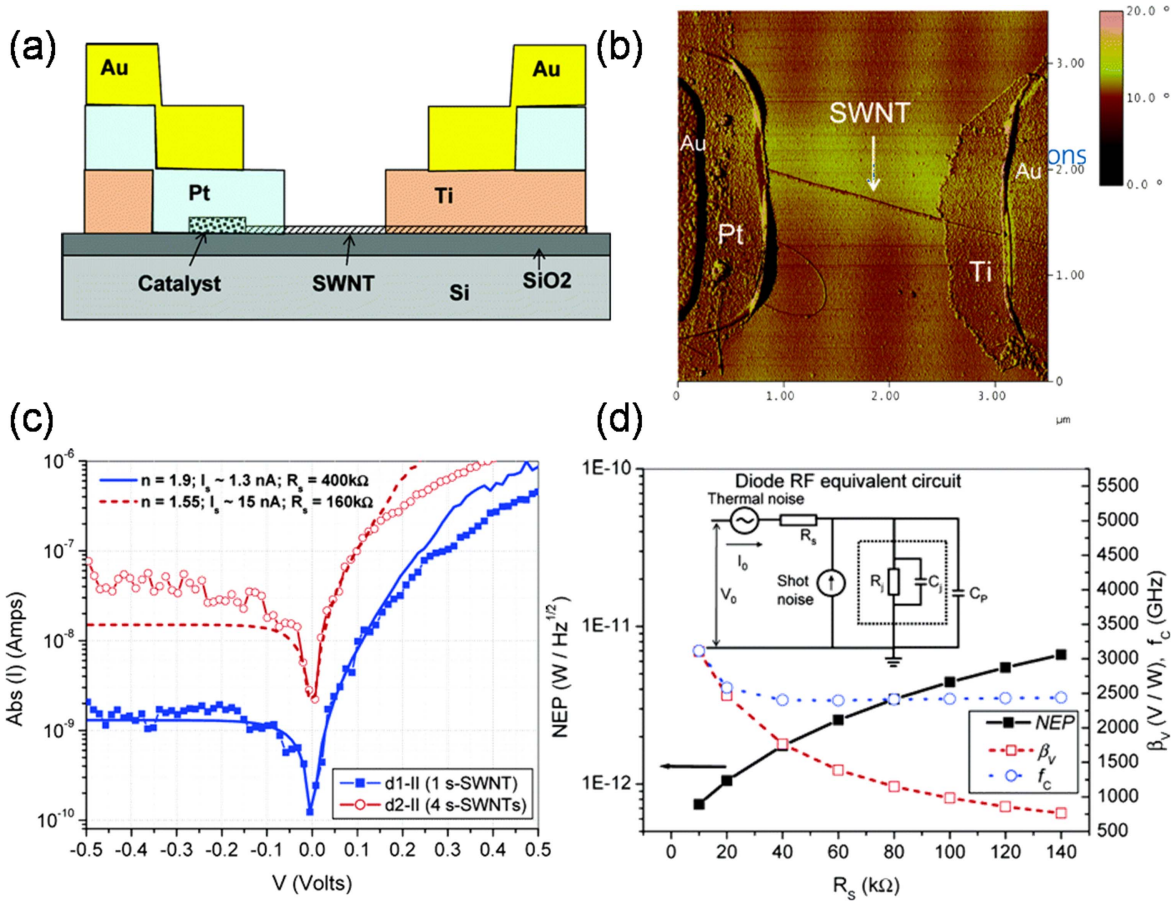

Figure 20. (a) Schematic representation of SWNT-Schottky diode showing the Ti-Schottky and the Pt-Ohmic metal layers deposited through angled evaporation, (b) AFM phase plot image of a typical SWNT-Schottky diode. The s-SWNT diameter varied from 1 to 3 nm while its length varied from 1.7 to 2.5 μm. (c) Ideality curve fits in low bias range for d1-II (with single s-SWNT) and d2-II (with four s-SWNTs) Schottky diodes. The curve shows the absolute magnitude of the current plotted against the corresponding voltage. The diode fits give $n = 1.5$–1.9 and $I_S = 1.3$–15 nA for the two diodes. (d) The dependence of the voltage responsivity (β_V), the noise equivalent power (NEP), and the cut-off frequency (f_C) on the series resistance of a hypothetical 100-nanotube SWNT-Schottky diode. The values are calculated for direct detection at 2.5 THz frequency signal at room temperature. The inset shows the diode RF equivalent circuit used in this model. Reprinted with permission from [202]. Copyright (2005) American Chemical Society.

substrates exhibit lower noise than those based on glass/quartz. This is a key consideration for integration into HF flexible electronics. Han *et al* and Vaillancourt *et al* [211, 212] note the need for CNTs of a high electronic grade, which are free from amorphous carbon that can coat CNT sidewalls. Using such solution processed CNTs they realised TFTs on flexible substrates operating at >300 MHz. Building on this early work, Vaillancourt *et al* [213] reported all inkjet-printed CNT-based TFTs operating up to 5 GHz, though operating with a low transimpedance gain of <0.05. The improvement in performance was attributed to incorporating circuit elements directly on the polyimide substrate rather than using external measurement circuitry. Chimot *et al* [214] employed AC DEP to fabricate TFTs with a channel length of 800 nm on 250 μm thick PET substrates, demonstrating the compatibility of the process with flexible substrates. The devices have extrinsic f_T values of up to 1 GHz, and show constant values of transconductance when measured at DC for bending radii down to 3.3 mm.

Yang *et al* [215] fabricated CNT Schottky diodes on a polyether ether ketone (PEEK) substrate. The authors highlight the compatibility of this substrate with chemicals used during processing as well as the relatively high glass transition temperature and low thermal expansion coefficient of PEEK in the selection of this substrate. A novel undercut method was employed to form closely spaced asymmetric electrodes on the order of 1 μm in the form of a log periodic array antenna. CNTs were aligned between the electrodes using AC DEP (figure 21). The diode was measured at a fixed frequency of 18 GHz, and for a radiated power input of 13 dBm gave a 0 bias output of ~1.5 mV and a maximum output of 9 mV when biased at +0.4 V. The authors again noted impedance mismatch as a limiting factor in the HF operation of the device but highlight the progress made by adopting many CNTs in parallel as well as in minimising the channel length.

CNTs are typically grown on rigid substrates via chemical vapour deposition (CVD), arc discharge or laser ablation [216–218]. Unfortunately, these growth processes are often carried out at high temperature (>500 °C), hence rendering them incompatible with inexpensive flexible substrate materials. To circumvent this issue, direct transfer of CNTs onto flexible substrates has been demonstrated by spin coating a polymeric layer such as poly(vinyl alcohol) (PVA) [219], poly(methyl

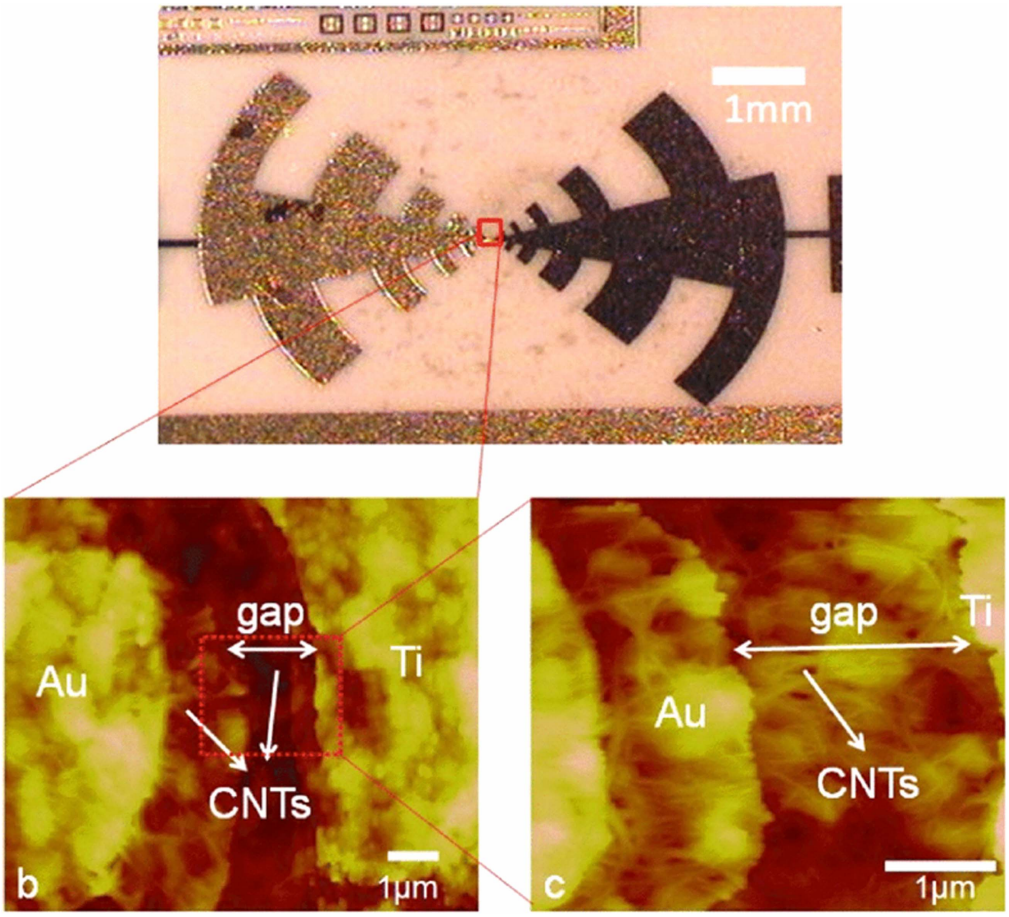

Figure 21. (a) Photomicrograph of a log-periodic antenna with CNT Schottky diodes. (b) AFM scan of the CNT diode region. (c) Close-up view of CNT rich region. Reprinted, with permission, from [215]. Copyright © (2011) IEEE.

methacrylate) (PMMA) [220], or polyimide [221] onto the as-grown CNTs followed by a subsequent peel off step. Furthermore, once grown, CNTs may be dispersed in solution, and stabilised from re-aggregation via solvent or surfactant stabilisation [222, 223], enabling their possible use in printable electronics. These different routes demonstrate the versatility of CNTs and their potential for application in large-volume RF flexible electronics.

6.1.3. Challenges. A consideration in any transfer technique is the alignment of CNTs with regard to the conductive electrodes. The use of electron microscopy to find CNTs and pattern electrodes around them is obviously not feasible for large-area applications. Cobas *et al* [203] report a fully photolithographic route towards the fabrication of aligned Ohmic and Schottky contacts, requiring no sophisticated patterning techniques. However, as the authors are depositing electrodes 'blind' on top of the CNTs, the yield of electrodes connected by CNTs is low.

Furthermore, separation of semiconducting and metallic CNTs still remains a major problem. When fabricating devices from single CNTs, Manohara *et al* noted that device yield decreases due to the possibility of the existence of a metallic CNT [202]. Lu *et al* [201] reported 40% of their CNT Schottky diodes failing due to the presence of metallic CNTs. However, new insights into the growth mechanisms of SWCNTs may in future provide a greater yield of semiconducting CNTs. Loebick *et al* [224] have found that a lower 600 °C temperature led to a yield of ~93% semiconducting SWCNTs when using CoMn bimetallic catalysts. Che *et al* [225] have demonstrated a yield of up to 97.6% semiconducting SWCNTs via CVD by employing 2-propanol (IPA) as the carbon feedstock. Islam *et al* [226] provide a recent detailed review on methods for both growing high yield semiconducting SWCNTs and separating metallic and semiconducting SWCNTs after growth, while Hersam [227] provides an account of progress towards monodisperse SWCNT dispersions.

Wang *et al* [228] have noted that density gradient ultracentrifugation (DGU) is a particularly scalable technique for the isolation of semiconducting SWCNTs. The achieved deposition of SWCNTs onto a poly-L-lysine solution-treated polyimide substrate by simple immersion. Resultant TFTs with channel lengths of 4 μm exhibited mobilities of 50 $cm^2\,V^{-1}\,s^{-1}$ and values of intrinsic f_T and f_{max} of 170 and 118 MHz respectively.

The most reliable route towards semiconducting CNT isolation may be the so-called polymer sorting route, where polyfluorene-based conjugated polymers have been shown to yield semiconducting CNT purities of >99.9% [229]. Cao *et al* [230] have taken advantage of these high purity

dispersions and employing the process of dose-controlled, floating evaporative self-assembly developed by Joo *et al* [231], have demonstrated TFTs with extrinsic values of f_T and f_{max} of 40 GHz. The measured devices display some reproducibility, with a reported ~20% device-to-device variation. This is promising for the development of scalable solution deposited CNT devices in the UHF regime. However, at present, scaling of the production of such devices is not feasible, the TFT in this case having a channel length of just 100 nm. While the reduction in the channel length for both TFTs and diodes based on CNTs is a critical issue for device performance (as discussed above), the routine fabrication of sub-100 nm separated electrodes at a low-cost production level is not trivial. In the case of diodes, the fabrication steps become even more complex, as asymmetric electrodes must be employed.

Conventional nanogap patterning techniques, including electron beam lithography [232, 233], mechanical break junctions [234, 235] and electromigration [236, 237], are typically neither compatible with large-area flexible substrates nor asymmetric electrodes essential for Schottky diodes. Emerging patterning techniques may hold some promise in this area in fabricating asymmetric nanogap electrodes [238, 239]. However, the lack of scalability of these fabrication techniques is an issue.

In recent years, significant effort has been focusing on the development of alternative asymmetric nanogap electrode fabrication techniques with the help of SAMs [240–244]. Recently, the group of Anthopoulos reported on adhesion lithography (a-Lith), a technique based on the modification of surface energies of conductive electrodes using SAMs for the large-area patterning of asymmetric nanogap electrodes [95]. These nanogap electrodes are routinely fabricated with separation <20 nm. Uniquely, this is a large-area compatible technique, capable of producing many nanogap electrode sets simultaneously. As the technique is highly reproducible and compatible with flexible substrates [94, 245], it may be a promising avenue for the pursuit of HF nanomaterial based devices, and pave the way towards large-area plastic nanoelectronics.

6.2. Graphene

Graphene is a quasi-2D crystalline allotrope of carbon. Since its discovery in 2004 [246] it has been the centre of a vast amount of research owing to its unique mechanical, optoelectronic, spintronic and plasmonic properties. The electrical properties of graphene have been at the forefront of the investigation into graphene. The original article reported the fabrication of a graphene TFT with a mobility of 10 000 $cm^2 V^{-1} s^{-1}$ [246]. Since then, devices have been fabricated with mobilities of up to 200 000 $cm^2 V^{-1} s^{-1}$ [247, 248].

Graphene has several of the inherent advantages associated with CNTs, but it has some of its own unique advantages too. Quantisation of conductance does not occur in graphene as in CNTs. Thus impedance mismatch at radio frequencies is not an issue [249, 250]. As a result, devices have been demonstrated with superior frequency performance, the record to date being a TFT with an intrinsic value of f_T of 427 GHz [251], though a channel length as small as 67 nm was needed to achieve this. Current levels in graphene Schottky diodes have reached the mA level, far exceeding those reported for CNT Schottky diodes [252]. Despite the rectification ratio being low due to the absence of a bandgap in graphene, the measured device impedance of 60 Ω allows the observed operation of the diode in the frequency range 40–65 GHz.

6.2.1. CVD graphene for flexible devices. The electronic properties of graphene were first studied using mechanically exfoliated samples from graphite. The technique, while in no way industrially scalable, is still often used in device fabrication. For example, Petrone *et al* [253] recently demonstrated flexible graphene TFTs passivated by layers of hexagonal boron nitride (hBN) on either side on a PEN substrate to achieve extrinsic values of f_T and f_{max} of 12 and 10.6 GHz, respectively. The high quality of the devices was attributed to the enhanced dielectric environment provided by the hBN encapsulation.

While mechanically exfoliated graphene was often favoured in the early days of graphene research for high quality electronic device fabrication, CVD-grown graphene has become competitive in terms of performance. This high temperature technique is generally carried out on copper substrates, but the resultant films can be transferred to flexible substrates by dissolution of the copper and lifting out of the floating graphene films onto new substrates [254].

Several groups have demonstrated the potential of highly flexible devices using transferred CVD graphene. Petrone *et al* [255] were the first to report graphene TFTs with performance in the GHz regime with strains over 0.5%. Specifically, the devices were fabricated on 127 μm thick PEN with channel lengths of 900 nm and exhibited values of f_T and f_{max} 6.3 GHz and 2.5 GHz, respectively. Yeh *et al* [256] implemented a self-aligned-T-gate structure on PET films with a native AlO_x gate dielectric and demonstrated devices with f_T of 32 and 13 GHz when the device was under a bending radius of 2.5 mm (2.5% strain). The TFTs were used to demonstrate low noise amplifiers and frequency mixers in the range 1–10 GHz. Lee *et al* [257] fabricated graphene TFTs on polyimide substrates, which exhibited electron mobilities of 3900 $cm^2 V^{-1} s^{-1}$ and intrinsic values of f_T of 25 GHz. The passivation of these devices with fluoropolymers provided water resistance, while the potential of the technology for application in flexible electronics was further highlighted with the demonstration of functional devices down to an impressive bending radius of 0.7 mm.

Wei *et al* [258] further boosted the observed value of f_T on flexible substrates to 39 GHz, by reducing the channel length to 180 nm via e-beam lithography on polyimide substrates, and again employing an Al gate with native AlO_x as the dielectric. The flexible devices were seen to have a good stability, showing a variation in these values of less than 15% after 1000 bending cycles to a bending radius of

12 mm. In a practical demonstration, Yogeesh *et al* [259, 260] fabricated a graphene TFT on polyimide and employed it as a demodulator for an AM radio signal at 2.4 GHz. The graphene was fabricated on Cu via CVD and transferred to the flexible substrate via wet-transfer. The authors combined the graphene demodulator with a graphite antenna and further demonstrated a thermoacoustic speaker based on monolayer graphene for compatibility.

6.2.2. Solution phase graphene. A more straightforward route to enabling graphene on flexible substrates is via solution phase exfoliation of graphene 2D flakes from graphite and subsequent deposition. Different methodologies to achieve stable graphene dispersions exist, including graphene oxide exfoliation and subsequent reduction [261], surfactant stabilised exfoliation [262], solvent stabilised exfoliation [263], sterically stabilised polymer exfoliation [264] and intercalation [265]. It is highly important that monolayer dispersions are obtained for device fabrication, and research is progressing on the realisation of complete monolayer graphene dispersions through techniques such as DGU [266] and cascade centrifugation [267].

Sire *et al* [268] fabricated near monodisperse suspensions of graphene with flake dimensions on the order of a few hundred nm in diameter via aqueous surfactant exfoliation of graphite followed by DGU. Graphene monolayers were aligned between S/D electrodes separated by 260 nm via DEP on polyimide substrates. While the authors do note that DEP is not a feasible large-area deposition technique, they were able to demonstrate flexible graphene TFTs with extrinsic values of f_T and f_{max} of 2.2 GHz and 550 MHz respectively. The fact that such high frequencies have been achieved in TFTs made on plastic substrates via deposition of graphene from liquid phase is encouraging for the future of large-area printed high-frequency flexible graphene electronics.

Kaur *et al* [269] employed graphene oxide in an aqueous dispersion in the only demonstration of solution phase fabricated graphene Schottky diodes to date (figure 22). In general, high temperatures are needed for the reduction of graphene oxide. The authors overcame this dilemma by adding hydrazine hydrate to the graphene oxide dispersion, and later annealing the diodes at 100 °C. PEEK was again chosen as the substrate due to its chemically inert nature, its low thermal expansion and its high glass transition temperature. The authors fabricated sub-micron asymmetric Ti/Pd electrode gaps using an undercut method and aligned the graphene flakes via DEP. The graphene was not fully reduced, thus leaving some presence of a band gap which enabled rectification at the cost of carrier mobility. The diode was capable of outputting a DC signal of just over 2 mV for an input power of 10 dBm at a frequency of 26 GHz.

6.2.3. Alternative 2D materials. As already mentioned, the absence of a bandgap in graphene represent a major bottleneck for several electronic applications, including rectifying devices such as diodes. Solutions to this major issue include use of partially reduced graphene oxide [269] or opening up a bandgap by using graphene nanoribbons [270]. A different approach investigated recently is to employ alternative quasi-2D materials for RF electronics. One such material which has been studied in this regard is a member of the transition metal dichalcogenide family, molybdenum disulphide (MoS_2) [271]. Like graphene, MoS_2 can be exfoliated from bulk material. While exhibiting intrinsically lower electron and hole mobilities than graphene, TFTs based on few layer MoS_2 were reported to exhibit effective velocities of 2.8×10^6 cm s^{-1} and monolayer MoS_2 TFTs to exhibit effective velocities of 1.1×10^6 cm s^{-1} under high-field saturation in TFTs, rendering sub-micron devices suitable for GHz operation [272, 273]. Furthermore, the presence of a direct bandgap in monolayer MoS_2 makes it interesting for both optoelectronics and more practical HF flexible electronics [274]. As such, there have been reports of MoS_2 TFTs with sub-micron channel lengths operating into the GHz regime. Krasnozhon *et al* [275, 276] found superior values of f_T up to 6 GHz in TFTs based on trilayer MoS_2 as opposed to monolayer MoS_2, attributing this behaviour to the lower contact resistance in the thicker stack. This was evidenced by more pronounced saturation behaviour in the trilayer device. However, the frequency performance of the TFT device degraded for thicker channel layers. Here the MoS_2 was grown via CVD and transferred using a similar process as used in graphene TFTs.

Chang *et al* [277] demonstrated flexible MoS_2 TFTs fabricated on 125 μm thick polyimide substrate. The nanochannel devices were shown to exhibit an f_T of 2.7 GHz and operating stability through 10 000 bending cycles to a bending radius of 12.5 mm. Furthermore, the authors showed that these devices could successfully be used for AM demodulation. Using short channel lengths of 68 nm, Cheng *et al* [278] demonstrated self-aligned gate TFTs with values of f_T and f_{max} of 4.7 GHz and 5.4 GHz, respectively, on polyimide substrates with no observable degradation in their DC characteristics after 1000 bending cycles to a bending radius of 5 mm. Devices with slightly longer channel lengths of 116 nm were also employed as flexible RF amplifiers operating at 300 MHz, clearly highlighting the important role of channel length in maximum performance attainable in MoS_2 TFTs.

Another alternative 2D material is monolayer black phosphorous (BP), known as phosphorene [279]. This recently isolated single layer allotrope of phosphorous has the advantages a high hole mobility and the presence of a direct bandgap. Zhu *et al* [280] recently demonstrated flexible top-gated BP transistors on PI substrates exhibiting low-field hole mobility of 233 cm^2 V^{-1} s^{-1} and f_T and f_{max} of ~17.5 GHz and 14.5 GHz, respectively, in TFTs with channel length L of 0.5 μm. The authors attribute the exceptional performance of their BP-TFTs to the use of optimised dielectric coatings which enhanced the air-stability of the active channel during microfabrication. Table 4 summarises the performance characteristics of the above-mentioned nanomaterials-based rectifiers.

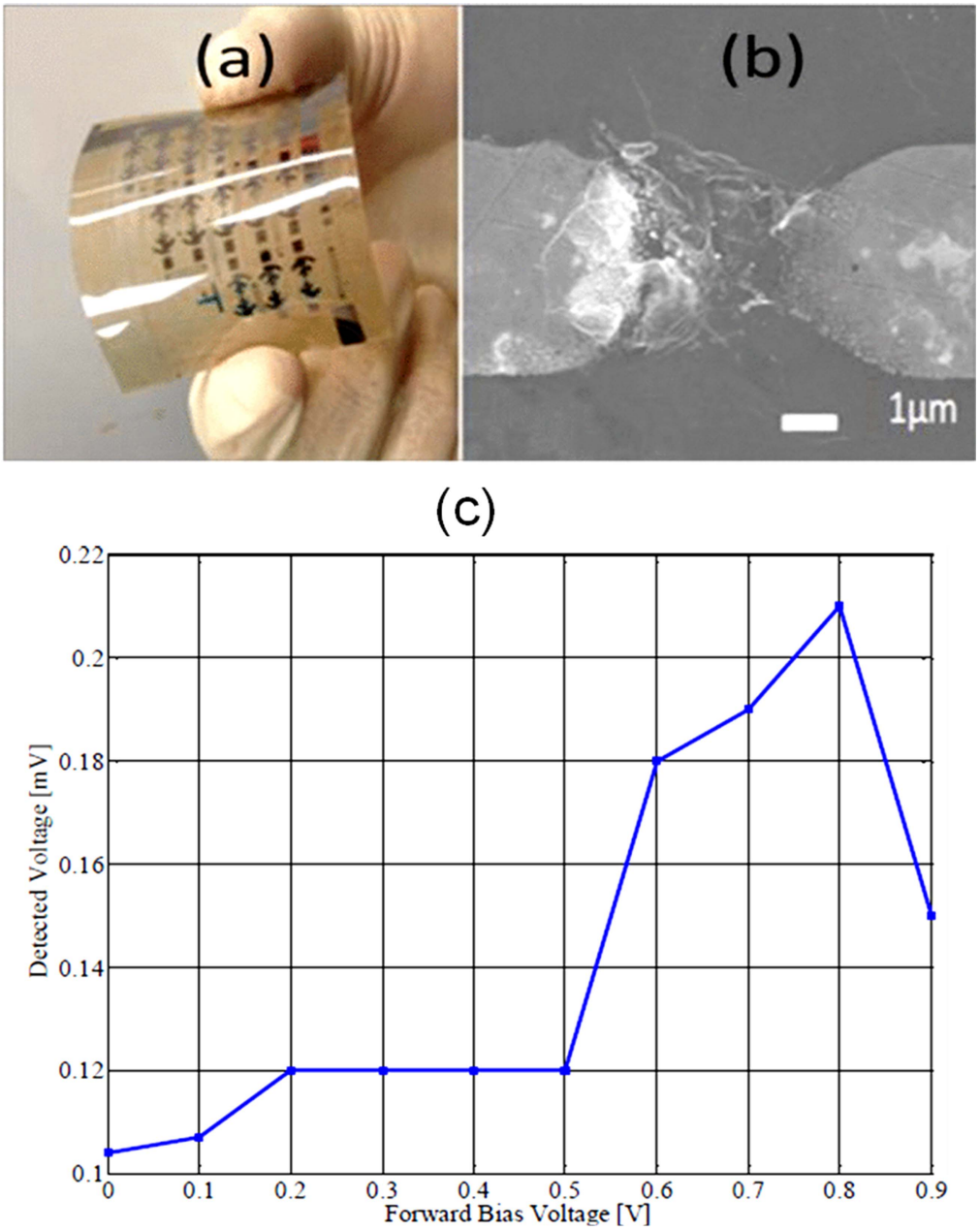

Figure 22. (a) Photo of the as-fabricated devices on PEEK substrate. (b) SEM image of aligned RGO between electrodes. (c) Measured output voltage as a function of applied bias voltage at a fixed power of −10 dBm and frequency of 10 GHz. Reprinted, with permission, from [269]. Copyright © (2013) IEEE.

7. Outlook

We have summarised recent progress in the development of transistor and diode-based rectifiers for application in flexible RF electronics. It is worth noting that over the last decade, there has been increasing interest in transferring research advances obtained on rigid substrates onto plastic (flexible) substrates. The growing demand for flexible, conformable RFID tags, wireless communication and wireless energy harvesting systems that could be produced at a low-cost is a key driver for this technology push. Research has manifested through a number of avenues, including adapting conventional Si-based technology and related materials via transfer methods onto flexible substrates, to employing large-area vacuum processed MOSs and organic semiconductors, which are reaching maturity in the display industry. Both of these latter material families are of interest due to the varying degrees of potential solution processability. Finally, carbon nanomaterials and their analogues possess excellent electronic transport properties, which could be exploited for flexible HF applications, if fabrication challenges can be overcome. A common theme that has presented itself across all material classes is that, important as choice and optimisation of material is, the choice and optimisation of device architecture is crucial for high performance also.

Figure 23 summarises the main classes of materials analysed in this review article with respect to their frequency

Table 4. Summary of performance characteristics of various nanomaterials-based rectifying devices.

Nanomaterial	Device type	Substrate	Performance	Year	Ref.
CNTs	Schottky diode Ti/CNT/Pt	Si	$f_c = 540$ GHz (@ ± 0.17 V)	2005	[202]
	Schottky diode Cr/CNT/Pt	sapphire, quartz	$f_c = 400$ GHz (predicted)	2008	[203]
	Schottky diode Ti/CNT/Au	PEEK	$V_{out} = 1.8$ mV (@ 18 GHz) ($P_{in} = 13$ dBm)	2011	[215]
	TFT	PET	$f_T = 1$ GHz	2007	[214]
	TFT		$f_T = 7$ GHz $f_{max} = 15$ GHz	2012	[207]
	TFT	PI	$f_{max} = 118$ MHz	2012	[228]
Graphene	TFT	glass	$f_T = 427$ GHz	2012	[251]
	TFT	PI	$f_T = 2.2$ GHz $f_{max} = 550$ MHz	2012	[268]
	TFT	PI	$f_T = 25$ GHz $f_{max} = 2.1$ GHz	2013	[257]
	TFT	PI	$f_{T(intrinsic)} = 25$ GHz	2014	[259]
	TFT	PEN	$f_T = 12$ GHz $f_{max} = 10.6$ GHz	2015	[253]
Graphene oxide	Schottky diode Ti/r-GO/Pd	PEEK	$V_{out} = 0.1$ mV (@ 10 GHz) ($P_{in} = -10$ dBm)	2013	[269]
Black Phosphorus	TFT	PI	$f_{T(intrinsic)} = 17.5$ GHz $f_{max(intrinsic)} = 14.5$ GHz	2016	[280]

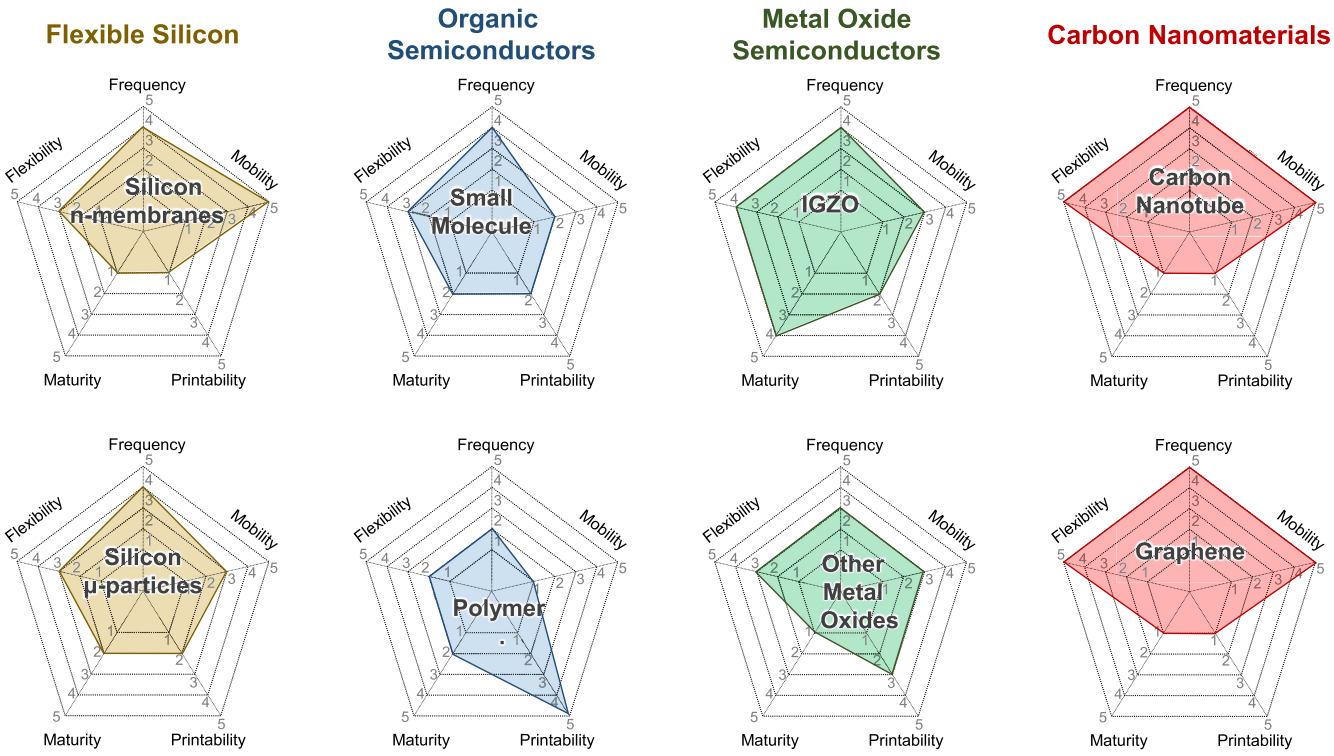

Figure 23. Main classes of semiconductor materials analysed in this review with respect to their: (i) frequency performance, (ii) charge carrier mobility, (iii) demonstrated processability via solution-phase techniques, (iv) technological maturity with regard to demonstrators relevant to the target end-application, and (v) mechanical flexibility.

performance, charge carrier mobility, their demonstrated capability to be processed through solution-phase (printing etc) techniques, the technological maturity with regard to demonstrators relevant to the target application area and their mechanical flexibility. The scoring scheme that was followed in order to construct this chart is explained in Table A2 in the appendix. From this figure, we may extract that polymeric materials are proven the most suitable for large-area printing

deposition but they still lack in terms of device performance. Interestingly, the opposite is observed for the nanomaterial class of materials (high performance but low maturity and technology readiness level). High performance may be obtained from flexible silicon, but at the expense of complex processing procedures. Printed silicon particles may be a more scalable approach but the true potential of this technique has yet to be realised. Finally, considering the inorganic metal oxide-based materials, which are the hitherto champion materials as regards performance versus maturity level, it is evident that more emphasis should be given on the printability and ink formulation issues they face, or to reducing the cost in large-area vacuum deposition techniques.

There is no doubt that single-crystalline silicon rectifiers will remain at the forefront of technological progress for rigid substrate RFID technology, since they present the advantages of (a) very high mobility that leads to operating frequencies up to the wireless communications (microwave) bands, and (b) compatibility with already established scalable fabrication processes that enable facile integration of the various electronic components in the final circuit/system. Successful transfer of this concept to flexible substrates is expected to deliver the best of both worlds, i.e., functionality versus scalability. One major hurdle for this approach is whether these techniques will be cost-competitive to the much simpler and less time-consuming rapidly evolving printing technologies. The current approach of transferring nanomembranes from rigid to flexible substrates, though capable of delivering high quality results on a small scale, it appears not to be scalable in a high-throughput industrial sense. Exploiting the properties of monocrystalline Si through the solution processing of microparticles may be more scalable, but still is a way off commercialisation.

MOSs, with IGZO leading the field, have demonstrated significant technological maturity to be a strong candidate to succeed Si in the flexible RF rectification race. Several examples of working TFT-based rectifiers integrated with additional circuitry in the HF band have been made. This, coupled with the proven industrial maturity of IGZO for relatively large-area deposition (display industry) is promising for the adoption of IGZO for flexible HF RFID technology. Recently, it was shown that flexible devices based on IGZO may well operate at Bluetooth frequencies and, thus, extend their range of applications up to and beyond UHF electronics. Of note is that diodes rather than TFTs have been the device type to achieve these levels of UHF performance. Alternative metal oxides, including binary as well as more complex oxides, should not be discounted however, and may provide an easier route towards solution processed, and thus significantly lower cost, RF devices.

Organic semiconductors arguably are the material class that shows the greatest level of interest and development for HF RFID applications. Progress on small molecules and polymers has shown that both are capable of operation and integration with devices at 13.56 MHz. While the majority of work on small molecules has focused on vacuum processed techniques, there is promise in printable large-area small molecule organic electronics, through combining blend materials with lateral devices, the use of precursors and soluble small molecule derivatives and primarily through the emergence of new high mobility solution-processable small molecules combined with novel deposition techniques. This is clear when one considers that even vacuum-deposited small molecule devices with the highest operating frequency (>1 GHz) exhibit carrier mobilities of $<1\ cm^2\ V^{-1}\ s^{-1}$. Doubtless the operating frequency limits of small molecule-based devices will be pushed in coming years as solution processed small molecules, which have shown substantially higher mobility ($>10\ cm^2\ V^{-1}\ s^{-1}$) [281] are tested for frequency response. Conjugated polymers are most likely to find applications at 13.56 MHz. Further optimisation of processing combined with the development of novel high mobility polymers may well yield more efficient rectifiers. Undoubtedly such developments will make this particular class of semiconducting materials highly interesting primarily due to their unmatched solution processability and layer uniformity—two much sought-after characteristics required for efficient large-area electronics manufacturing.

Finally, the scientifically exciting class of nanomaterials, such as CNTs, graphene and other emerging 2D nanostructures, combine inherent flexibility with ultra-high carrier mobility, and hold promise for extremely high levels of performance. However, their unique properties also hold some cause for concern. For example, in the case of CNTs, the quantum conductance arising from the quasi-1D nature of the material leads to a problem of impedance mismatch. In the case of graphene, the electronic band properties, which give rise to extremely high mobilities, are coupled with the lack of a bandgap, meaning achieving rectification in devices of significant levels is a challenge. There are of course, strategies to overcome these issues, namely device and material engineering, as well as looking to the new class of emerging 2D nanomaterials. However, a final problem comes in the large-area deposition of these materials for high throughput device fabrication. Thus, while possibly holding the greatest natural potential for HF flexible electronics, it is evident that nanomaterials are the furthest from commercial realisation in this regard.

In all four classes of materials discussed here, there is much scope for development and improvement. Those most compatible with large-area deposition techniques (i.e. organics) suffer from the poorest performance at RF, while those with the highest performance at RF (i.e. nanomaterials) suffer the lowest level of large-area deposition development. With complex challenges yet to be overcome and huge potential for the societal impact of the realised technology, we thus conclude that the field of flexible HF rectifiers and electronics as a whole will continue to be an active area of research over the coming years.

Acknowledgments

The authors are grateful to the European Research Council (ERC) AMPRO grant number 280221, the European Union's Horizon 2020 research and innovation programme, under the Marie Skłodowska-Curie grant agreement 706707, and the Engineering and Physical Sciences Research Council (EPSRC) Centre for Innovative Manufacturing in Large Area Electronics (CIM-LAE) grant no. EP/K03099X/1 for financial support.

Appendix

Table A1. Corresponding values of device operating frequency and carrier mobility as shown graphically in figure 7(a).

Reference	Frequency (MHz)	Device type	Mobility ($cm^2\ V^{-1}\ s^{-1}$)	Material
Silicon nanomembrane				
[54]	1900	TFT	230	Si
[61]	4900	TFT	160	Si
Metal oxide semiconductor				
[100]	25	TFT	15.1	IGZO
[98]	27	Heterojunction diode	15.06/2.11	IGZO/Cu2O
[107]	135	TFT	17.94	IGZO
[108]	384	TFT	12.7	IGZO
[90]	1800	Schottky diode	10	IGZO
[113]	6800	Schottky diode	10	IGZO
Organic semiconductor (small molecule)				
[108]	0.4	TFT	0.01	F_{16}CuPc
[126]	0.25	TFT	0.1	Pentacene
[129]	4	TFT	0.2	DNTT
[130]	7	TFT	0.3	DNTT
[131]	20	TFT	0.44	DNTT
[140]	50	Schottky diode	0.15	Pentacene
[142]	700	Schottky diode	0.15	Pentacene
[143]	1240	Schottky diode	0.11	Pentacene
[155]	700	Schottky diode	0.42	C_{60}
[154]	10	TFT	0.73	Pentacene
[154]	27.7	TFT	2.22	C_{60}
[42]	22	TFT	3	C_{10}-DNTBT
[161]	1	TFT	0.03	TIPS pentacene
Organic semiconductor (polymer)				
[173]	1	TFT	0.5	Lisicon® S1200
[175]	3.3	TFT	6.4	P(NDI2OD-T2)
Nanomaterial				
[228]	170	TFT	50	CNT
[251]	427 000	TFT	2000	Graphene
[257]	25 000	TFT	3900	Graphene
[259]	2400	TFT	8000	Graphene
[268]	2200	TFT	102	Graphene
[255]	7200	TFT	1500	Graphene
[258]	39 000	TFT	2500	Graphene
[256]	32 000	TFT	3000	Graphene
[275]	6000	TFT	8.3	Trilayer MoS_2
[277]	2700	TFT	54	MoS_2
[274]	2800	TFT	55	MoS_2

Table A2. The following scoring scheme was followed to construct the chart in figure 23 with data taken from respective references in the text.

Score	1	2	3	4	5
Frequency (MHz)	$<$13.56	$\sim$13.56	$\sim$100	$\sim$1000	$\sim$10 000
Mobility ($cm^2\ V^{-1}\ s^{-1}$)	$<$1	1	10	$\sim$100	$>$100
Printability	Solution processable material	Spin coated demonstration	More scalable demonstration (e.g. spray/dip coat)	Printing demonstration (gravure, inkjet etc)	Large scale (roll to roll) demonstration
Maturity	Little or no demos of target application but some promise	Maturity in academic literature	Commercial prototypes	Commercial applications in other areas	Commercial maturity
Flexibility	Performs under some strain	Measured $>$10 mm	$10 > x > 1$	$<$1	Theoretical limitation of bending up to 90°

ORCID iDs

Dimitra G Georgiadou https://orcid.org/0000-0002-2620-3346
Thomas D Anthopoulos https://orcid.org/0000-0002-0978-8813

References

[1] Bradley J, Reberger C, Dixit A and Gupta V 2013 Internet of everything: a $4.6 trillion public-sector opportunity: http://internetofeverything.cisco.com/sites/default/files/docs/en/ioe_public_sector_vas_white%20paper_121913final.pdf: Cisco

[2] Reindl L, Scholl G, Ostertag T, Ruppel C C W, Bulst W E and Seifert F 1996 SAW devices as wireless passive sensors *1996 IEEE Ultrasonics Symp. Proc.* pp 363–7

[3] Stockman H 1948 Communication by means of reflected power *Proc. IRA* **36** 1196–204

[4] Landt J 2005 The history of RFID *IEEE Potentials* **24** 8–11

[5] Milanovic V, Gaitan M, Marshall J C and Zaghloul M E 1996 CMOS foundry implementation of Schottky diodes for RF detection *IEEE Trans. Electron Devices* **43** 2210–4

[6] Rao K V S, Nikitin P V and Lam S F 2005 Antenna design for UHF RFID tags: a review and a practical application *IEEE Trans. Antennas Propag.* **53** 3870–6

[7] Akshay Uttama Nambi S N, Prabhakar T V, Jamadagni H S, Kishan G, Pramod B K, Rakesh C M and Sanjay Naik R 2012 *Wireless Networks and Computational Intelligence: 6th Int. Conf. on Information Processing, ICIP 2012 (Bangalore, India, 10–12 August 2012)* (Berlin: Springer) pp 1–10

[8] Patel M and Wang J 2010 Applications, challenges, and prospective in emerging body area networking technologies *IEEE Wirel. Commun. Mag.* **17** 80–8

[9] Rathnayaka A J D, Potdar V M and Kuruppu S J 2011 Evaluation of wireless home automation technologies *2011 IEEE 5th Int. Conf. on Digital Ecosystems and Technologies (IEEE-DEST)* pp 76–81

[10] Jabbar H, Song Y S and Jeong T T 2010 RF energy harvesting system and circuits for charging of mobile devices *IEEE Trans. Consum. Electron.* **56** 247–53

[11] Visser H J and Vullers R J M 2013 RF energy harvesting and transport for wireless sensor network applications: principles and requirements *Proc. IEEE* **101** 1410–23

[12] Pinuela M, Mitcheson P D and Lucyszyn S 2013 Ambient RF energy harvesting in urban and semi-urban environments *IEEE Trans. Microw. Theory Tech.* **61** 2715–26

[13] Das R and Harrop P 2016 RFID Forecasts, Players and Opportunities 2016–2026 www.IDTechEx.com/RFID: IDTechEx Research

[14] Nathanson D and Wimmer T 2009 RFID Readers, Track 1, Volume 2: The 2009 RFID Business Planning Service—An Executive Brief, http://vdcresearch.com/_Documents/executivebrief/wp-attachment-2528.pdf: VDC Research

[15] Perret E 2014 *Radio Frequency Identification and Sensors: from RFID to Chipless RFID* (New York: Wiley)

[16] Arias A C, MacKenzie J D, McCulloch I, Rivnay J and Salleo A 2010 Materials and applications for large area electronics: solution-based approaches *Chem. Rev.* **110** 3–24

[17] 2016 *Printed Electronics: Materials, Technologies and Applications* (New York: Wiley)

[18] Caironi M and Yong-Young N 2015 *Large Area and Flexible Electronics* (New York: Wiley)

[19] Koden M 2017 *OLED Display and Lighting* (UK: Wiley-IEEE)

[20] Tang C W and Vanslyke S A 1987 Organic electroluminescent diodes *Appl. Phys. Lett.* **51** 913–5

[21] Friend R H *et al* 1999 Electroluminescence in conjugated polymers *Nature* **397** 121–8

[22] Sariciftci N S, Smilowitz L, Heeger A J and Wudl F 1992 Photoinduced electron-transfer from a conducting polymer to buckminsterfullerene *Science* **258** 1474–6

[23] Sirringhaus H *et al* 1999 Two-dimensional charge transport in self-organized, high-mobility conjugated polymers *Nature* **401** 685–8

[24] Brabec C J, Sariciftci N S and Hummelen J C 2001 Plastic solar cells *Adv. Funct. Mater.* **11** 15–26

[25] Caironi M, Anthopoulos T D, Noh Y-Y and Zaumseil J 2013 Organic and hybrid materials for flexible electronics *Adv. Mater.* **25** 4208–9

[26] Facchetti A 2014 Printed diodes operating at mobile phone frequencies *Proc. Natl Acad. Sci. USA* **111** 11917–8

[27] Cantatore E, Geuns T C T, Gelinck G H, van Veenendaal E, Gruijthuijsen A F A, Schrijnemakers L, Drews S and de Leeuw D M 2007 A 13.56 MHz RFID system based on organic transponders *IEEE J. Solid-State Circuits* **42** 84–92

[28] Bohm M, Ullmann A, Zipperer D, Knobloch A, Glauert W H and Fix W 2006 Printable electronics for polymer RFID applications *2006 IEEE Int. Solid State Circuits Conf.—Digest of Technical Papers* pp 1034–41

[29] Rost H and Mildner W 2008 Latest Advances: On the Way to Printed Electronics, Kunststoffe International https://kunststoffe.de/en/journal/archive/article/latest-advances-on-the-way-to-printed-electronics-585302.html pp 60–4

[30] Riethus K and Rost H 2012 PolyIC's Approach to Printed Electronics: http://polyic.com/fileadmin/images/content-images/presse_news_events/News/Artikel_Convertech_PolyIC.pdf: PolyIC GmbH & Co. KG pp 36–9

[31] Finkenzeller K 2010 *RFID Handbook: Fundamentals and Applications in Contactless Smart Cards, Radio Frequency Identification and Near-Field Communication* (New York: Wiley)

[32] Juels A 2006 RFID security and privacy: a research survey *IEEE J. Sel. Areas Commun.* **24** 381–94

[33] http://idtechex.com/research/reports/rfid-forecasts-players-and-opportunities-2016-2026-000451.asp IDTechEx Research

[34] Zhou Y, Froppier B and Razban T 2012 Schottky diode rectifier for power harvesting application *2012 IEEE Int. Conf. on RFID-Technologies and Applications (RFID-TA)* pp 429–32

[35] Sani N *et al* 2014 All-printed diode operating at 1.6 GHz *Proc. Natl Acad. Sci. USA* **111** 11943–8

[36] Sze S M and Ng K K 2007 *Physics of Semiconductor Devices* (New York: Wiley)

[37] Bhatnagar M, McLarty P K and Baliga B J 1992 Silicon-carbide high-voltage (400 V) Schottky barrier diodes *IEEE Electron Device Lett.* **13** 501–3

[38] Lin G-C, Lee M-W and Hsu Y-C 2012 An AC–DC rectifier for RF energy harvesting system *2012 Asia-Pacific Microwave Conf. Proc. (APMC)* pp 1052–4

[39] Koji K and Takashi I 2007 High efficiency CMOS rectifier circuit with self-Vth-cancellation and power regulation functions for UHF RFIDs *2007 IEEE Asian Solid-State Circuits Conf. (ASSCC)* pp 119–22

[40] Shen J, Wang B, Liu S, Wang X A, Ruan Z and Li S 2013 A passive UHF RFID tag with a dynamic-Vth-cancellation rectifier *J. Semiconduct.* **34** 095005

[41] Chasin A, Volskiy V, Libois M, Myny K, Nag M, Rockele M, Vandenbosch G A E, Genoe J, Gielen G and Heremans P 2014 An integrated a-IGZO UHF energy harvester for passive RFID tags *IEEE Trans. Electron Devices* **61** 3289–95

[42] Uno M *et al* 2015 Short-channel solution-processed organic semiconductor transistors and their application in high-speed organic complementary circuits and organic rectifiers *Adv. Electron. Mater.* **1** 6

[43] McSpadden J O, Fan L and Chang K 1998 Design and experiments of a high-conversion-efficiency 5.8 GHz rectenna *IEEE Trans. Microw. Theory Tech.* **46** 2053–60

[44] Heremans P, Tripathi A K, de de Meux A, Smits E C P, Hou B, Pourtois G and Gelinck G H 2016 Mechanical and electronic properties of thin-film transistors on plastic, and their integration in flexible electronic applications *Adv. Mater.* **28** 4266–82

[45] Nisato G, Lupo D and Ganz S 2016 *Organic and Printed Electronics: Fundamentals and Applications* (USA: Pan Stanford Publishing)

[46] Wong W S and Saleo A 2009 *Flexible Electronics: Materials and Applications* (Berlin: Springer)

[47] Kao H L, Chin A, Hung B F, Lee C F, Lai J M, McAlister S P, Sarnudra G S, Yoo W J and Chi C C 2005 Low noise RF MOSFETs on flexible plastic substrates *IEEE Electron Device Lett.* **26** 489–91

[48] Lecavelier des Etangs-Levallois A, Dubois E, Lesecq M, Danneville F, Poulain L, Tagro Y, Lepilliet S, Gloria D, Raynaud C and Troadec D 2011 150 GHz RF SOI-CMOS technology in ultrathin regime on organic substrate *IEEE Electron Device Lett.* **32** 1510–2

[49] Lecavelier des Etangs-Levallois A, Lesecq M, Danneville F, Tagro Y, Lepilliet S, Hoel V, Troadec D, Gloria D, Raynaud C and Dubois E 2013 Radio-frequency and low noise characteristics of SOI technology on plastic for flexible electronics *Solid-State Electron.* **90** 73–8

[50] Lecavelier des Etangs-Levallois A *et al* 2013 A converging route towards very high frequency, mechanically flexible, and performance stable integrated electronics *J. Appl. Phys.* **113** 153701

[51] Rogers J A, Lagally M G and Nuzzo R G 2011 Synthesis, assembly and applications of semiconductor nanomembranes *Nature* **477** 45–53

[52] Reuss R H 2005 Macroelectronics: perspectives on technology and applications *Proc. IEEE* **93** 1239–56

[53] Yuan H-C, Ma Z, Roberts M M, Savage D E and Lagally M G 2006 High-speed strained-single-crystal-silicon thin-film transistors on flexible polymers *J. Appl. Phys.* **100** 013708

[54] Yuan H-C and Ma Z 2006 Microwave thin-film transistors using Si nanomembranes on flexible polymer substrate *Appl. Phys. Lett.* **89** 212105

[55] Yuan H-C, Celler G K and Ma Z 2007 7.8 GHz flexible thin-film transistors on a low-temperature plastic substrate *J. Appl. Phys.* **102** 034501

[56] Sun L, Qin G, Seo J-H, Celler G K, Zhou W and Ma Z 2010 12 GHz thin-film transistors on transferrable silicon nanomembranes for high-performance flexible electronics *Small* **6** 2553–7

[57] Qin G, Yuan H-C, Celler G K, Zhou W, Ma J and Ma Z 2011 RF model of flexible microwave single-crystalline silicon nanomembrane PIN diodes on plastic substrate *Microelectron. J.* **42** 509–14

[58] Ma Z, Zhang K, Seo J-H, Zhou H, Sun L, Yuan H-C, Qin G, Pang H and Zhou W 2011 Fast flexible electronics based on printable thin mono-crystalline silicon *ECS Trans.* **34** 137–42

[59] Qin G, Yuan H-C, Qin Y, Seo J-H, Wang Y, Ma J and Ma Z 2013 Fabrication and characterization of flexible microwave single-crystal germanium nanomembrane diodes on a plastic substrate *IEEE Electron Device Lett.* **34** 160–2

[60] Qin G, Cai T, Yuan H-C, Seo J-H, Ma J and Ma Z 2014 Flexible radio-frequency single-crystal germanium switch on plastic substrates *Appl. Phys. Lett.* **104** 163501

[61] Seo J-H, Chang T-H, Lee J, Sabo R, Zhou W, Cai Z, Gong S and Ma Z 2015 Microwave flexible transistors on cellulose nanofibrillated fiber substrates *Appl. Phys. Lett.* **106** 262101

[62] Jung Y H *et al* 2015 High-performance green flexible electronics based on biodegradable cellulose nanofibril paper *Nat. Commun.* **6** 7170

[63] Menard E, Nuzzo R G and Rogers J A 2005 Bendable single crystal silicon thin film transistors formed by printing on plastic substrates *Appl. Phys. Lett.* **86** 093507

[64] Ahn J-H, Kim H-S, Lee K J, Zhu Z, Menard E, Nuzzo R G and Rogers J A 2006 High-speed mechanically flexible single-crystal silicon thin-film transistors on plastic substrates *IEEE Electron Device Lett.* **27** 460–2

[65] Sun Y, Menard E, Rogers J A, Kim H-S, Kim S, Chen G, Adesida I, Dettmer R, Cortez R and Tewksbury A 2006 Gigahertz operation in flexible transistors on plastic substrates *Appl. Phys. Lett.* **88** 183509

[66] Wang C, Chien J-C, Fang H, Takei K, Nah J, Plis E, Krishna S, Niknejad A M and Javey A 2012 Self-aligned, extremely high frequency III–V metal–oxide–semiconductor field-effect transistors on rigid and flexible substrates *Nano Lett.* **12** 4140–5

[67] Ko H *et al* 2010 Ultrathin compound semiconductor on insulator layers for high-performance nanoscale transistors *Nature* **468** 286–9

[68] Kooy N, Mohamed K, Pin L T and Guan O S 2014 A review of roll-to-roll nanoimprint lithography *Nanoscale Res. Lett.* **9** 320

[69] Seo J-H, Ling T, Gong S, Zhou W, Ma A L, Guo L J and Ma Z 2016 Fast flexible transistors with a nanotrench structure *Sci. Rep.* **6** 24771

[70] Sani N, Wang X, Granberg H, Ersman P A, Crispin X, Dyreklev P, Engquist I, Gustafsson G and Berggren M 2016 Flexible lamination-fabricated ultra-high frequency diodes based on self-supporting semiconducting composite film of silicon micro-particles and nano-fibrillated cellulose *Sci. Rep.* **6** 28921

[71] Klasens H A and Koelmans H 1964 A tin oxide field-effect transistor *Solid-State Electron.* **7** 701–2

[72] Boesen G F and Jacobs J E 1968 ZnO field-effect transistor *Proc. IEEE* **56** 2094–5

[73] Nomura K, Ohta H, Takagi A, Kamiya T, Hirano M and Hosono H 2004 Room-temperature fabrication of transparent flexible thin-film transistors using amorphous oxide semiconductors *Nature* **432** 488–92

[74] Wager J F, Yeh B, Hoffman R L and Keszler D A 2014 An amorphous oxide semiconductor thin-film transistor route to oxide electronics *Curr. Opin. Solid State Mater. Sci.* **18** 53–61

[75] Ghaffarzadeh K and Das R 2014 *Metal Oxide TFT Backplanes for Displays 2014–2024: Technologies, Forecasts, Players Read* (IDTechEx)

[76] Yu X, Marks T J and Facchetti A 2016 Metal oxides for optoelectronic applications *Nat. Mater.* **15** 383–96

[77] Suresh A, Gollakota P, Wellenius P, Dhawan A and Muth J F 2008 Transparent, high mobility InGaZnO thin films deposited by PLD *Thin Solid Films* **516** 1326–9

[78] von Wenckstern H *et al* 2007 Homoepitaxy of ZnO by pulsed-laser deposition *Phys. Status Solidi (RRL)—Rapid Res. Lett.* **1** 129–31

[79] Illiberi A, Cobb B, Sharma A, Grehl T, Brongersma H, Roozeboom F, Gelinck G and Poodt P 2015 Spatial atmospheric atomic layer deposition of InxGayZnzO for thin film transistors *ACS Appl. Mater. Interfaces* **7** 3671–5

[80] Ellinger C R and Nelson S F 2014 Selective area spatial atomic layer deposition of ZnO, Al_2O_3, and aluminum-doped ZnO using poly(vinyl pyrrolidone) *Chem. Mater.* **26** 1514–22

[81] Pan C A and Ma T P 1980 High-quality transparent conductive indium oxide films prepared by thermal evaporation *Appl. Phys. Lett.* **37** 163–5
[82] Fouad O A, Ismail A A, Zaki Z I and Mohamed R M 2006 Zinc oxide thin films prepared by thermal evaporation deposition and its photocatalytic activity *Appl. Catalysis* B **62** 144–9
[83] Lee J-H *et al* 2008 42.2: World's largest (15-inch) XGA AMLCD panel using IGZO oxide TFT *SID Symp. Dig. Tech. Pap.* **39** 625–8
[84] Wang Y-L, Covert L N, Anderson T J, Lim W, Lin J, Pearton S J, Norton D P, Zavada J M and Ren F 2008 RF characteristics of room-temperature-deposited, small gate dimension indium zinc oxide TFTs *Electrochem. Solid State Lett.* **11** H60–2
[85] Wang H-C, Lin C-K, Chiu H-C and Hsueh K-P 2009 ZnO based thin-film transistor with high-k gadolinium and praseodymium oxide as gate dielectric *2009, IEEE Int. Conf. of Electron Devices and Solid-State Circuits, 2009, EDSSC* pp 205–8
[86] Thomas S R, Pattanasattayavong P and Anthopoulos T D 2013 Solution-processable metal oxide semiconductors for thin-film transistor applications *Chem. Soc. Rev.* **42** 6910–23
[87] Heo S J and Jung T S 2013 Recent advances in low-temperature solution-processed oxide backplanes *J. Inf. Disp.* **14** 79–87
[88] Kim M-G, Kanatzidis M G, Facchetti A and Marks T J 2011 Low-temperature fabrication of high-performance metal oxide thin-film electronics via combustion processing *Nat. Mater.* **10** 382–8
[89] Banger K K, Yamashita Y, Mori K, Peterson R L, Leedham T, Rickard J and Sirringhaus H 2011 Low-temperature, high-performance solution-processed metal oxide thin-film transistors formed by a 'sol–gel on chip' process *Nat. Mater.* **10** 45–50
[90] Kim Y-H, Heo J-S, Kim T-H, Park S, Yoon M-H, Kim J, Oh M S, Yi G-R, Noh Y-Y and Park S K 2012 Flexible metal-oxide devices made by room-temperature photochemical activation of sol–gel films *Nature* **489** 128–32
[91] Lin Y-H, Faber H, Zhao K, Wang Q, Amassian A, McLachlan M and Anthopoulos T D 2013 High-performance ZnO transistors processed via an aqueous carbon-free metal oxide precursor route at temperatures between 80 °C and 180 °C *Adv. Mater.* **25** 4340–6
[92] Lin Y-H *et al* 2015 High electron mobility thin-film transistors based on solution-processed semiconducting metal oxide heterojunctions and quasi-superlattices *Adv. Sci.* **2** 1500058
[93] Semple J, Rossbauer S, Burgess C H, Zhao K, Jagadamma L K, Amassian A, McLachlan M A and Anthopoulos T D 2016 Radio frequency coplanar ZnO Schottky nanodiodes processed from solution on plastic substrates *Small* **12** 1993–2000
[94] Semple J, Rossbauer S and Anthopoulos T D 2016 Analysis of Schottky contact formation in coplanar Au/ZnO/Al nanogap radio frequency diodes processed from solution at low temperature *ACS Appl. Mater. Interfaces* **8** 23167–74
[95] Beesley D J, Semple J, Jagadamma L K, Amassian A, McLachlan M A, Anthopoulos T D and deMello J C 2014 Sub-15 nm patterning of asymmetric metal electrodes and devices by adhesion lithography *Nat. Commun.* **5** 3933
[96] Park H, Kang H, Lee Y, Park Y, Noh J and Cho G 2012 Fully roll-to-roll gravure printed rectenna on plastic foils for wireless power transmission at 13.56 MHz *Nanotechnology* **23** 344006
[97] Kang H, Park H, Park Y, Jung M, Kim B C, Wallace G and Cho G 2014 Fully roll-to-roll gravure printable wireless (13.56 MHz) sensor-signage tags for smart packaging *Sci. Rep.* **4** 5387
[98] Chen W C, Hsu P C, Chien C W, Chang K M, Hsu C J, Chang C H, Lee W K, Chou W F, Hsieh H H and Wu C C 2014 Room-temperature-processed flexible n-InGaZnO/p-Cu2O heterojunction diodes and high-frequency diode rectifiers *J. Phys. D: Appl. Phys.* **47** 365101
[99] Kawamura T, Uchiyama H, Saito S, Wakana H, Mine T, Hatano M, Torii K and Onai T 2008 1.5 V operating fully-depleted amorphous oxide thin film transistors achieved by 63 mV dec^{-1} subthreshold slope *2008 IEEE Int. Electron Devices Meeting* pp 1–4
[100] Kawamura T, Wakana H, Fujii K, Ozaki H, Watanabe K, Yamazoe T, Uchiyama H and Torii K 2010 Oxide TFT rectifier achieving 13.56 MHz wireless operation with DC output up to 12 V *2010 IEEE Int. Electron Devices Meeting (IEDM)* pp 21.4.1–4
[101] Ozaki H, Kawamura T, Wakana H, Yamazoe T and Uchiyama H 2011 20 μW operation of an a-IGZO TFT-based RFID chip using purely NMOS 'active' load logic gates with ultra-low-consumption power *2011 Symp. on VLSI Circuits (VLSIC)* pp 54–5 http://ieeexplore.ieee.org/document/5986421
[102] Tripathi A K *et al* 2011 Low-voltage gallium–indium–zinc–oxide thin film transistors based logic circuits on thin plastic foil: building blocks for radio frequency identification application *Appl. Phys. Lett.* **98** 162102
[103] Myny K, Tripathi A K, van der Steen J L and Cobb B 2015 Flexible thin-film NFC tags *IEEE Commun. Mag.* **53** 182–9
[104] Myny K, Cobb B, van der Steen J-L, Tripathi A K, Genoe J, Gelinck G, Heremans P and IEEE 2015 Flexible thin-film NFC tags powered by commercial USB reader device at 13.56 MHz *2015 IEEE Int. Solid-State Circuits Conf. (ISSCC) (San Francisco, CA)* pp 294–6
[105] Tripathi A K, Myny K, Hou B, Wezenberg K and Gelinck G H 2015 Electrical characterization of flexible InGaZnO transistors and 8-b transponder chip down to a bending radius of 2 mm *IEEE Trans. Electron Devices* **62** 4063–8
[106] Cho S H, Kim S W, Cheong W S, Byun C W, Hwang C-S, Cho K I and Bae B S 2010 Oxide thin film transistor circuits for transparent RFID applications *IEICE Trans. Electron.* **E93.C** 1504–10
[107] Yang B D, Oh J M, Kang H J, Park S H, Hwang C S, Ryu M K and Pi J E 2013 A transparent logic circuit for RFID tag in a-IGZO TFT technology *ETRI J.* **35** 610–6
[108] Muenzenrieder N, Petti L, Zysset C, Kinkeldei T, Salvatore G A and Troester G 2013 Flexible self-aligned amorphous InGaZnO thin-film transistors with submicrometer channel length and a transit frequency of 135 MHz *IEEE Trans. Electron Devices* **60** 2815–20
[109] Su L-Y and Huang J 2015 Demonstration of radio-frequency response of amorphous IGZO thin film transistors on the glass substrate *Solid-State Electron.* **104** 122–5
[110] Chasin A, Steudel S, Vanaverbeke F, Myny K, Nag M, Tung-Huei K, Schols S, Gielen G, Genoe J and Heremans P 2012 UHF IGZO Schottky diode *2012 IEEE Int. Electron Devices Meeting (IEDM)* pp 12.4.1–4
[111] Chasin A, Nag M, Bhoolokam A, Myny K, Steudel S, Schols S, Genoe J, Gielen G and Heremans P 2013 Gigahertz operation of a-IGZO Schottky diodes *IEEE Trans. Electron Devices* **60** 3407–12
[112] Chasin A, Steudel S, Myny K, Nag M, Ke T-H, Schols S, Genoe J, Gielen G and Heremans P 2012 High-performance a-In–Ga–Zn–O Schottky diode with oxygen-treated metal contacts *Appl. Phys. Lett.* **101** 113505
[113] Zhang J, Li Y, Zhang B, Wang H, Xin Q and Song A 2015 Flexible indium–gallium-–zinc–oxide Schottky diode operating beyond 2.45 GHz *Nat. Commun.* **6** 7561

[114] Köhler A and Bässler H 2009 Triplet states in organic semiconductors *Mater. Sci. Eng.: R: Rep.* **66** 71–109
[115] Shirakawa H 2001 Nobel lecture: the discovery of polyacetylene film—the dawning of an era of conducting polymers *Rev. Mod. Phys.* **73** 713–8
[116] Chiang C K, Fincher C R, Park Y W, Heeger A J, Shirakawa H, Louis E J, Gau S C and Macdiarmid A G 1977 Electrical conductivity in doped polyacetylene *Phys. Rev. Lett.* **39** 1098–101
[117] Bässler H and Köhler A 2012 *Unimolecular and Supramolecular Electronics I: Chemistry and Physics Meet at Metal-Molecule Interfaces* ed M R Metzger (Berlin: Springer) pp 1–65
[118] Reese C and Bao Z 2007 Organic single-crystal field-effect transistors *Mater. Today* **10** 20–7
[119] Anthony J E 2008 The larger acenes: versatile organic semiconductors *Angew. Chem., Int. Ed.* **47** 452–83
[120] Salleo A 2007 Charge transport in polymeric transistors *Mater. Today* **10** 38–45
[121] Baeg K J, Caironi M and Noh Y Y 2013 Toward printed integrated circuits based on unipolar or ambipolar polymer semiconductors *Adv. Mater.* **25** 4210–44
[122] Zaki T, Rodel R, Letzkus F, Richter H, Zschieschang U, Klauk H and Burghartz J N 2013 AC characterization of organic thin-film transistors with asymmetric gate-to-source and gate-to-drain overlaps *Org. Electron.* **14** 1318–22
[123] Zschieschang U *et al* 2013 Megahertz operation of flexible low-voltage organic thin-film transistors *Org. Electron.* **14** 1516–20
[124] Uemura T *et al* 2014 Split-gate organic field-effect transistors for high-speed operation *Adv. Mater.* **26** 2983–8
[125] Palfinger U *et al* 2010 Fabrication of n- and p-type organic thin film transistors with minimized gate overlaps by self-aligned nanoimprinting *Adv. Mater.* **22** 5115–9
[126] Gold H *et al* 2015 Self-aligned flexible organic thin-film transistors with gates patterned by nano-imprint lithography *Org. Electron.* **22** 140–6
[127] Ante F *et al* 2012 Contact resistance and megahertz operation of aggressively scaled organic transistors *Small* **8** 73–9
[128] Xu Y, Liu C, Scheideler W, Darmawan P, Li S, Balestra F, Ghibaudo G and Tsukagoshi K 2013 How small the contacts could be optimal for nanoscale organic transistors? *Org. Electron.* **14** 1797–804
[129] Uno M, Nakayama K, Soeda J, Hirose Y, Miwa K, Uemura T, Nakao A, Takimiya K and Takeya J 2011 High-speed flexible organic field-effect transistors with a 3D structure *Adv. Mater.* **23** 3047–51
[130] Nakahara R, Uno M, Uemura T, Takimiya K and Takeya J 2012 Flexible three-dimensional organic field-effect transistors fabricated by an imprinting technique *Adv. Mater.* **24** 5212–6
[131] Uno M, Cha B-S, Kanaoka Y and Takeya J 2015 High-speed organic transistors with three-dimensional organic channels and organic rectifiers based on them operating above 20 MHz *Org. Electron.* **20** 119–24
[132] Lin Y Y, Gundlach D J, Nelson S F and Jackson T N 1997 Stacked pentacene layer organic thin-film transistors with improved characteristics *IEEE Electron Device Lett.* **18** 606–8
[133] Gundlach D J, Jia L L and Jackson T N 2001 Pentacene TFT with improved linear region characteristics using chemically modified source and drain electrodes *IEEE Electron Device Lett.* **22** 571–3
[134] Klauk H, Halik M, Zschieschang U, Schmid G, Radlik W and Weber W 2002 High-mobility polymer gate dielectric pentacene thin film transistors *J. Appl. Phys.* **92** 5259–63
[135] Kroto H W, Heath J R, O'Brien S C, Curl R F and Smalley R E 1985 C60: buckminsterfullerene *Nature* **318** 162–3
[136] Haddon R C, Perel A S, Morris R C, Palstra T T M, Hebard A F and Fleming R M 1995 C60 thin film transistors *Appl. Phys. Lett.* **67** 121–3
[137] Brabec C J, Gowrisanker S, Halls J J M, Laird D, Jia S J and Williams S P 2010 Polymer-fullerene bulk-heterojunction solar cells *Adv. Mater.* **22** 3839–56
[138] Baude P F, Ender D A, Haase M A, Kelley T W, Muyres D V and Theiss S D 2003 Pentacene-based radio-frequency identification circuitry *Appl. Phys. Lett.* **82** 3964–6
[139] Marien H, Steyaert M, Steudel S, Vicca P, Smout S, Gelinck G and Heremans P 2010 An organic integrated capacitive DC–DC up-converter *2010 Proc. ESSCIRC* pp 510–3
[140] Steudel S, Myny K, Arkhipov V, Deibel C, De Vusser S, Genoe J and Heremans P 2005 50 MHz rectifier based on an organic diode *Nat. Mater.* **4** 597–600
[141] Steudel S, De Vusser S, Myny K, Lenes M, Genoe J and Heremans P 2006 Comparison of organic diode structures regarding high-frequency rectification behavior in radio-frequency identification tags *J. Appl. Phys.* **99** 7
[142] Steudel S, Myny K, Vicca P, Cheyns D, Genoe J and Heremans P 2008 Ultra-high frequency rectification using organic diodes *2008 IEEE Int. Electron Devices Meeting (IEDM)* pp 1–4
[143] Kang C M *et al* 2016 1 GHz pentacene diode rectifiers enabled by controlled film deposition on SAM-treated Au anodes *Adv. Electron. Mater.* **2** 1500282
[144] Cvetkovic N V, Sidler K, Savu V, Brugger J, Tsamados D and Ionescu A M 2012 Organic half-wave rectifier fabricated by stencil lithography on flexible substrate *Microelectron. Eng.* **100** 47–50
[145] Myny K, Steudel S, Vicca P, Genoe J and Heremans P 2008 An integrated double half-wave organic Schottky diode rectifier on foil operating at 13.56 MHz *Appl. Phys. Lett.* **93** 093305
[146] Gutierrez-Heredia G, Martinez-Landeros V H, Aguirre-Tostado F S, Shah P, Gnade B E, Sotelo-Lerma M and Quevedo-Lopez M A 2012 Full bridge circuit based on pentacene schottky diodes fabricated on plastic substrates *Semicond. Sci. Technol.* **27** 085013
[147] Myny K, Steudel S, Vicca P, Beenhakkers M J, van Aerle N A J M, Gelinck G H, Genoe J, Dehaene W and Heremans P 2009 Plastic circuits and tags for 13.56 MHz radio-frequency communication *Solid-State Electron.* **53** 1220–6
[148] Ma H, Yip H-L, Huang F and Jen A K Y 2010 Interface engineering for organic electronics *Adv. Funct. Mater.* **20** 1371–88
[149] DiBenedetto S A, Facchetti A, Ratner M A and Marks T J 2009 Molecular self-assembled monolayers and multilayers for organic and unconventional inorganic thin-film transistor applications *Adv. Mater.* **21** 1407–33
[150] Love J C, Estroff L A, Kriebel J K, Nuzzo R G and Whitesides G M 2005 Self-assembled monolayers of thiolates on metals as a form of nanotechnology *Chem. Rev.* **105** 1103–69
[151] Seong Hyun K, Jung Hun L, Sang Chul L, Yong Suk Y and Taehyoung Z 2004 Improved contact properties for organic thin-film transistors using self-assembled monolayer *Japan. J. Appl. Phys.* **43** L60
[152] Hong J-P, Park A-Y, Lee S, Kang J, Shin N and Yoon D Y 2008 Tuning of Ag work functions by self-assembled monolayers of aromatic thiols for an efficient hole injection for solution processed triisopropylsilylethynyl pentacene organic thin film transistors *Appl. Phys. Lett.* **92** 143311
[153] Kitamura M and Arakawa Y 2011 High current-gain cutoff frequencies above 10 MHz in n-channel C60 and p-channel

pentacene thin-film transistors *Japan. J. Appl. Phys.* **50** 01BC01
[154] Kitamura M, Kuzumoto Y, Aomori S, Kamura M, Na J H and Arakawa Y 2009 Threshold voltage control of bottom-contact n-channel organic thin-film transistors using modified drain/source electrodes *Appl. Phys. Lett.* **94** 083310
[155] Im D, Moon H, Shin M, Kim J and Yoo S 2011 Towards gigahertz operation: ultrafast low turn-on organic diodes and rectifiers based on C-60 and tungsten oxide *Adv. Mater.* **23** 644–8
[156] Pal B N, Sun J, Jung B J, Choi E, Andreou A G and Katz H E 2008 Pentacene-zinc oxide vertical diode with compatible grains and 15 MHz rectification *Adv. Mater.* **20** 1023
[157] Olthof S, Tress W, Meerheim R, Lüssem B and Leo K 2009 Photoelectron spectroscopy study of systematically varied doping concentrations in an organic semiconductor layer using a molecular p-dopant *J. Appl. Phys.* **106** 103711
[158] Kleemann H, Schumann S, Jörges U, Ellinger F, Leo K and Lüssem B 2012 Organic pin-diodes approaching ultra-high-frequencies *Org. Electron.* **13** 1114–20
[159] Herwig P T and Müllen K 1999 A soluble pentacene precursor: synthesis, solid-state conversion into pentacene and application in a field-effect transistor *Adv. Mater.* **11** 480–3
[160] Kjellander B K C, Smaal W T T, Myny K, Genoe J, Dehaene W, Heremans P and Gelinck G H 2013 Optimized circuit design for flexible 8 bit RFID transponders with active layer of ink-jet printed small molecule semiconductors *Org. Electron.* **14** 768–74
[161] Higgins S G *et al* 2015 Self-aligned megahertz organic transistors solution-processed on plastic *Adv. Electron. Mater.* **1** 1500024
[162] Uemura T, Hirose Y, Uno M, Takimiya K and Takeya J 2009 Very high mobility in solution-processed organic thin-film transistors of highly ordered [1]benzothieno[3,2-b] benzothiophene derivatives *Appl. Phys. Express* **2** 111501
[163] Mitsui C *et al* 2014 High-performance solution-processable N-shaped organic semiconducting materials with stabilized crystal phase *Adv. Mater.* **26** 4546–51
[164] Smith J, Bashir A, Adamopoulos G, Anthony J E, Bradley D D C, Heeney M, McCulloch I and Anthopoulos T D 2010 Air-stable solution-processed hybrid transistors with hole and electron mobilities exceeding 2 cm^2 V^{-1} s^{-1} *Adv. Mater.* **22** 3598–602
[165] Smith J, Hamilton R, McCulloch I, Stingelin-Stutzmann N, Heeney M, Bradley D D C and Anthopoulos T D 2010 Solution-processed organic transistors based on semiconducting blends *J. Mater. Chem.* **20** 2562–74
[166] Smith J, Hamilton R, Qi Y, Kahn A, Bradley D D C, Heeney M, McCulloch I and Anthopoulos T D 2010 The influence of film morphology in high-mobility small-molecule:polymer blend organic transistors *Adv. Funct. Mater.* **20** 2330–7
[167] Smith J, Zhang W, Sougrat R, Zhao K, Li R, Cha D, Amassian A, Heeney M, McCulloch I and Anthopoulos T D 2012 Solution-processed small molecule-polymer blend organic thin-film transistors with hole mobility greater than 5 cm^2 V^{-1} s^{-1} *Adv. Mater.* **24** 2441–6
[168] Hunter S and Anthopoulos T D 2013 Observation of unusual, highly conductive grain boundaries in high-mobility phase separated organic semiconducting blend films probed by lateral-transport conductive-AFM *Adv. Mater.* **25** 4320–6
[169] Hunter S, Chen J and Anthopoulos T D 2014 Microstructural control of charge transport in organic blend thin-film transistors *Adv. Funct. Mater.* **24** 5969–76
[170] Stingelin-Stutzmann N, Smits E, Wondergem H, Tanase C, Blom P, Smith P and De Leeuw D 2005 Organic thin-film electronics from vitreous solution-processed rubrene hypereutectics *Nat. Mater.* **4** 601–6
[171] Shin N *et al* 2013 Vertically segregated structure and properties of small molecule–polymer blend semiconductors for organic thin-film transistors *Adv. Funct. Mater.* **23** 366–76
[172] de Zerio Mendaza A D, Melianas A, Rossbauer S, Bäcke O, Nordstierna L, Erhart P, Olsson E, Anthopoulos T D, Inganäs O and Müller C 2015 High-entropy mixtures of pristine fullerenes for solution-processed transistors and solar cells *Adv. Mater.* **27** 7325–31
[173] Kang H K, Kitsomboonloha R, Ulmer K, Stecker L, Grau G, Jang J W and Subramanian V 2014 Megahertz-class printed high mobility organic thin-film transistors and inverters on plastic using attoliter-scale high-speed gravure-printed sub-5 μm gate electrodes *Org. Electron.* **15** 3639–47
[174] Higgins S G, Muir B V O, Dell'Erba G, Perinot A, Caironi M and Campbell A J 2016 Self-aligned organic field-effect transistors on plastic with picofarad overlap capacitances and megahertz operating frequencies *Appl. Phys. Lett.* **108** 023302
[175] Bucella S G, Luzio A, Gann E, Thomsen L, McNeill C R, Pace G, Perinot A, Chen Z H, Facchetti A and Caironi M 2015 Macroscopic and high-throughput printing of aligned nanostructured polymer semiconductors for MHz large-area electronics *Nat. Commun.* **6** 10
[176] Altazin S, Clerc R, Gwoziecki R, Verilhac J-M, Boudinet D, Pananakakis G, Ghibaudo G, Chartier I and Coppard R 2014 Physics of the frequency response of rectifying organic Schottky diodes *J. Appl. Phys.* **115** 64509
[177] Lilja K E, Bäcklund T G, Lupo D, Hassinen T and Joutsenoja T 2009 Gravure printed organic rectifying diodes operating at high frequencies *Org. Electron.* **10** 1011–4
[178] Kim K D, Koo J B, Lee J K, Yang Y S, You I K and Noh Y Y 2010 Variations in the electric characteristics of an organic schottky diode with the P3HT thickness *J. Korean Phys. Soc.* **57** 124–7
[179] Lin C-Y, Tsai C-H, Lin H-T, Chang L-C, Yeh Y-H, Pei Z, Peng Y-R and Wu C-C 2011 High-frequency polymer diode rectifiers for flexible wireless power-transmission sheets *Org. Electron.* **12** 1777–82
[180] Bose I, Tetzner K, Borner K and Bock K 2014 Air-stable, high current density, solution-processable, amorphous organic rectifying diodes (ORDs) for low-cost fabrication of flexible passive low frequency RFID tags *Microelectron. Reliab.* **54** 1643–7
[181] Heljo P S, Li M, Lilja K E, Majumdar H S and Lupo D 2013 Printed half-wave and full-wave rectifier circuits based on organic diodes *IEEE Trans. Electron Devices* **60** 870–4
[182] Heljo P, Lilja K E, Majumdar H S and Lupo D 2014 High rectifier output voltages with printed organic charge pump circuit *Org. Electron.* **15** 306–10
[183] Li M, Heljo P S and Lupo D 2014 Organic rectifying diode and circuit for wireless power harvesting at 13.56 MHz *IEEE Trans. Electron Devices* **61** 2164–9
[184] Jung M *et al* 2010 All-printed and roll-to-roll-printable 13.56 MHz-operated 1 bit RF tag on plastic foils *IEEE Trans. Electron Devices* **57** 571–80
[185] Altazin S, Clerc R, Gwoziecki R, Verilhac J-M, Boudinet D, Pananakakis G, Ghibaudo G, Chartier I and Coppard R 2014 Physics of the frequency response of rectifying organic Schottky diodes *J. Appl. Phys.* **115** 064509
[186] Iijima S 1991 Helical microtubules of graphitic carbon *Nature* **354** 56–8
[187] Treacy M M J, Ebbesen T W and Gibson J M 1996 Exceptionally high Young's modulus observed for individual carbon nanotubes *Nature* **381** 678–80

[188] Bellucci S 2005 Carbon nanotubes: physics and applications *Phys. Status Solidi* c **2** 34–47

[189] Pop E, Mann D, Wang Q, Goodson K and Dai H 2006 Thermal conductance of an individual single-wall carbon nanotube above room temperature *Nano Lett.* **6** 96–100

[190] Martel R, Schmidt T, Shea H R, Hertel T and Avouris P 1998 Single- and multi-wall carbon nanotube field-effect transistors *Appl. Phys. Lett.* **73** 2447–9

[191] Nihei M, Kawabata A and Awano Y 2003 Direct diameter-controlled growth of multiwall carbon nanotubes on nickel-silicide layer *Japan. J. Appl. Phys.* **42** 721–3

[192] Naeemi A and Meindl J D 2005 Monolayer metallic nanotube interconnects: promising candidates for short local interconnects *IEEE Electron Device Lett.* **26** 544–6

[193] Yao Z, Kane C L and Dekker C 2000 High-field electrical transport in single-wall carbon nanotubes *Phys. Rev. Lett.* **84** 2941–4

[194] Dürkop T, Getty S A, Cobas E and Fuhrer M S 2004 Extraordinary mobility in semiconducting carbon nanotubes *Nano Lett.* **4** 35–9

[195] Kocabas C, Kim H-S, Banks T, Rogers J A, Pesetski A A, Baumgardner J E, Krishnaswamy S V and Zhang H 2008 Radio frequency analog electronics based on carbon nanotube transistors *Proc. Natl Acad. Sci.* **105** 1405–9

[196] Rutherglen C and Burke P 2007 Carbon nanotube radio *Nano Lett.* **7** 3296–9

[197] Jensen K, Weldon J, Garcia H and Zettl A 2007 Nanotube radio *Nano Lett.* **7** 3508–11

[198] Rutherglen C, Jain D and Burke P 2009 Nanotube electronics for radiofrequency applications *Nat. Nanotechnol.* **4** 811–9

[199] Collins P G, Bradley K, Ishigami M and Zettl A 2000 Extreme oxygen sensitivity of electronic properties of carbon nanotubes *Science* **287** 1801–4

[200] Zhang R, Zhang Y, Zhang Q, Xie H, Qian W and Wei F 2013 Growth of half-meter long carbon nanotubes based on Schulz–Flory distribution *ACS Nano* **7** 6156–61

[201] Lu C, An L, Fu Q, Liu J, Zhang H and Murduck J 2006 Schottky diodes from asymmetric metal-nanotube contacts *Appl. Phys. Lett.* **88** 133501

[202] Manohara H M, Wong E W, Schlecht E, Hunt B D and Siegel P H 2005 Carbon nanotube Schottky diodes using Ti-Schottky and Pt-Ohmic contacts for high frequency applications *Nano Lett.* **5** 1469–74

[203] Cobas E and Fuhrer M S 2008 Microwave rectification by a carbon nanotube Schottky diode *Appl. Phys. Lett.* **93** 43120

[204] Cobas E D, Anlage S M and Fuhrer M S 2011 Single carbon nanotube Schottky diode microwave rectifiers *IEEE Trans. Microw. Theory Tech.* **59** 2726–32

[205] Kim Y-H and Kim H 2012 Anomalous length scaling of carbon nanotube-metal contact resistance: an *ab initio* study *Appl. Phys. Lett.* **100** 213113

[206] Krupke R, Hennrich F, Löhneysen H and Kappes M M 2003 Separation of metallic from semiconducting single-walled carbon nanotubes *Science* **301** 344–7

[207] Steiner M *et al* 2012 High-frequency performance of scaled carbon nanotube array field-effect transistors *Appl. Phys. Lett.* **101** 053123

[208] Li M and Zhang J 2014 AU-SWCNTS-HF Schottky diodes fabricated by dielectrophoresis *2014 12th IEEE Int. Conf. on Solid-State and Integrated Circuit Technology (ICSICT)* pp 1–3

[209] Park S, Vosguerichian M and Bao Z 2013 A review of fabrication and applications of carbon nanotube film-based flexible electronics *Nanoscale* **5** 1727–52

[210] Chen L, Xi N, Yang R, Song B, Zhou Z and Sun Z 2013 Substrate effect on single carbon nanotube based infrared sensors *2013 13th IEEE Conf. on Nanotechnology (IEEE-NANO)* pp 250–3

[211] Han X, Janzen D C, Vaillancourt J and Lu X 2007 Printable high-speed thin-film transistor on flexible substrate using carbon nanotube solution *IET Micro Nano Lett.* **2** 96–8

[212] Vaillancourt J, Lu X, Han X and Janzen D C 2006 High-speed thin-film transistor on flexible substrate fabricated at room temperature *Electron. Lett.* **42** 1365–6

[213] Vaillancourt J *et al* 2008 All ink-jet-printed carbon nanotube thin-film transistor on a polyimide substrate with an ultrahigh operating frequency of over 5 GHz *Appl. Phys. Lett.* **93** 243301

[214] Chimot N, Derycke V, Goffman M F, Bourgoin J P, Happy H and Dambrine G 2007 Gigahertz frequency flexible carbon nanotube transistors *Appl. Phys. Lett.* **91** 153111

[215] Yang X and Chahal P 2011 Large-area low-cost substrate compatible CNT Schottky diode for THz detection *2011 IEEE 61st Electronic Components and Technology Conf. (ECTC)* pp 2158–64

[216] Arora N and Sharma N N 2014 Arc discharge synthesis of carbon nanotubes: comprehensive review *Diam. Relat. Mater.* **50** 135–50

[217] Aqel A, El-Nour K M M A, Ammar R A A and Al-Warthan A 2012 Carbon nanotubes, science and technology:I. Structure, synthesis and characterisation *Arab. J. Chem.* **5** 1–23

[218] Kumar M and Ando Y 2010 Chemical vapor deposition of carbon nanotubes: a review on growth mechanism and mass production *J. Nanosci. Nanotechnol.* **10** 3739–58

[219] Aikawa S, Einarsson E, Thurakitseree T, Chiashi S, Nishikawa E and Maruyama S 2012 Deformable transparent all-carbon-nanotube transistors *Appl. Phys. Lett.* **100** 63502

[220] Jiao L, Xian X, Wu Z, Zhang J and Liu Z 2009 Selective positioning and integration of individual single-walled carbon nanotubes *Nano Lett.* **9** 205–9

[221] Kang S, Kocabas C, Ozel T, Shim M, Pimparkar N, Alam M A, Rotkin S V and Rogers J A 2007 High-performance electronics using dense, perfectly aligned arrays of single-walled carbon nanotubes *Nat. Nanotechnol.* **2** 230–6

[222] Vaisman L, Wagner H D and Marom G 2006 The role of surfactants in dispersion of carbon nanotubes *Adv. Colloid Interface Sci.* **128–130** 37–46

[223] Fu K and Sun Y-P 2003 Dispersion and solubilization of carbon nanotubes *J. Nanosci. Nanotechnol.* **3** 351–64

[224] Loebick C, Podila R, Reppert J, Chudow J, Ren F, Haller G L, Rao A M and Pfefferle L D 2010 Selective synthesis of subnanometer diameter semiconducting single-walled carbon nanotubes *J. Am. Chem. Soc.* **132** 11125–31

[225] Che Y, Wang C, Liu J, Liu B, Lin X, Parker J, Beasley C, Wong H S P and Zhou C 2012 Selective synthesis and device applications of semiconducting single-walled carbon nanotubes using isopropyl alcohol as feedstock *ACS Nano* **6** 7454–62

[226] Islam A E, Rogers J A and Alam M A 2015 Recent progress in obtaining semiconducting single-walled carbon nanotubes for transistor applications *Adv. Mater.* **27** 7908–37

[227] Hersam M C 2008 Progress towards monodisperse single-walled carbon nanotubes *Nat. Nanotechnol.* **3** 387–94

[228] Wang C, Chien J-C, Takei K, Takahashi T, Nah J, Niknejad A M and Javey A 2012 Extremely bendable, high-performance integrated circuits using semiconducting carbon nanotube networks for digital, analog, and radio-frequency applications *Nano Lett.* **12** 1527–33

[229] Ouyang M, Huang J-L and Lieber C M 2002 Fundamental electronic properties and applications of single-walled carbon nanotubes *Acc. Chem. Res.* **35** 1018–25

[230] Cao Y, Brady G J, Gui H, Rutherglen C, Arnold M S and Zhou C 2016 Radio frequency transistors using aligned semiconducting carbon nanotubes with current-gain cutoff

frequency and maximum oscillation frequency simultaneously greater than 70 GHz *ACS Nano* **10** 6782–90
[231] Joo Y, Brady G J, Arnold M S and Gopalan P 2014 Dose-controlled, floating evaporative self-assembly and alignment of semiconducting carbon nanotubes from organic solvents *Langmuir* **30** 3460–6
[232] Duan H, Hu H, Hui H, Shen Z and Yang J K W 2013 Free-standing sub-10 nm nanostencils for the definition of gaps in plasmonic antennas *Nanotechnology* **24** 185301
[233] Duan H, Hu H, Kumar K, Shen Z and Yang J K W 2011 Direct and reliable patterning of plasmonic nanostructures with Sub-10 nm gaps *ACS Nano* **5** 7593–600
[234] Reichert J, Weber H B, Mayor M and Löhneysen V H 2003 Low-temperature conductance measurements on single molecules *Appl. Phys. Lett.* **82** 4137–9
[235] Weber H B, Reichert J, Weigend F, Ochs R, Beckmann D, Mayor M, Ahlrichs R and Löhneysen H V 2002 Electronic transport through single conjugated molecules *Chem. Phys.* **281** 113–25
[236] Stepanov A S, Soldatov E S and Snigirev O V 2009 Formation of molecular transistor electrodes by electromigration *SPIE Proc. Int. Conf. on Micro- and Nano-Electronics 2009* 26 February 2010 p 752112
[237] Lambert M F, Goffman M F, Bourgoin J P and Hesto P 2003 Fabrication and characterization of sub-3 nm gaps for single-cluster and single-molecule experiments *Nanotechnology* **14** 772
[238] Guillorn M A, Carr D W, Tiberio R C, Greenbaum E and Simpson M L 2000 Fabrication of dissimilar metal electrodes with nanometer interelectrode distance for molecular electronic device characterization *J. Vac. Sci. Technol.* B **18** 1177
[239] Deshmukh M M, Prieto A L, Gu Q and Park H 2003 Fabrication of asymmetric electrode pairs with nanometer separation made of two distinct metals *Nano Lett.* **3** 1383–5
[240] Hino T, Tanaka H, Ozawa H, Iida Y and Ogawa T 2008 A new utilization of organic molecules for nanofabrication using the molecular ruler method *Colloids Surf.* A **313** 369–72
[241] Negishi R, Hasegawa T, Terabe K, Aono M, Ebihara T, Tanaka H and Ogawa T 2006 Fabrication of nanoscale gaps using a combination of self-assembled molecular and electron beam lithographic techniques *Appl. Phys. Lett.* **88** 223111
[242] Tanaka H, Anderson M E, Horn M W and Weiss P S 2004 Position-selected molecular ruler *Japan. J. Appl. Phys.* **43** 950–3
[243] Anderson M E, Srinivasan C, Jayaraman R, Weiss P S and Horn M W 2005 Utilizing self-assembled multilayers in lithographic processing for nanostructure fabrication: Initial evaluation of the electrical integrity of nanogaps *Microelectron. Eng.* **78** 248–52
[244] Johnson S, Evans D, Davies G A, Linfield E H and Wälti C 2009 The fabrication of embedded co-planar electrodes using a self-assembled monolayer molecular resist *Nanotechnology* **20** 155304
[245] Georgiadou D G, Semple J and Anthopoulos T D 2017 Adhesion lithography for fabrication of printed radio-frequency diodes *SPIE Newsroom* (https://doi.org/10.1117/2.1201611.006783)
[246] Novoselov K S, Geim A K, Morozov S V, Jiang D, Zhang Y, Dubonos S V, Grigorieva I V and Firsov A A 2004 Electric field effect in atomically thin carbon films *Science* **306** 666–9
[247] Akturk A and Goldsman N 2008 Electron transport and full-band electron–phonon interactions in graphene *J. Appl. Phys.* **103** 53702
[248] Bolotin K I, Sikes K J, Jiang Z, Klima M, Fudenberg G, Hone J, Kim P and Stormer H L 2008 Ultrahigh electron mobility in suspended graphene *Solid State Commun.* **146** 351–5
[249] Deligeorgis G, Dragoman M, Neculoiu D, Dragoman D, Konstantinidis G, Cismaru A and Plana R 2009 Microwave propagation in graphene *Appl. Phys. Lett.* **95** 73107
[250] Dragoman M, Neculoiu D, Cismaru A, Muller A A, Deligeorgis G, Konstantinidis G, Dragoman D and Plana R 2011 Coplanar waveguide on graphene in the range 40 MHz–110 GHz *Appl. Phys. Lett.* **99** 33112
[251] Cheng R, Bai J, Liao L, Zhou H, Chen Y, Liu L, Lin Y C, Jiang S, Huang Y and Duan X 2012 High-frequency self-aligned graphene transistors with transferred gate stacks *Proc. Natl Acad. Sci.* **109** 11588–92
[252] Dragoman M, Deligeorgis G, Muller A, Cismaru A, Neculoiu D, Konstantinidis G, Dragoman D, Dinescu A and Comanescu F 2012 Millimeterwave Schottky diode on grapene monolayer via asymmetric metal contacts *J. Appl. Phys.* **112** 84302
[253] Petrone N, Chari T, Meric I, Wang L, Shepard K L and Hone J 2015 Flexible graphene field-effect transistors encapsulated in hexagonal boron nitride *ACS Nano* **9** 8953–9
[254] Li X *et al* 2009 Large-area synthesis of high-quality and uniform graphene films on copper foils *Science* **324** 1312–4
[255] Petrone N, Meric I, Hone J and Shepard K L 2013 Graphene field-effect transistors with gigahertz-frequency power gain on flexible substrates *Nano Lett.* **13** 121–5
[256] Yeh C-H, Lain Y-W, Chiu Y-C, Liao C-H, Moyano D, Hsu S S H and Chiu P-W 2014 Gigahertz flexible graphene transistors for microwave integrated circuits *ACS Nano* **8** 7663–70
[257] Lee J, Ha T-J, Li H, Parrish K N, Holt M, Dodabalapur A, Ruoff R S and Akinwande D 2013 25 GHz embedded-gate graphene transistors with high-K dielectrics on extremely flexible plastic sheets *ACS Nano* **7** 7744–50
[258] Wei W, Pallecchi E, Haque S, Borini S, Avramovic V, Centeno A, Amaia Z and Happy H 2016 Mechanically robust 39 GHz cut-off frequency graphene field effect transistors on flexible substrates *Nanoscale* **8** 14097–103
[259] Yogeesh M N, Parish K, Lee J, Tao L and Akinwande D 2014 Towards the design and fabrication of graphene based flexible GHz radio receiver systems *2014 IEEE MTT-S Int. Microwave Symp. (IMS2014)* pp 1–4
[260] Yogeesh M N, Parrish K N, Lee J, Park S, Tao L and Akinwande D 2015 Towards the realization of graphene based flexible radio frequency receiver *Electronics* **4** 933–46
[261] Paredes J I, Villar-Rodil S, Martínez-Alonso A and Tascón J 2008 Graphene oxide dispersions in organic solvents *Langmuir* **24** 10560–4
[262] Lotya M *et al* 2009 Liquid phase production of graphene by exfoliation of graphite in surfactant/water solutions *J. Am. Chem. Soc.* **131** 3611–20
[263] Hernandez Y, Nicolosi V, Lotya M, Blighe F M, Sun Z, De S, McGovern I T, Holland B, Byrne M and Gun'Ko Y K 2008 High-yield production of graphene by liquid-phase exfoliation of graphite *Nat. Nanotechnol.* **3** 563–8
[264] Wajid A S, Das S, Irin F, Ahmed H S, Shelburne J L, Parviz D, Fullerton R J, Jankowski A F, Hedden R C and Green M J 2012 Polymer-stabilized graphene dispersions at high concentrations in organic solvents for composite production *Carbon* **50** 526–34
[265] Viculis L M, Mack J J, Mayer O M, Hahn T H and Kaner R B 2005 Intercalation and exfoliation routes to graphite nanoplatelets *J. Mater. Chem.* **15** 974–8
[266] Green A A and Hersam M C 2009 Solution phase production of graphene with controlled thickness via density differentiation *Nano Lett.* **9** 4031–6

[267] Backes C *et al* 2016 Production of highly monolayer enriched dispersions of liquid-exfoliated nanosheets by liquid cascade centrifugation *ACS Nano* **10** 1589–601
[268] Sire C, Ardiaca F, Lepilliet S, Seo J-W T, Hersam M C, Dambrine G, Happy H and Derycke V 2012 Flexible gigahertz transistors derived from solution-based single-layer graphene *Nano Lett.* **12** 1184–8
[269] Kaur A, Yang X, Park K Y and Chahal P 2013 Reduced graphene oxide based Schottky diode on flex substrate for microwave circuit applications *IEEE 63rd Electronic Components and Technology Conf.* pp 1037–42
[270] Lu Y H and Feng Y P 2009 Band-gap engineering with hybrid graphane–graphene nanoribbons *J. Phys. Chem.* C **113** 20841–4
[271] Mak K, Lee C, Hone J, Shan J and Heinz T F 2010 Atomically thin MoS_2: a new direct-gap semiconductor *Phys. Rev. Lett.* **105** 136805
[272] Fiori G, Szafranek B U N, Iannaccone G and Neumaier D 2013 Velocity saturation in few-layer MoS_2 transistor *Appl. Phys. Lett.* **103** 233509
[273] Zou X *et al* 2014 Interface engineering for high-performance top-gated MoS_2 field-effect transistors *Adv. Mater.* **26** 6255–61
[274] Sanne A *et al* 2015 Radio frequency transistors and circuits based on CVD MoS_2 *Nano Lett.* **15** 5039–45
[275] Krasnozhon D, Dutta S, Nyffeler C, Leblebici Y and Kis A 2015 High-frequency, scaled MoS_2 transistors *2015 IEEE Int. Electron Devices Meeting (IEDM) (Washington, DC, 2015)* pp 27.4.1–4
[276] Krasnozhon D, Lembke D, Nyffeler C, Leblebici Y and Kis A 2014 MoS_2 transistors operating at gigahertz frequencies *Nano Lett.* **14** 5905–11
[277] Chang H Y, Yogeesh M, Ghosh R, Rai A, Sanne A, Yang S, Lu N, Banerjee S and Akinwande D 2016 Large-area monolayer MoS_2 for flexible low-power RF nanoelectronics in the GHz regime *Adv. Mater.* **28** 1818–23
[278] Cheng R, Jiang S, Chen Y, Liu Y, Weiss N, Cheng H-C, Wu H, Huang Y and Duan X 2014 Few-layer molybdenum disulfide transistors and circuits for high-speed flexible electronics *Nat. Commun.* **5** 5143
[279] Liu H, Neal A T, Zhu Z, Luo Z, Xu X, Tománek D and Ye P D 2014 Phosphorene: an unexplored 2D semiconductor with a high hole mobility *ACS Nano* **8** 4033–41
[280] Zhu W, Park S, Yogeesh M N, McNicholas K M, Bank S R and Akinwande D 2016 Black phosphorus flexible thin film transistors at gighertz frequencies *Nano Lett.* **16** 2301–6
[281] Paterson A F *et al* 2016 Small molecule/polymer blend organic transistors with hole mobility exceeding 13 $cm^2 V^{-1} s^{-1}$ *Adv. Mater.* **28** 7791–8